Report 3024

NAVAL SHIP RESEARCH AND DEVELOPMENT CENTER
Washington, D.C. 20007

THE EFFECTS OF VARIATIONS OF SEVERAL PARAMETERS ON THE WAKE IN WAY OF THE PROPELLER PLANE FOR SERIES 60–0.60 C_B MODELS

by

Jerald W. Grant and Alan C. M. Lin

HYDROMECHANICS LABORATORY
RESEARCH AND DEVELOPMENT REPORT

June 1969

Report 3024

THE EFFECTS OF VARIATIONS OF SEVERAL PARAMETERS ON THE WAKE IN WAY OF THE PROPELLER PLANE FOR SERIES 60–0.60 C_B MODELS

The Naval Ship Research and Development Center is a U.S. Navy center for laboratory effort directed at achieving improved sea and air vehicles. It was formed in March 1967 by merging the David Taylor Model Basin at Carderock, Maryland and the Marine Engineering Laboratory at Annapolis, Maryland. The Mine Defense Laboratory, Panama City, Florida became part of the Center in November 1967.

Naval Ship Research and Development Center
Washington, D.C. 20007

DEPARTMENT OF THE NAVY
NAVAL SHIP RESEARCH AND DEVELOPMENT CENTER
WASHINGTON, D. C. 20007

THE EFFECTS OF VARIATIONS OF SEVERAL PARAMETERS ON THE WAKE IN WAY OF THE PROPELLER PLANE FOR SERIES 60–0.60 C_B MODELS

by

Jerald W. Grant and Alan C. M. Lin

June 1969 Report 3024

TABLE OF CONTENTS

LIST OF FIGURES

APPENDIXES

LIST OF TABLES

NOTATION

CONVENTIONAL SYMBOL	SYMBOL APPEARING ON PLOTS	DEFINITION
D	–	Propeller diameter
J_a	–	Apparent advance coefficient $J_a = \frac{V}{nD}$ (dimensionless)
N	N	Harmonic number
n	–	Propeller revolutions per unit time
P	P	Pressure factor $P = \frac{(V_b)^2\,\text{Max}}{(V_b)^2\,\text{Mean}} - 1$
r/R or x	RADIUS or RAD.	Distance (r) from the propeller axis expressed as a ratio of the propeller radius (R), expressed as a decimal
V	V	Actual model or ship velocity
V_b	–	Resultant inflow velocity to blade
$\overline{V}_b$	–	Mean resultant inflow velocity to blade
V_r	VR	Radial component of the water velocity (positive toward the shaft centerline)
$\overline{V}_r$	–	Mean radial velocity component
V_r/V	VR/V	Radial velocity component ratio
$\overline{V}_r/V$	VRBAR	Mean radial velocity component ratio
V_t	VT	Tangential component of the water velocity (positive in a counterclockwise direction)
$\overline{V}_t$	–	Mean tangential velocity component
V_t/V	VT/V	Tangential velocity component ratio
$\overline{V}_t/V$	VTBAR	Mean tangential velocity component ratio
$(\widetilde{V}_t/V)_N$	AMPLITUDE	Amplitude of N th harmonic of tangential velocity component ratio
V_x	VX	Longitudinal (normal to the plane of survey) component of the water velocity (positive in the astern direction)

$\bar{V}_x$	–	Mean longitudinal velocity component
$V_{x'}/V$	VX/V	Longitudinal velocity component ratio
$\bar{V}_{x'}/V$	VXBAR	Mean longitudinal velocity component ratio
$(\tilde{V}_x/V)_N$	AMPLITUDE	Amplitude of N th harmonic of longitudinal velocity component ratio
$1-w_x$	1–WX	Volumetric mean wake velocity ratio $1 - w_x = \dfrac{2\pi \displaystyle\int_{x = r_{hub}/R}^{x = r_{'}/R} (\bar{V}_{x_c}/V) \cdot x \cdot dx}{\text{Disk Area} - \text{Hub Area}}$ where $(V_{x_c}/V) = (V_{x'}/V) - (V_t/V) \tan \beta$
$\bar{\beta}$	BBAR	Mean advance angle in degrees
$+\Delta\beta$	BPOS	Variation of the maximum advance angle from the mean
$-\Delta\beta$	BNEG	Variation of the minimum advance angle from the mean
θ	ANGLE IN DEGREES	Position angle (angular coordinate) in degrees
τ	–	Section shape coefficient

ABSTRACT

This report presents the results of a series of wake surveys conducted on Series 60–0.60 C_B models with three different afterbody configurations. These tests were conducted with variations of the following parameters: speed, propeller position, displacement, trim, and deadwood area.

This presentation includes the circumferential distributions of the longitudinal, tangential, and radial velocity component ratios; the radial distribution of the mean velocity component ratios; the radial distribution of the volumetric mean wake velocity ratio; the radial distribution of the amplitudes of the harmonics of the longitudinal and tangential velocity component ratios; and the radial distribution of the pressure factor and of the mean advance angle and the maximum positive and negative variations thereof.

The most pronounced effect was achieved by removing a portion of the deadwood in way of the stern aperture. This alteration yielded a higher mean longitudinal velocity while reducing the harmonic amplitudes. The displacement and speed also had an effect on the wake distribution. The testing of the moderate U- and V-shaped sterns, however, did not indicate changes of the magnitude that were anticipated.

ADMINISTRATIVE INFORMATION

The work reported herein was sponsored by the Maritime Administration under Purchase Order P1-MA66-939.

INTRODUCTION

The Naval Ship Research and Development Center (NSRDC) has undertaken a program to determine how the variation of certain parameters would affect the velocity distribution in the propeller plane of a single-screw merchant vessel. The parameters which have been under study in this program include the shape of the stern sections, the longitudinal position of the propeller with respect to the hull, the extent of deadwood, and the ship speed, displacement, and trim. This report presents the results of several tests conducted to determine the magnitude of the effects resulting from the variation of these parameters.

BACKGROUND

The nonuniformity of the velocity distribution (wake) in the propeller plane of a ship is of particular interest since it is a factor involved in the problems of propeller vibration, cavitation, and noise. Since the trends in ship design are generally directed toward greater

displacements and/or higher speeds, they lead to higher horsepower requirements. Inasmuch as contemporary marine propellers are often required to absorb in excess of 2×10^4 horsepower, they are particularly vulnerable to the effects of cavitation and vibration. Naval architects who design such high powered ships must give serious consideration to the wake distribution in designing a suitable propeller. The result of their design efforts should be a well chosen stern shape in conjunction with a wake-adapted propeller. Consequently, an incomplete or inadequate knowledge of the wake can lead to a poor design choice with associated problems which may adversely affect the life of the machinery and the performance of the propeller.

Since the wake is dominated by viscous effects, there is no acceptable method for estimating this complex wake distribution, and experimental methods must be used to measure the velocity distribution. During the past 25 years, a considerable number of such experiments have been conducted. The greater part of these data has been reanalyzed and is presented in References 1 through 5.*

Difficulties may arise when an attempt is made to make meaningful comparisons between the results of tests of different models because these tests are not always conducted at precisely the same speed, displacement, trim, or propeller clearance. Therefore, it is essential to determine the effects of all these variables on the wake. The most important finding from previous tests to determine these effects has been "the comparative inconsistency of the test data."[6] On the basis of the findings reported in Reference 6, it was decided that improvements in the wake-measurement equipment were needed both with regard to the accuracy of measurement and to the speed of data acquisition.

This equipment consisted of a pitot tube assembly, a clamping mechanism, a transverse mount, a fore-and-aft mount, a base plate, a field target, and a manometer board; see Reference 1** for a description of procedure. The mounting and aligning techniques which had to be used with this equipment were quite intricate and tedious. The nature of the mechanism made it unlikely that the pitot tube could be positioned at a certain point in the plane of measurement consistently enough to provide acceptable repeatability.

Since both accuracy and speed were affected by this method of pitot tube positioning it was imperative that the new equipment circumvent these deficiencies. The device designed to facilitate the positioning of the measuring element consists of a rake of five spherically headed pitot tubes. This rake can be inserted into the propeller shaft bossing and positioned so that it can be rotated in the desired plane of measurement. This apparatus has greatly simplified the testing procedure in that for a typical experiment (i.e., at a given speed and displacement condition), adjustments must be made only to the angular position of the rake, and the rake of pitot tubes can be quickly positioned within ± 1 deg in the model propeller disk.

---

*References are listed on page 102.

**A description of this procedure can be found on page 3 of Reference 1.

Another deficiency of the instrumentation formerly employed for wake surveys involved the use of manometers to measure the pressures on the spherical head of the pitot tube. This method precluded the rapid acquisition of data and limited the accuracy of measurement. The recently developed system uses variable reluctance pressure transducers which are coupled to digital voltmeters through a Wheatstone-bridge circuit. This electronic equipment has been linked with automatic recording devices which greatly expedite the acquisition of data; a more detailed description of this equipment is available in Appendix A. The development of this instrumentation, in conjunction with the pitot-tube rake, has made it possible to obtain repeatable data which can be used to make expeditious and meaningful comparisons when varying test conditions or design parameters. For a discussion of the repeatability of this data acquisition system, the reader is referred to pages 186–188 of Reference 7.

APPROACH

The purpose of this project is to determine the effects of several parameters on the wake distribution. Since previous tests suggested that the stern-section shape could significantly affect wake,[3] it was decided to determine the effects of stern shape on three models with identical dimensions and hull coefficients; any variation of these other parameters could overshadow the effects of the stern variations. This decision necessitated the development of two hulls with different stern-section shapes, but with the same principal dimensions and hull coefficients as those of an existing wax model (NSRDC Model 4210-5). The other two hull forms developed were designated NSRDC Model 5112 (U-shaped stern) and Model 5113 (V-shaped stern).* Numeric and pictoral descriptions of these three models are presented in Figures 1 through 5.

Since it had already been determined from previous tests that the velocity distribution in the propeller plane is sensitive to the position of that plane in the stern aperture (see page 13 of Reference 6), it was decided that this program should include some investigation in this area. The most obvious investigation of this type is the measurement of velocities in two or more propeller planes. Although the effects of this variable had been investigated previously,[6] it seemed desirable to substantiate this with some additional data. Another investigation in this area is to study the effects of changing the shape of the propeller aperture by an alteration of the deadwood. It was believed that a cutaway of deadwood would lead to a more uniform wake since it effectively changes the propeller clearance in the lower portion of the propeller disk.

A minor goal of this program was to determine the effects of certain operational variables on the wake. Since the naval architect must often design a ship to operate at two or

*These hull forms were designed by Dr. Kuo.

more dissimilar conditions of displacement and/or speed, he needs some information concerning the effects of these variables. Therefore, it was decided that experiments should be conducted at various conditions of speed, displacement, and trim. Such information is also helpful in comparisons of wake surveys conducted on models of similar vessels.

EXPERIMENTAL PROCEDURE

This program used NSRDC Model 4210-5 and the recently constructed Models 5112 (U-shaped stern) and 5113 (V-shaped stern) to represent conventional single-screw ships of the clearwater-stern type. The principal dimensions and coefficients for the corresponding ships of 400-foot length are given in Figure 1. The difference in afterbody shape is clearly shown by the section shape coefficient (τ) in Figure 1 and the comparative afterbody plan in Figure 2. (The geometrical definition of the section shape coefficient (τ), including an arbitrary determination of which values of τ might be classified as U- or V-shaped, is given in Appendix B.) Photographs showing the profile, stern section, and stern quarter are presented in Figures 3 through 5. Figure 6 indicates the radii that were surveyed.

Table 1 summarizes the testing program established to determine the effects of several parameters on the wake distribution behind a single-screw merchant ship. The test at the design displacement, speed, and plane of survey was conducted to provide a meaningful standard for purposes of comparison. This test is designated Test 35. The other eight tests were conducted in accordance with the conditions outlined in Table 1.

After each model was fitted with the pitot-tube rake and the standard towing equipment, it was prepared for testing in the NSRDC deep-water towing tank. At this point it seems desirable to explain some of the techniques employed to ensure the repeatability of this series of experiments:

1. Underway Trim. The models were ballasted to the desired displacement and trim. Each model was towed in the tank at the test speed, where it was free to assume its normal underway trim for this speed. The ogive towing struts were then locked, keeping the model at the underway trim for the duration of a test. This procedure eliminated, for practical purposes, any pitching, heaving, or rolling of the model during a test.

2. Ballast. When weights were being placed in the model to bring it to the desired displacement and draft, the actual position and denomination of each weight was marked within the model. This procedure was followed so that the model could be returned easily and accurately to the same displacement and trim.

3. Propeller Location. Since velocity measurements were to be conducted with the rake in two different propeller planes, it was necessary to have a means of precisely positioning the rake in each plane of measurement. A fairing piece was constructed with a diameter and a shape equal to that of an appropriate propeller hub. When locked in place on the rake shaft, this fairing piece served as a positioning device. A split bushing with an outside diameter

TABLE 1

Summary of Testing Program

Test Number	Model Number	Displacement (Percent Design)	Speed	Plane of Survey	Remarks
35	4210-5	100	100	35	Even Keel
36	4210-5	100	65*	35	Even Keel
37	4210-5	100	30*	35	Even Keel
38	4210-5	100	100	10*	Even Keel
39	4210-5	80*	100	35	Even Keel
40	4210-5	80*	100	35	Trimmed by Stern*
41	4210-5	100	100	35	Deadwood Removal*
42	5112*	100	100	35	Even Keel (U-Shape)
43	5113*	100	100	35	Even Keel (V-Shape)

NOTE: Speed is expressed as a percentage of the design speed. The location of the plane of survey, which is expressed as a percentage of the propeller diameter, is measured from the stern frame at the 0.7 propeller radius. The asterisks denote those parameters which were changed from the conditions existing during the base test, Test 35.

equal to the maximum diameter of the fairing was machined to a length equal to 25 percent of the propeller diameter. When this bushing was placed on the rake shaft, the rake could easily be positioned at the after (35 percent) propeller plane. The removal of the split bushing made it possible to slide the rake forward to the forward (10 percent) propeller plane. Figure 7 is a sketch of these planes of measurement.

4. Deadwood Cutaway. The conduct of the last test with Model 4210-5, designated Test 41, was facilitated by having a removable portion of deadwood. During Tests 35 through 40, the removable deadwood was bolted in place and faired to the hull with soft, water-resistant putty. The bolts and deadwood were then removed and the excess putty was wiped from the hull for Test 41. The extent of deadwood removal is clearly discernable in Figures 3 through 5 and in Figure 7.

PRESENTATION OF RESULTS

All of the information presented herein has been plotted in composite form. Each graph compares the results from one or more tests with the base or standard test, Test 35. Essentially, the graphical information given in this report is composed of two types. The first consists of three-dimensional velocity component ratios, which were calculated directly from test data; they are presented as nondimensional vectors in the cylindrical coordinate system. All of the other information presented was derived from the velocity component ratios.

The graphical results from the entire testing program are presented in Figures 8 through 62.* Table 2 defines this presentation by relating each group of information to the appropriate Figure numbers. This information has been grouped into five basic categories to facilitate the comparisons which must be made. These five categories consist of groups of tests which demonstrate the effects of speed, propeller position, displacement and trim, deadwood removal and stern-section shape.

TABLE 2

Chart Defining Location of Information

Figure numbers for use in locating plots which illustrate the effects of specific parameters.

Specific Parameters under Study and Corresponding Test Numbers	Specific Type of Information Presented			
	Circumferential Distribution of Velocity Ratios	Mean Velocity Component Ratios	Harmonic Content of Velocity Distribution $(\tilde{V}_x/V)$ $(\tilde{V}_T/V)$	Advance Angle and Pressure Factor
Speed (Tests 35, 36, and 37)	8–12	13	14–15 16–17	18
Propeller Position (Tests 35 and 38)	19–23	24	25–26 27–28	29
Displacement and Trim (Tests 35, 39, and 40)	30–34	35	36–37 38–39	40
Deadwood Removal (Tests 35 and 41)	41–45	46	47–48 49–50	51
Stern-Section Shape (Tests 35, 42, and 43)	52–56	57	58–59 60–61	62

The first type of information presented for each of the tests is the circumferential distribution of velocity component ratios. As indicated in Table 2, this information is presented in Figures 8–12, 19–23, 30–34, 41–45, and 52–56. These figures consist of plots of the longitudinal, tangential, and radial velocity component ratios for each of the test radii. Since all of these graphs are presented in comparative form, it was necessary to devise a key to distinguish between the symbols used. This key, which is located at the bottom of each of the figures, shows the model number, the test number, the displacement as a percent of

*Some additional tests were conducted to determine the wake distribution behind a Series 60–0.60 C_B model which had a major bossing modification to accommodate a large, six-component dynamometer. The results of these tests are published in Appendix C.

the design condition, the trim, the model speed in knots, the propeller location and the test date. Directly below this key is shown the actual test radius as a ratio of the propeller radius (R), expressed as a decimal.

The second type of information, which is plotted against the radius ratio in Figures 13, 24, 35, 46, and 57, consists of the mean velocity component ratios. The mean longitudinal, tangential, and radial velocity component ratios, which are calculated for each test radius and for several interpolated radii, are merely the arithmetic mean of the interpolated circumferential velocity distribution. The volumetric mean wake velocity ratio, which is calculated in accordance with the formula given in the notation, is also plotted against the radius ratio in the aforementioned figures.

The third type of information is a harmonic analysis of the circumferential distribution of the longitudinal and tangential velocity component ratios which was performed with the results from each test. The harmonic amplitudes, which are the coefficients of a Fourier series of harmonically related sine and cosine functions, are plotted against the radius ratio in Figures 14–17, 25–28, 36–39, 47–50, and 58–61. These graphs show the results for harmonic numbers (N) from one through eight.

The fourth type of information is the radial distribution of the mean advance angle ($\bar{\beta}$), the maximum positive ($+\Delta\beta$) and negative ($-\Delta\beta$) variation of the advance angle, and the pressure factor (P). This information is presented in graphical form in Figures 18, 29, 40, 51, and 62. It is necessary to mention here that an apparent advance coefficient (J_a) of 0.922 was used in the calculation of the advance angles. Appendix D presents details of the calculation methods and the computerized techniques. It includes velocity diagram which defines the relationships of the geometrical nomenclature in this report.

DISCUSSION

This discussion is divided into five sections to describe the effects brought about by variation of each of the five specific parameters under study.

EFFECTS OF SPEED

Model 4210-5 was tested at three speeds (see Table 3) to determine the effects of speed on the wake.

The results from these tests are presented in Figures 8 through 18. It can be seen from the plots of the velocity component ratios at each test radius, that the wake was most affected at the inner radii. It appears that the noticeable differences in both the magnitude of the velocities and the angular width of the velocity gradient may be attributed to the thickness of the boundary layer, which apparently varies significantly with speed. It should be noted, however, that pitot tubes of this type have definite limitations as to the magnitude of velocity gradient which can be measured accurately. The accuracy of the data taken

TABLE 3

Test Speeds

Test Number	Percentage of Design Speed	Model Speed knots	Speed-Length Ratio
35	100	4.38	0.979
36	65	2.85	0.637
37	30	1.31	0.294

immediately behind a skeg or shoulder, for example, is known to be less than for locations where the flow is more uniform. Unfortunately it is not within the state-of-the-art to make meaningful corrections to the data for shear flow effects of this type. This limitation is discussed at some length in Appendix D.

The effect of speed on the mean wake can be seen in Figure 13. The radial distribution of the mean longitudinal and the volumetric mean wake velocity component ratios for Tests 35 and 36, which define the mean wake at speeds equivalent to 100 and 65 percent of design, respectively, showed only a slight difference in the wake. The results from Test 37, however, revealed a mean longitudinal distribution which was significantly lower in magnitude than at the higher speeds. The results from Test 37, however, may be subject to the effects of instrumentation accuracy.*

The amplitudes of the harmonics of the circumferential distribution of the longitudinal and tangential velocity ratios are presented in Figures 14 through 17. The effects of speed were quite pronounced in the longitudinal harmonics and were evident in the lower harmonics of the tangential velocity distribution. It is of particular interest to note that at a radius ratio of 0.7 to 0.8, the amplitudes of the fourth through the sixth harmonic of the longitudinal velocity component ratios increased approximately 2 percent at the lower speeds. The effects of speed on the advance angle (β) and the pressure factor are shown in Figure 18.

EFFECTS OF PROPELLER POSITION

Experiments were conducted in two propeller planes to determine the effects of longitudinal position on the wake. These two planes of measurement (the locations are defined in Figure 7) were separated by a distance equal to 25 percent of the propeller diameter. The results from these tests are presented in Figures 19 through 29.

*It should be noted that errors in pressure readings, which could amount to as much as $\pm$ 0.02 in. of water, are quite significant when compared to the maximum pressure differentials of 0.25 in. of water recorded during Test 37. It is conceivable that such errors could contribute as much as $\pm$ 3 percentage points to the value of V_x/V.

It can be seen from the plots of the circumferential distribution of the velocity component ratios that the velocity distribution was most affected at the inner radii and about the vertical-centerline plane (0, 180, and 360 deg) of the ship for all radii. It is evident from these plots that the wake is slightly more uniform in the after propeller position.

The radial distributions of the second, fourth, and sixth longitudinal and tangential harmonic amplitudes (Figures 25 through 28) clearly show the effect of propeller position on wake. The greater amplitudes of the harmonics in the forward (10 percent) plane of measurement show that the wake in this plane is considerably less uniform than the wake at the 35 percent propeller position. Furthermore, the variation of the advance angle ($\pm\Delta\beta$), as presented in Figure 29, was greater for Test 38 than for Test 35.

EFFECTS OF DISPLACEMENT AND TRIM

These experiments were conducted at the design speed and in the after (35 percent) plane of measurement. The model was tested at 80 percent of design displacement in both the even keel (Test 39) and the trimmed (Test 40) conditions. The comparative plots of the circumferential distribution of the velocity component ratios at each radius (Figures 30 through 34) illustrate that there was some difference in wake between Tests 35 and 39. Although this difference was most evident at the inner radii, the outer radii were slightly affected about the vertical-centerline plane of the ship. In the trimmed condition at the light displacement (Test 40), the wake was nearly identical to the wake of the base test (Test 35).

The harmonic amplitudes of the longitudinal and tangential velocity distributions (Figures 36 through 39) illustrate that the flow in Test 39 was somewhat different from that in Test 35 and 40. The radial distribution of the mean longitudinal and tangential velocities, (Figure 35) as well as the advance angle and the pressure factor (Figure 40) further illustrate the aforementioned flow observations.

The similarity between the wake distributions measured in Tests 35 and 40 can be explained by noting that: (1) the propeller centerline was at the same immersion for both tests and (2) the model trim during Test 40 was less than 1.1 deg.

The wake distribution is known to be dominated by the hull shape in the immediate area of the propeller plane, i.e., the last few stations of a 20-station ship. Essentially then, the portion of the hull which has a predominant effect on the wake is at approximately the same draft and is inclined to the horizontal by roughly 1 deg. This reasoning is backed up by the test results presented in Figure 35 in that the wake at the inner radii, which is most dominated by the hull shape, was practically identical for the two test conditions.

EFFECTS OF DEADWOOD REMOVAL

It has been observed from the results of other experimentation[3, 6, 8] that one can expect a region of low velocity at both 0 and 180 deg for single-screw merchant ships. It was

decided by the authors that this series of experiments might well include some work directed toward reducing the nonuniformity of the wake. Since the velocity gradient near 180 deg is attributable to the deadwood below the propeller shaft, a modification of this area was undertaken. It was decided that it would be desirable to remove the portion of deadwood below a plane, which was passed through the hull, inclined by about 12 deg to the baseline at Station 18. This modification, which is illustrated in Figures 3 through 5 and in Figure 7, was undertaken and Test 41 was conducted to determine the effects.

It can be seen from the plots of the circumferential distribution of the velocity component ratios (Figures 41 through 45) that the deadwood removal or cutaway clearly affected the flow in the region bounded by the four inner radii. The unusual distribution for the two inner radii between 80 and 280 deg was partly due to the flow which follows this flattened contour. The velocity gradients which appeared in the vicinity of 120–160 and 200–240 deg were largely due to the sharp shoulders located where the plane of deadwood cutaway met the original hull shape. These low velocity regions, which are probably created by vortices which form about the sharp shoulders, might be reduced somewhat by a careful fairing in this area.

The harmonic content of the longitudinal velocity components (Figures 47 and 48) showed a slight increase in the amplitude of the lower odd-numbered harmonics compared to those of Test 35. The even harmonics and the odd harmonics above the fifth were less than the comparable harmonic amplitudes from Test 35. The harmonic amplitudes derived from the tangential velocity component ratios of Test 41 (Figures 49 and 50) were slightly lower than those of Test 35. The radial distribution of the mean velocity ratios (Figure 46) and of the advance angle (Figure 51) indicated, as do the other data, that the wake with the deadwood cutaway (Test 41) was somewhat superior.

EFFECTS OF STERN SECTION SHAPE

Experiments were conducted to determine the wake distribution behind the three hulls with different stern shapes as described in Figures 1 and 2. It can be seen from the plots of the circumferential distribution of the velocity component ratios (Figures 52 through 56) that the differences in the wake were quite small. Nevertheless, some statements can be made regarding the apparent differences. It would seem that the magnitude and width of the low velocity region near 180 deg was greatest for the U-shaped stern (Test 42) and least for the V-shaped stern (Test 43). The opposite effect seems to prevail in the region near top-dead-center (0 deg).

The harmonic analysis of the circumferential distribution of the longitudinal velocity component ratios (Figures 58 and 59) shows that for the first and third harmonic amplitudes, the results from Test 42 were superior to those of Tests 35 and 43. From the fourth harmonic up, however, the results for the U-shaped stern from (Test 42) were clearly less desirable than

the results from Tests 35 and 43, which were nearly equal. There appears to be little difference in the amplitudes of the harmonic content of the tangential velocity distribution (Figures 60 and 61).

Since the measured differences in wake distribution were small, it would be pointless to make any statements indicating which stern shape yields the most desirable wake distribution. The only conclusive statement which can be made is that the test results indicated a more favorable wake at 0 deg for the U-shape stern and at 180 deg for the V-shape stern.

CONCLUSIONS

Based on the test results which have been discussed, it appears that the following conclusions can be made:

1. The effect of speed on the wake pattern is not negligible. It affects the wake velocity more noticeably in the inner region of the propeller disk. A lower speed tends to show a greater retardation of the flow and results in a lower mean longitudinal velocity ratio. Moreover, the effect of speed on the amplitudes and radial distributions of the various harmonics of the velocity components is also significant.

2. A change in the longitudinal position of the propeller plane in the order of 25 percent of the propeller diameter indicates some change in the wake pattern, especially in the inner region of the propeller disk. Its effect on the harmonics of the velocity components is also significant, but it is not as prominent as that of speed. From the standpoint of uniformity, the aft position is favored.

3. The change in displacement, which amounts to a reduction of 20 percent, clearly affects the wake pattern. The effects of this change on the various harmonics are significant and are as prominent as those of speed. The results of the test at a trimmed condition at 80 percent of design displacement, however, indicate a negligible effect. This phenomenon can be explained more readily when one is aware that the test condition results in a propeller immersion equal to that at the design displacement.

4. The information gained from the experiment in the cutaway of deadwood indicates that it is possible to improve the wake pattern through modifications of this type. The effects of this modification are pronounced at the inner radii in both the circumferential velocity distributions and in the harmonic amplitudes.

5. The effects of afterbody section variations were not as pronounced as had been anti-anticipated. Since the test results indicated only slight differences in the wake, no conclusion regarding the superiority of one stern shape over the other can be made. It appears that the variations of the stern-section shape were not extreme enough to achieve conclusive results.

RECOMMENDATIONS

Since the experiment with the cutaway of deadwood yielded such marked effects, it would be advantageous to continue investigation in this area. It is the opinion of the authors that the present cutaway design could be improved by a careful fairing of the shoulders.

Considering what research has been completed, it seems desirable to explore the effects of greater variations in the stern-section shape. It is suggested that any investigation of this type should include hulls with pronounced U-shaped ($\tau \leqq 0.1$) and V-shaped ($\tau \geqq 0.04$) sterns.

It is further speculated that a pronounced U-shaped stern, in conjunction with a modification of the cutaway design, would lead to the most satisfactory solution to the problem of shaft-transmitted vibration associated with single-screw hulls. It is believed that a pronounced U-shaped stern would reduce the velocity defect (dip) about the top of the propeller disk while the cutaway would almost eliminate the defect at 180 deg.

ACKNOWLEDGMENTS

When any research project of this nature is undertaken, it is anticipated that there will be many people to thank upon its completion. The authors wish to thank at least some of these people formally by way of this report.

The authors wish to thank Mr. J.B. Hadler, Head of the Ship Powering Division, Mr. C.J. Wilson, Head of the Speed and Power Branch, and Mr. H.M. Cheng, for the aid and suggestions which helped to make this testing program both possible and fruitful. The endeavors of Messrs. Robert Archer and Jack Gordon who developed, improved, and maintained our excellent testing instrumentation are greatly appreciated by all those who have used this equipment.

The conduct of our testing program was greatly facilitated by Mr. Robert Hunt, whose time and effort are greatly appreciated. Last, but certainly not least, the authors want to thank Miss Nadine Hubble. It must again be stressed that nearly all the curves reported herein were plotted by a machine, guided by programmed instructions. Without her ingenious programming, countless hours would have been spent calculating and plotting, without the inherent accuracy of a machine.

MODEL NUMBER	4210-5	5112	5113
LBP, ft.	400.0	400.0	400.0
B, ft.	53.33	53.33	53.33
H, ft.	21.33	21.33	21.33
Δ, TONS	7808	7815	7815
L_E/LBP	0.5	0.5	0.5
L_X/LBP	0	0	0
L_R/LBP	0.5	0.5	0.5
C_B	0.60	0.60	0.60
C_X	.977	.977	.977
C_P	.614	.614	.614
C_{PF}	.581	.581	.581
C_{PA}	.646	.646	.646
C_{PE}	.581	.581	.581
C_{PR}	.646	.646	.646
C_{PV}	.850	.850	.848
C_{PVF}	.910	.910	.910
C_{PVA}	.802	.796	.793
C_W	.706	.688	.689
C_{WF}	.624	.624	.624
C_{WA}	.788	.752	.754
HALF ENT. ANGLE	7.0°	7.0°	7.0°
LWL, ft.	406.7	405.5	405.5
LCB, %LBP FROM [illegible] ...	1.5%A	1.3%A	1.4%A
L/B	7.5	7.5	7.5
B/H	2.5	2.5	2.5
$\Delta/.01L^3$	122.0	122.0	122.0
S, $ft.^2$	27,280	26,970	26,990
τ @ Sta. 18	.217	.181	.330

Figure 1 – Principal Dimensions and Hull Coefficients for Models 4210-5, 5112, and 5113

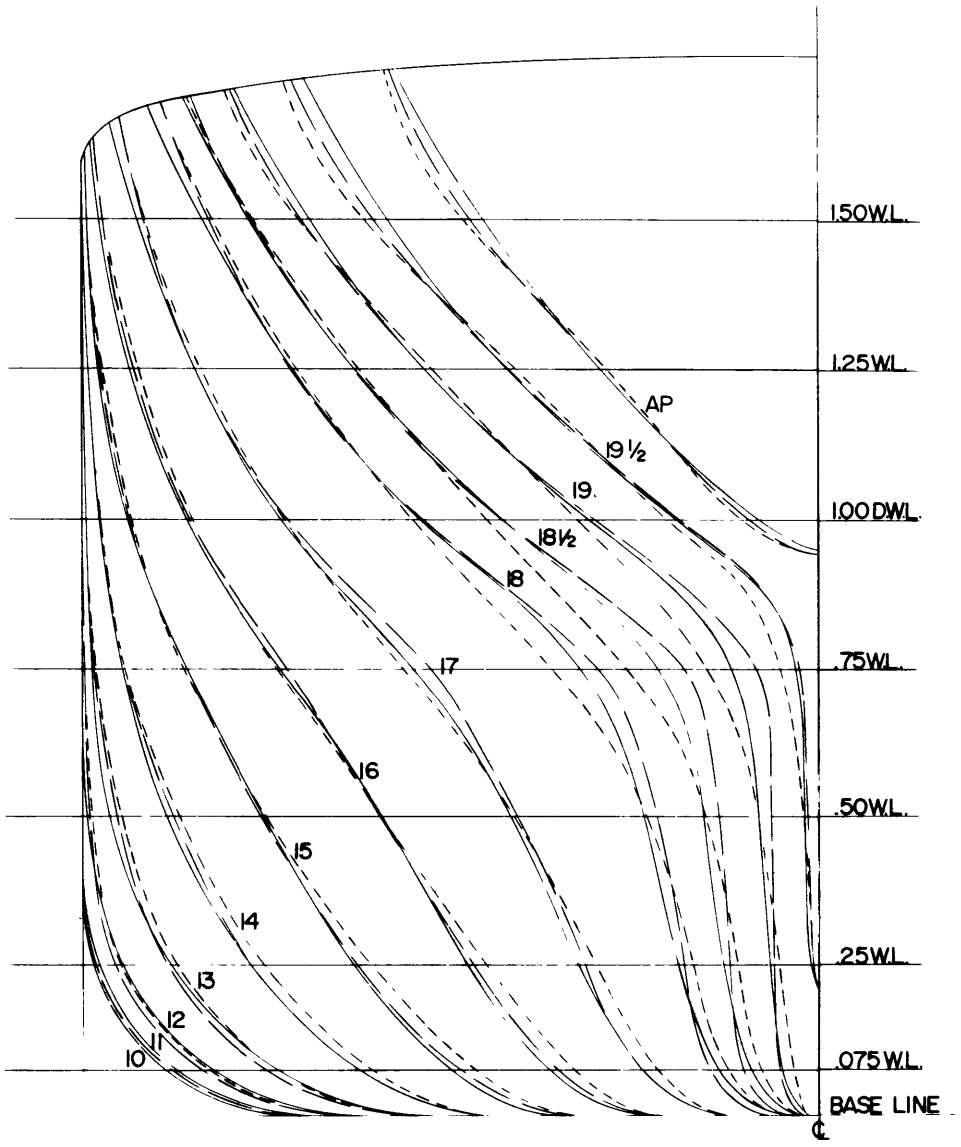

Figure 2 – Comparative Afterbody Plan of Models 4210-5 (Moderate U-Shaped), .5112 (U-Shaped), and 5113 (V-Shaped)

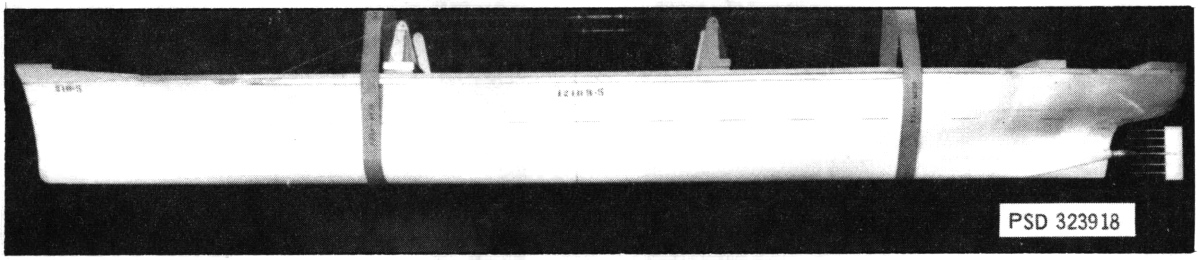

Figure 3a – Model 4210-5, Moderate U-Shape

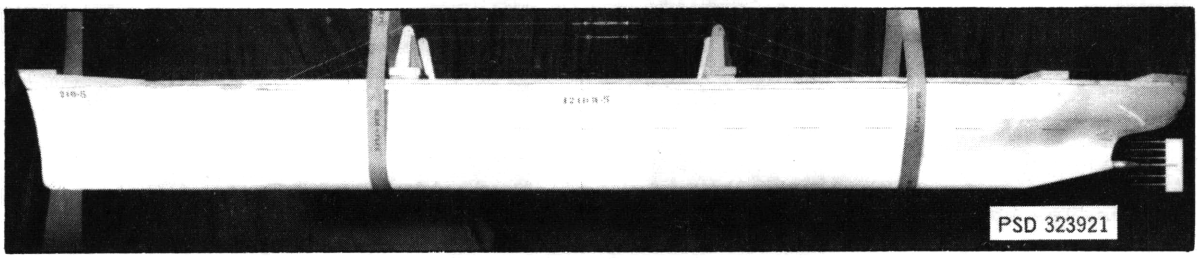

Figure 3b – Model 4210-5, Moderate U-Shape (Deadwood Cut Away)

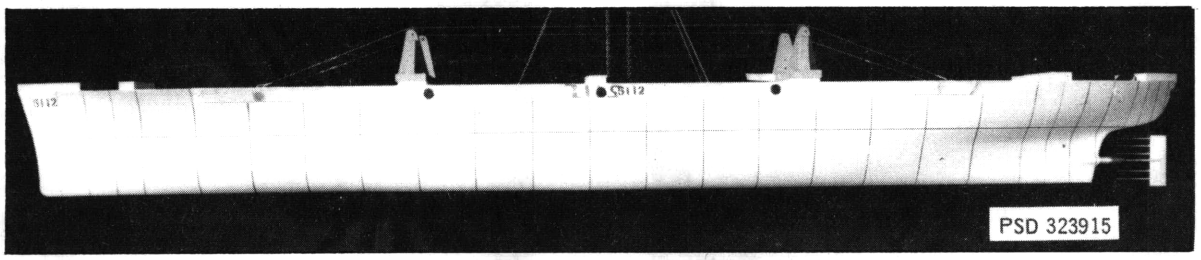

Figure 3c – Model 5112, U-Shape

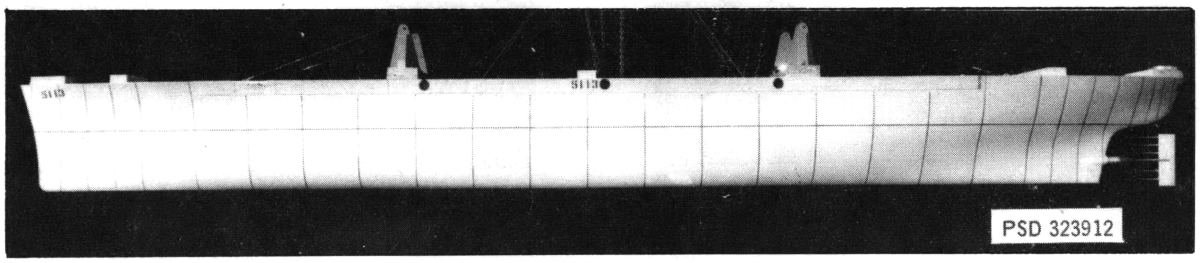

Figure 3d – Model 5113, V-Shape

Figure 3 – Profile Views of the Models Showing the Pitot Tube Rake Assembly

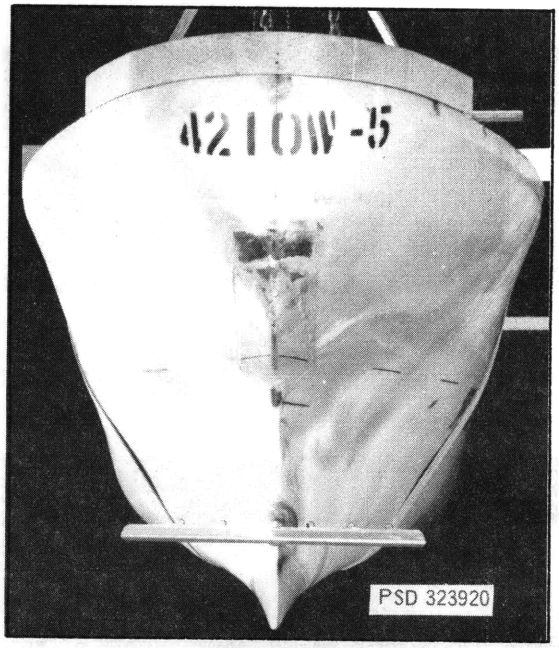

Figure 4a – Model 4210-5, Moderate U-Shape

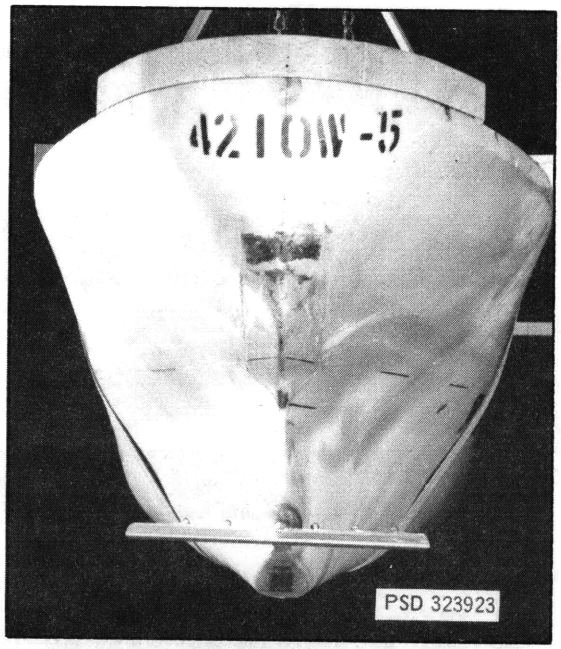

Figure 4b – Model 4210-5, Moderate U-Shape (Deadwood Cut Away)

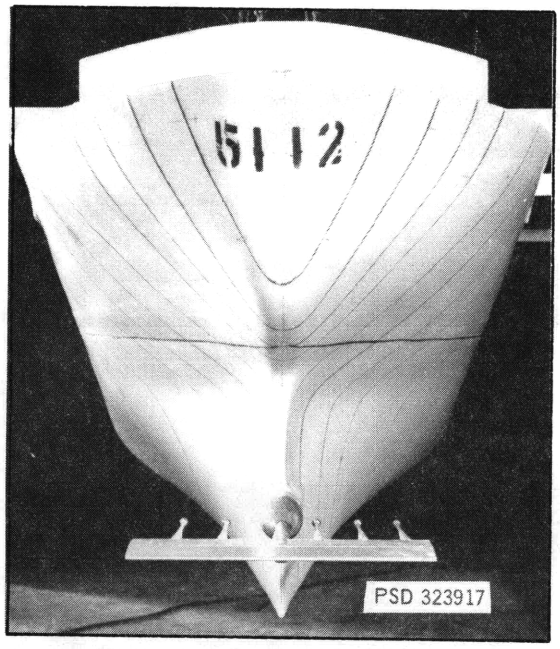

Figure 4c – Model 5112, U-Shape

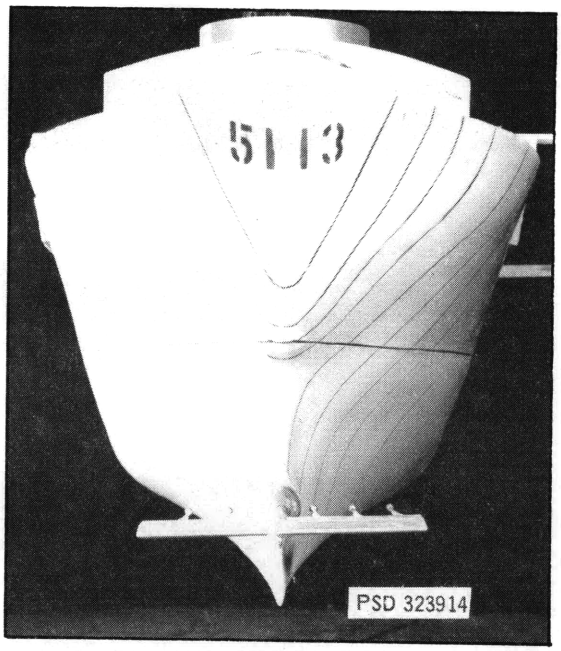

Figure 4d – Model 5113, V-Shape

Figure 4 – Stern Views of the Models Showing the Pitot Tube Rake Assembly

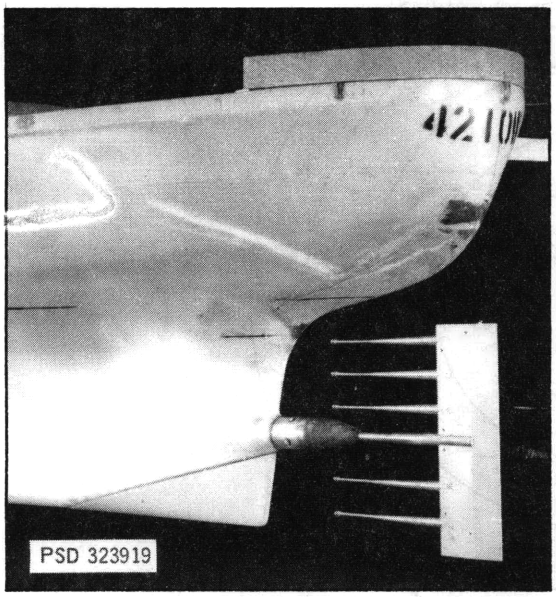

Figure 5a – Model 4210-5, Moderate U-Shape

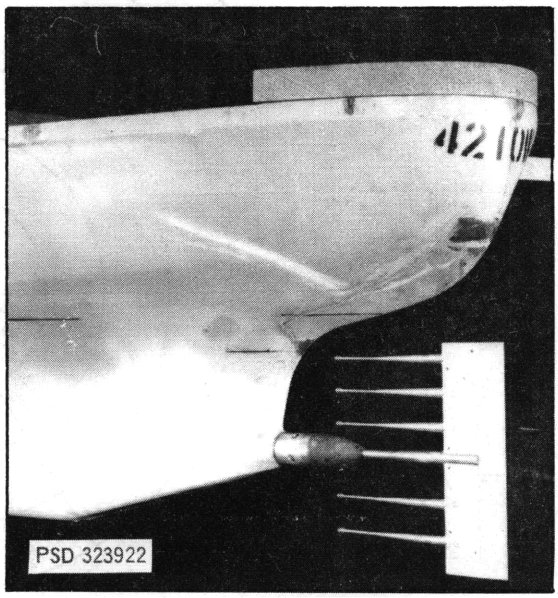

Figure 5b – Model 4210-5, Moderate U-Shape (Deadwood Cut Away)

Figure 5c – Model 5112, U-Shape

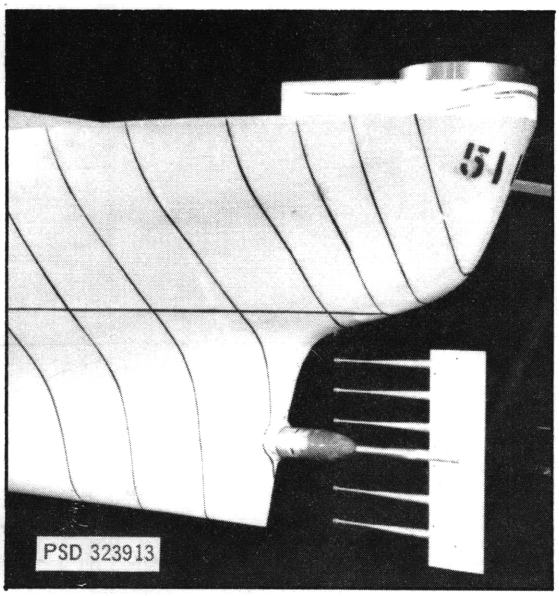

Figure 5d – Model 5113, V-Shape

Figure 5 – Stern-Quarter Views of the Models Showing the Pitot Tube Rake Assembly

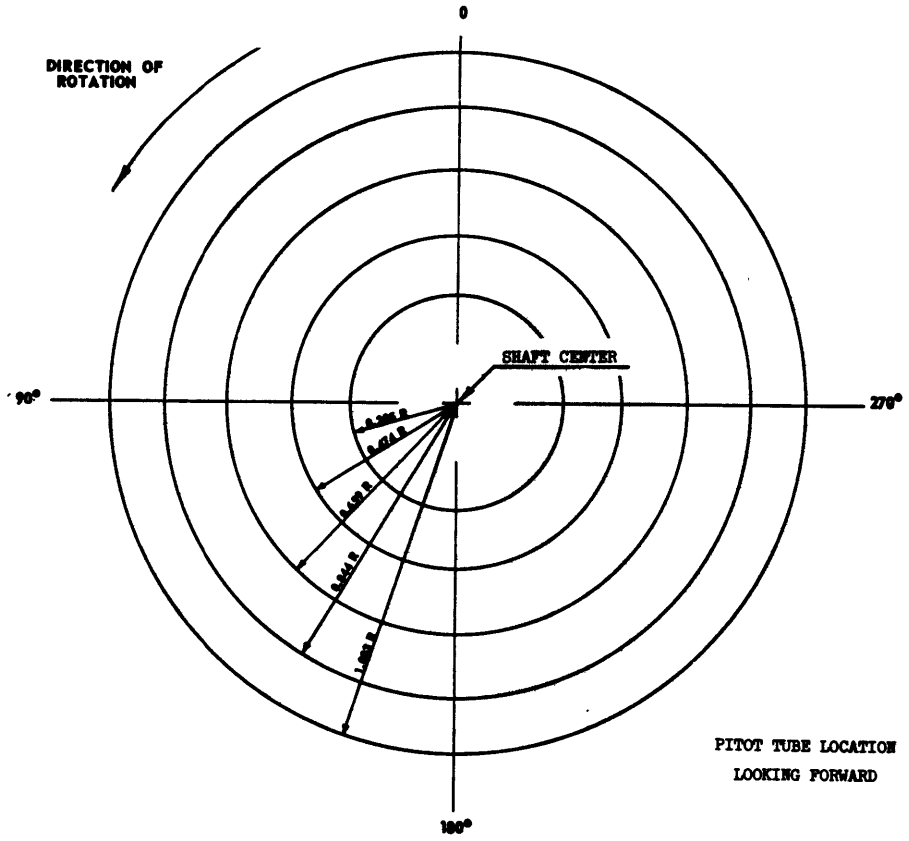

Figure 6 – Test Radii in the Propeller Plane

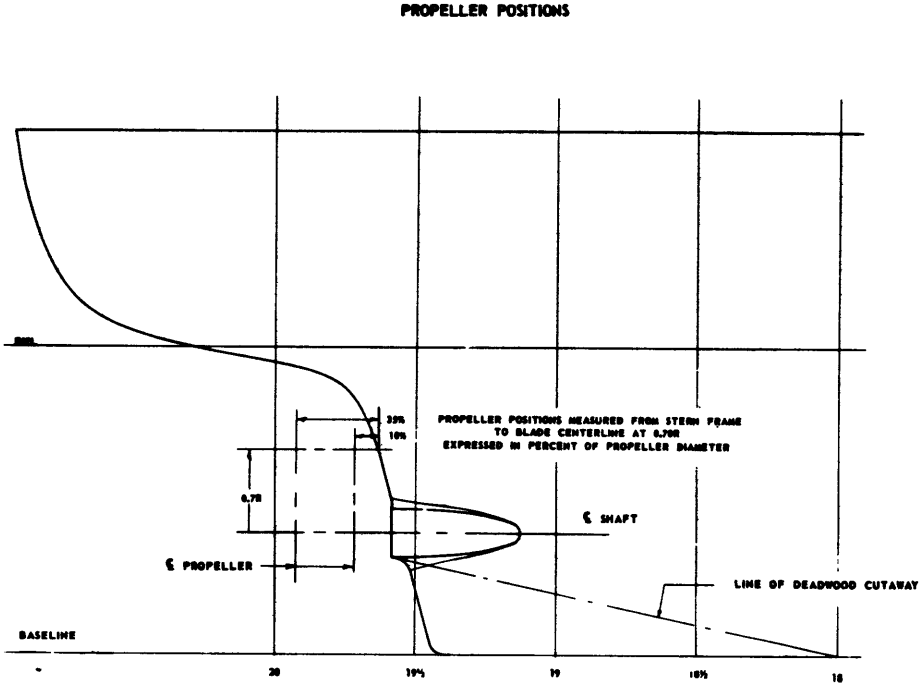

Figure 7 – Planes of Measurement

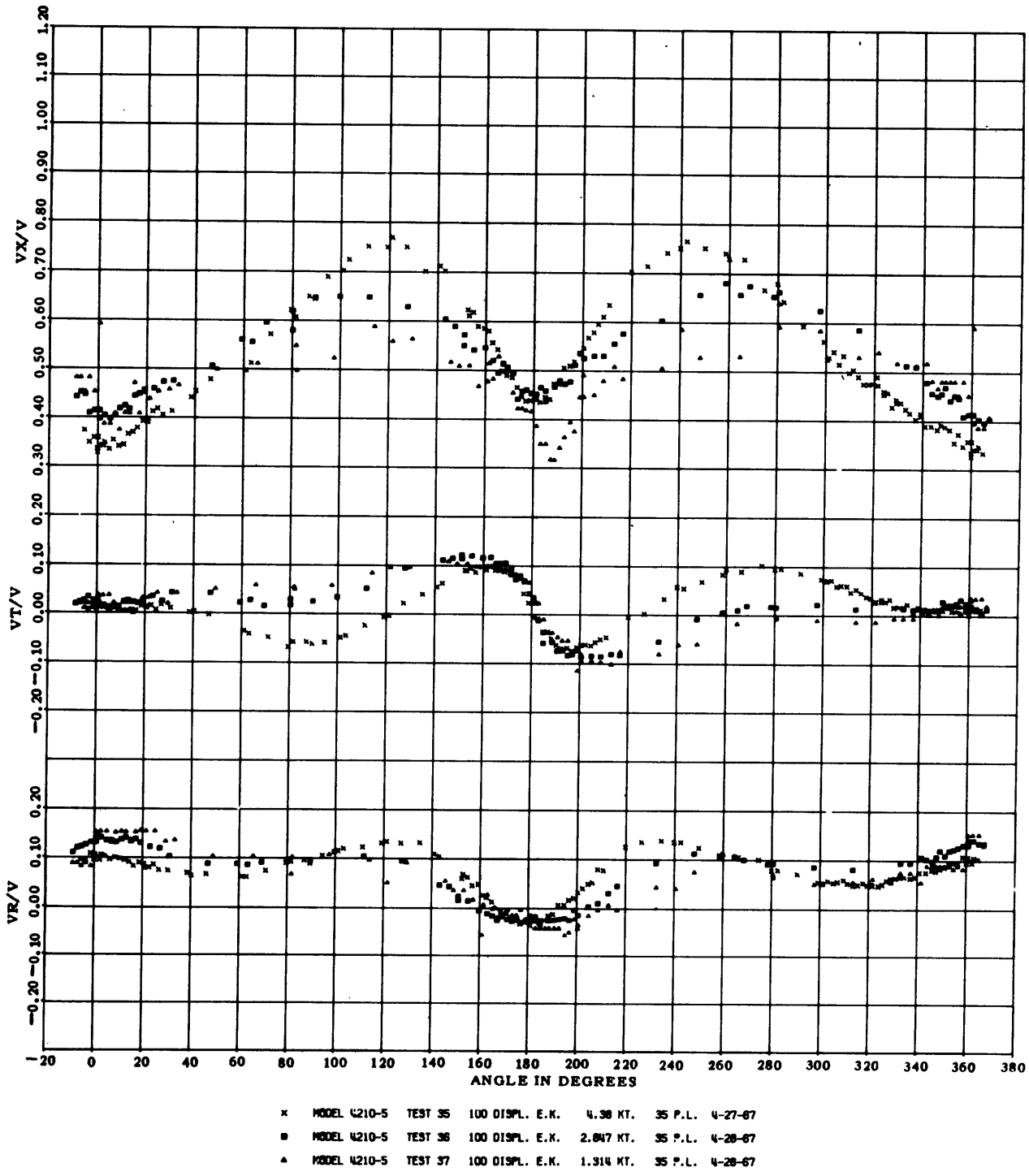

Figure 8 – Circumferential Distribution of Longitudinal, Tangential, and Radial Velocity Component Ratios at a Radius Ratio of 0.305 for Three Speeds: Composite of Tests 35, 36, and 37

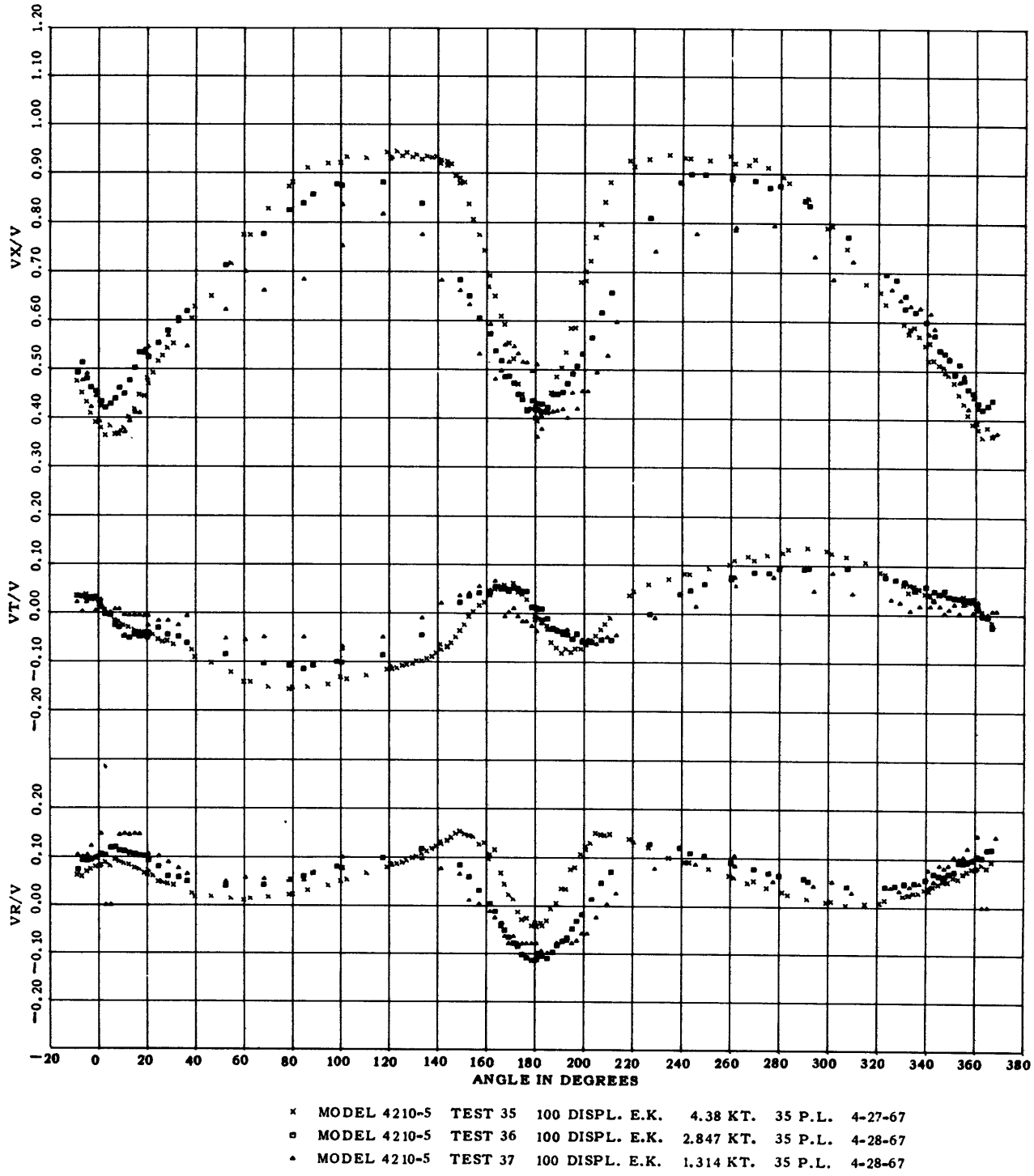

Figure 9 – Circumferential Distribution of Longitudinal, Tangential, and Radial Velocity Component Ratios at a Radius Ratio of 0.474 for Three Speeds: Composite of Tests 35, 36, and 37

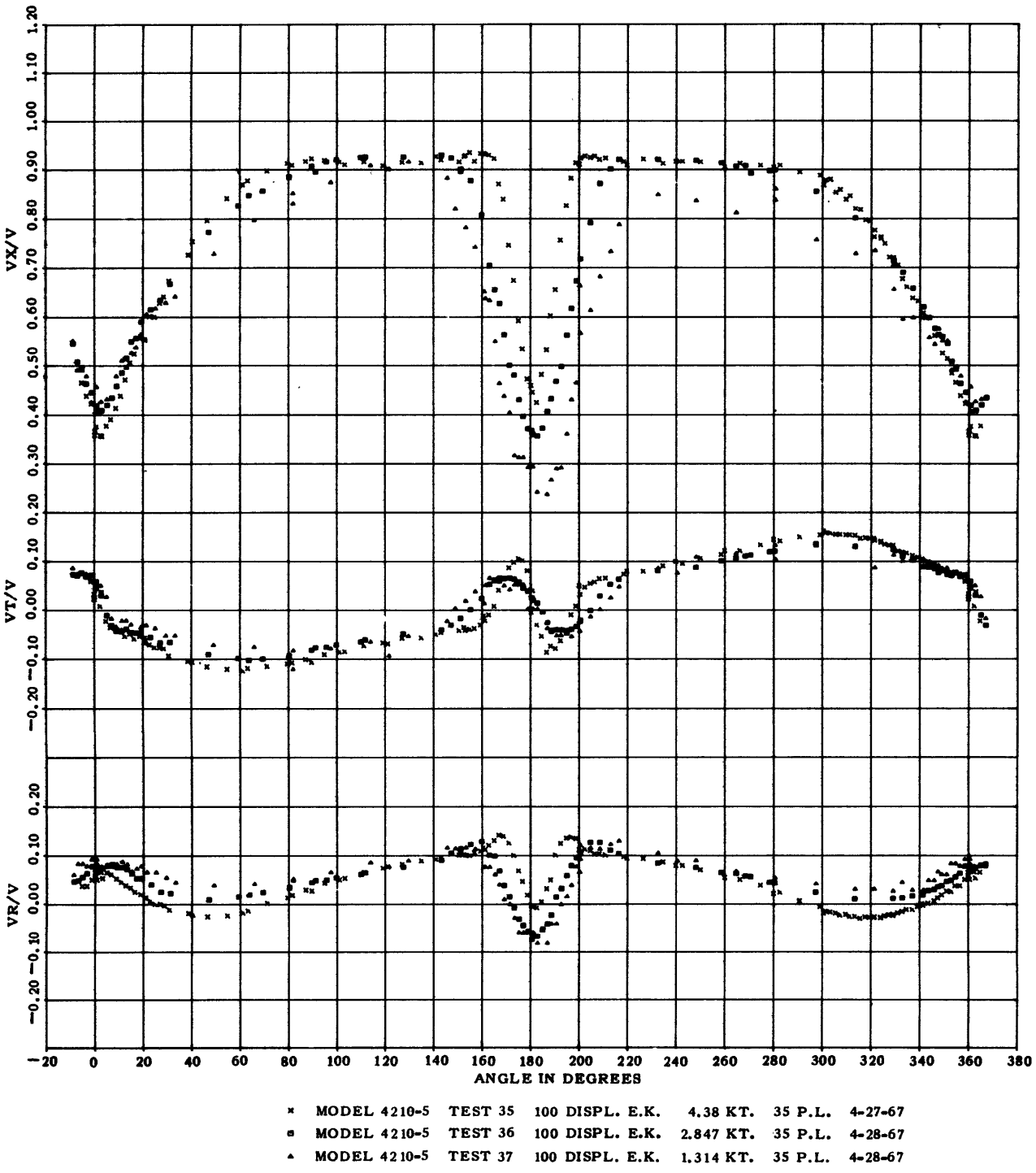

Figure 10– Circumferential Distribution of Longitudinal, Tangential, and Radial Velocity Component Ratios at a Radius Ratio of 0.659 for Three Speeds: Composite of Tests 35, 36, and 37

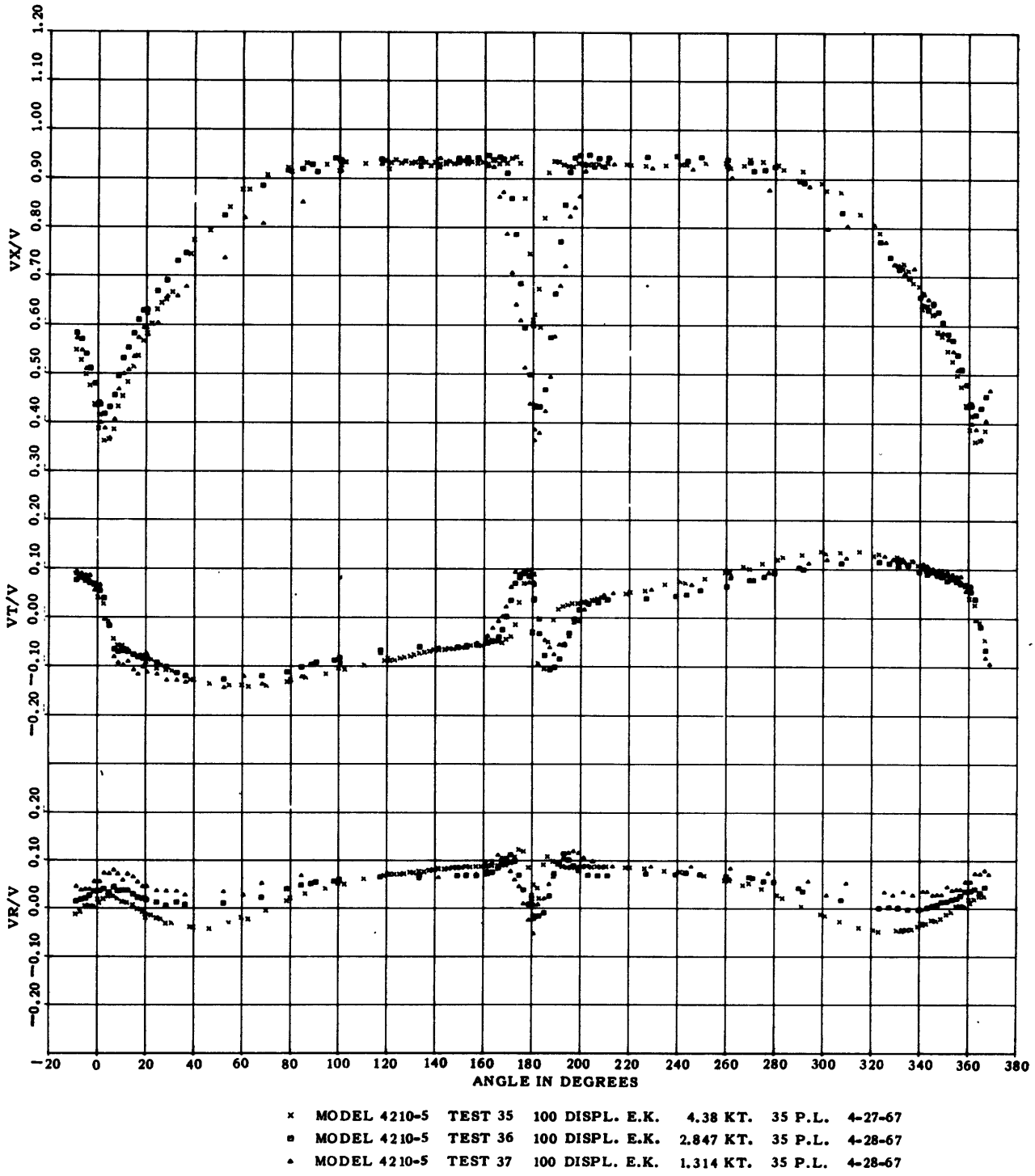

Figure 11 – Circumferential Distribution of Longitudinal, Tangential, and Radial Velocity Component Ratios at a Radius Ratio of 0.844 for Three Speeds: Composite of Tests 35, 36, and 37

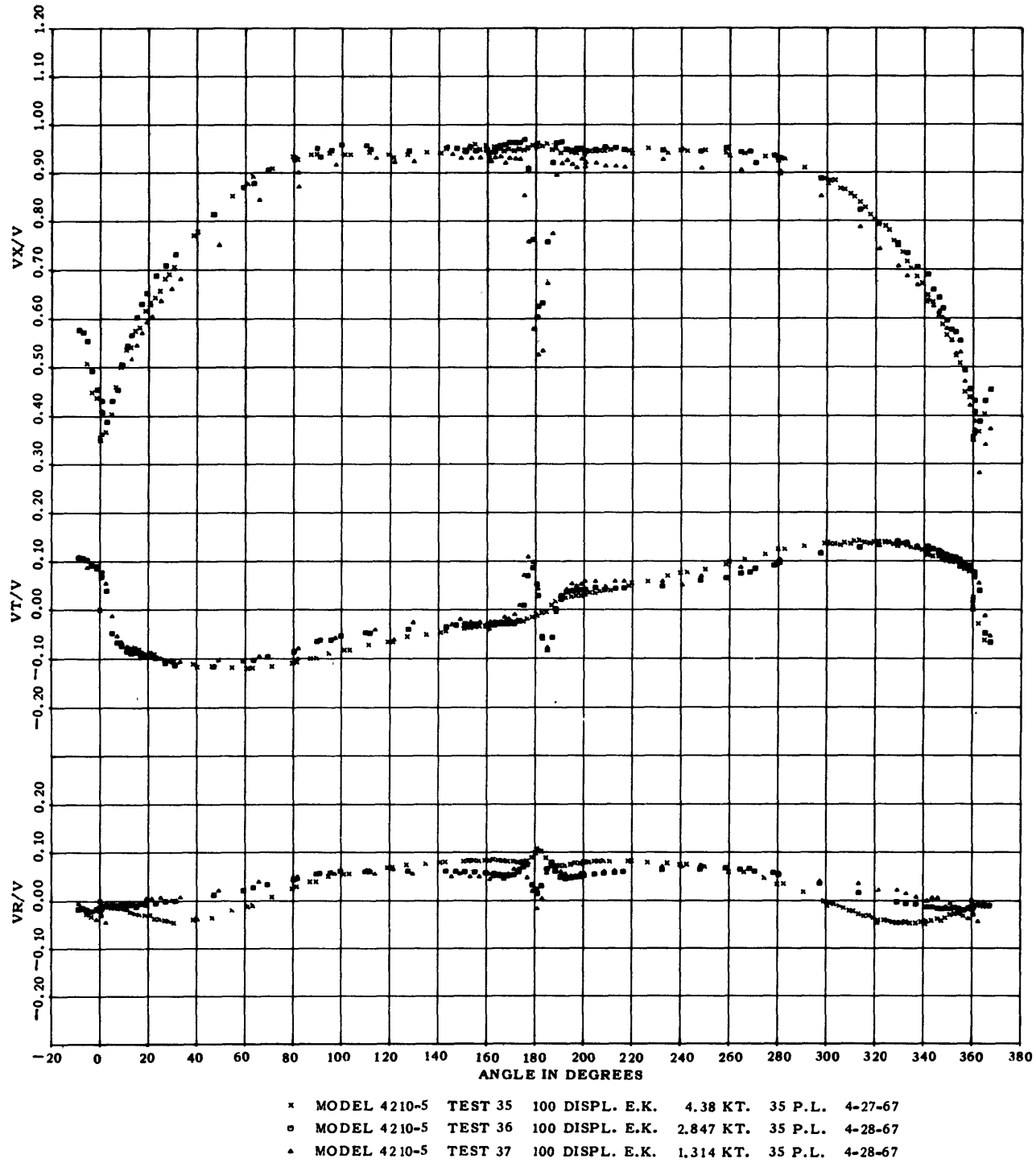

Figure 12 – Circumferential Distribution of Longitudinal, Tangential, and Radial Velocity Component Ratios at a Radius Ratio of 1.003 for Three Speeds: Composite of Tests 35, 36, and 37

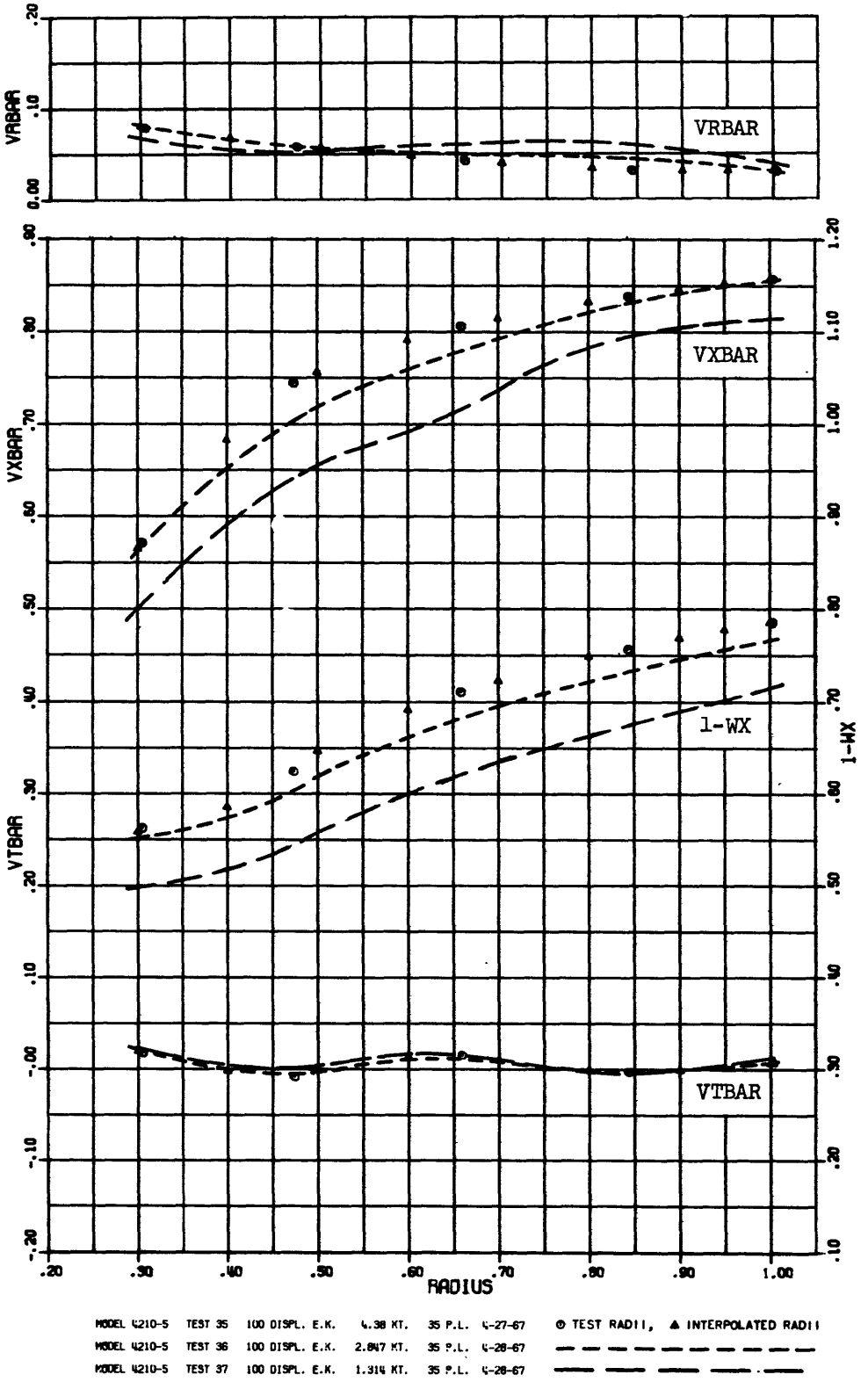

Figure 13 – Radial Distribution of the Volumetric Mean Wake Velocity Component Ratio and of the Mean Longitudinal, Tangential, and Radial Velocity Component Ratios for Three Speeds: Composite of Tests 35, 36, and 37

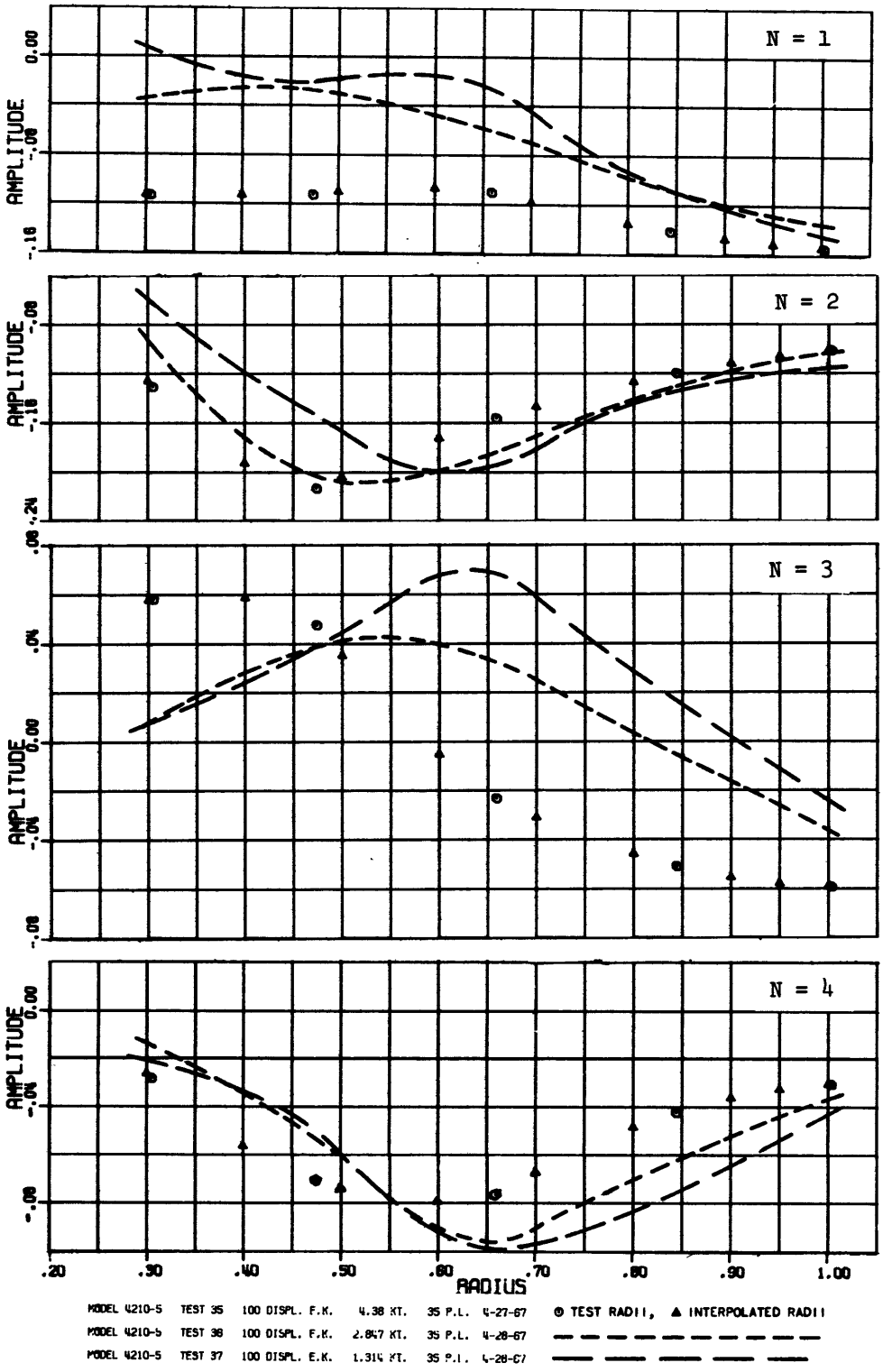

Figure 14 – Radial Distribution of the Amplitudes of the First through the Fourth Harmonic of the Circumferential Distribution of the Longitudinal Velocity Component Ratios for Three Speeds: Composite of Tests 35, 36, and 37

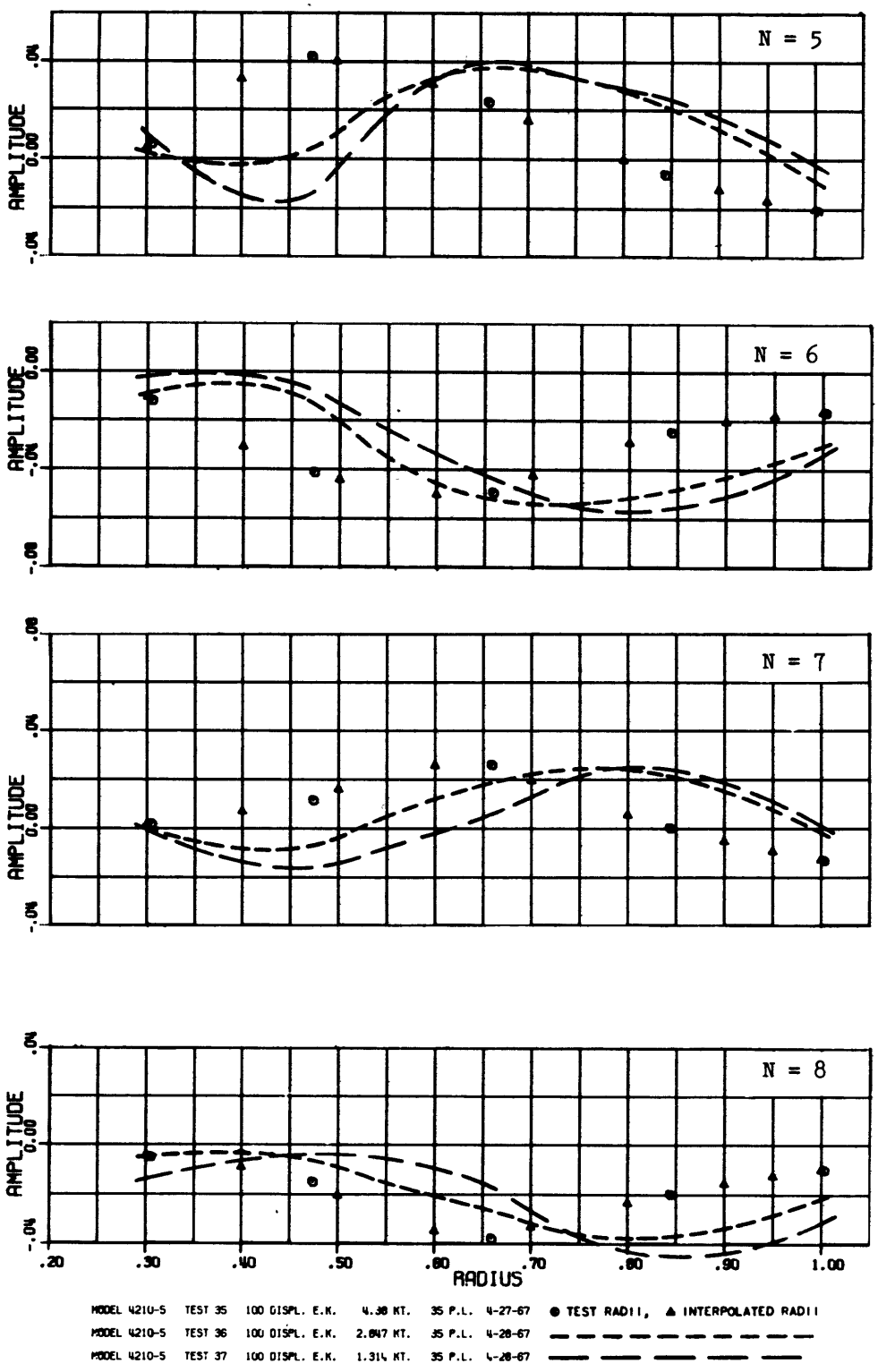

Figure 15 – Radial Distribution of the Amplitudes of the Fifth through the Eighth Harmonic of the Circumferential Distribution of the Longitudinal Velocity Component Ratios for Three Speeds: Composite of Tests 35, 36, and 37

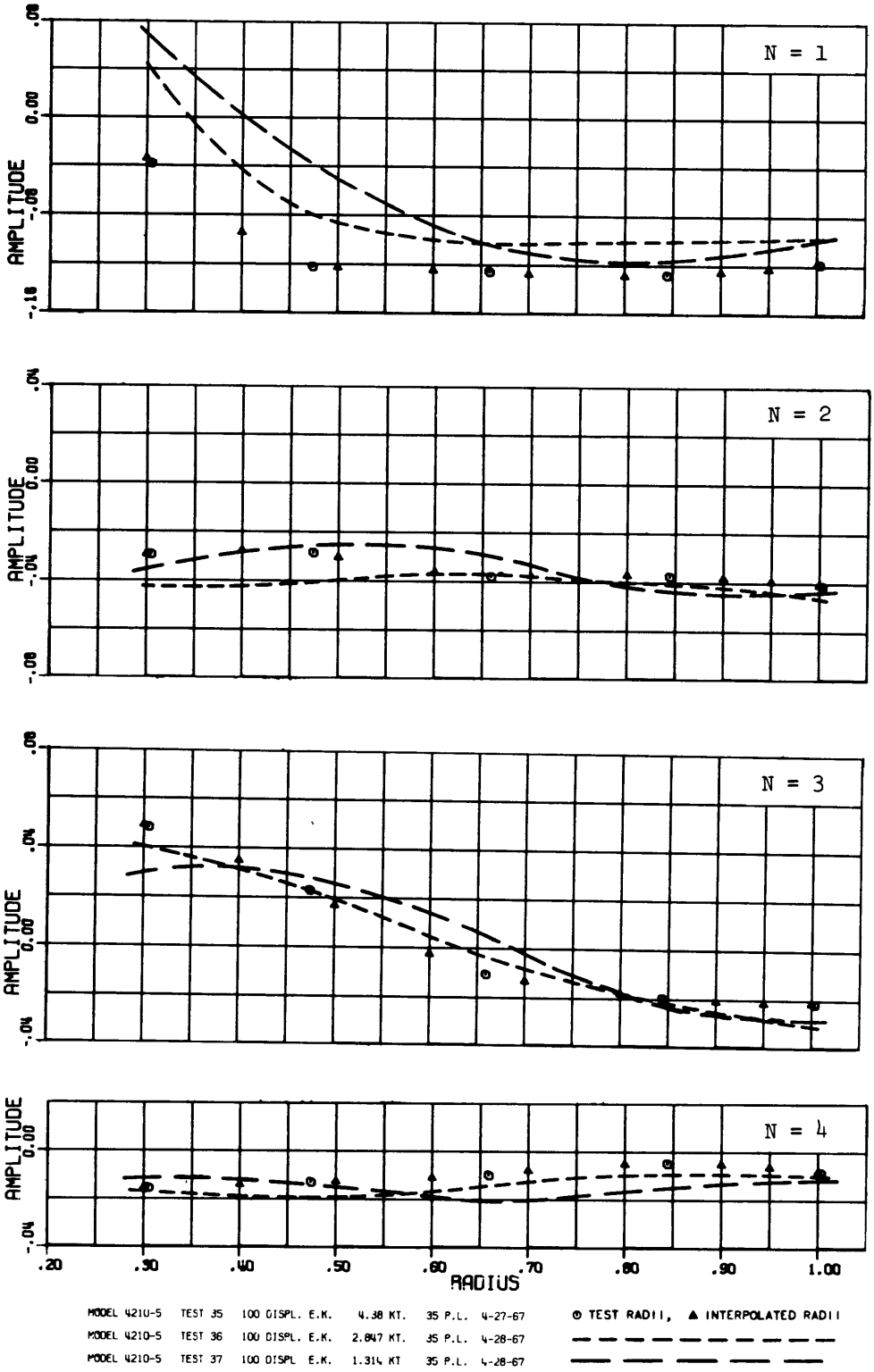

Figure 16 – Radial Distribution of the Amplitudes of the First through the Fourth Harmonic of the Circumferential Distribution of the Tangential Velocity Component Ratios for Three Speeds: Composite of Tests 35, 36, and 37

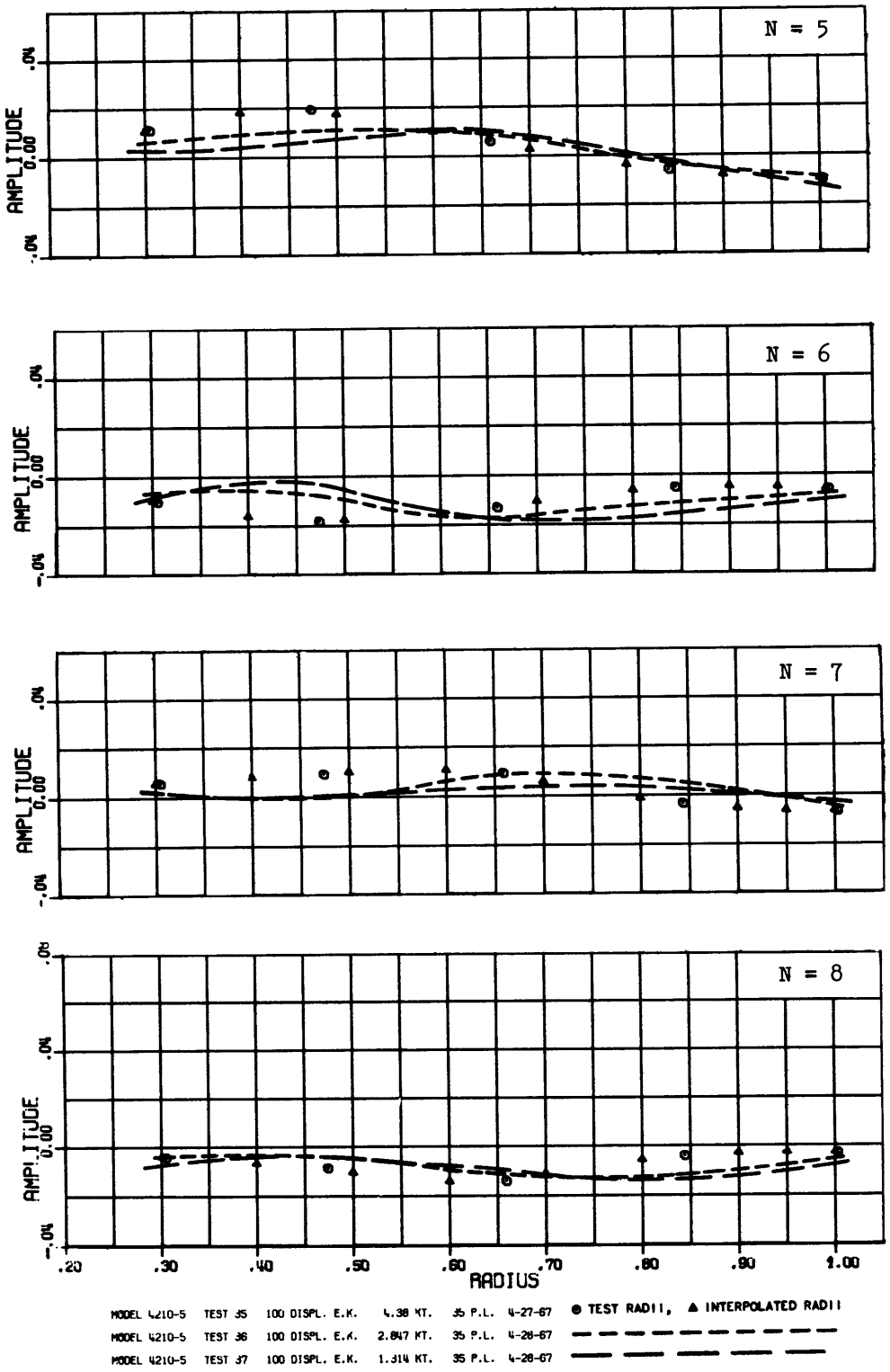

Figure 17 – Radial Distribution of the Amplitudes of the Fifth through the Eighth Harmonic of the Circumferential Distribution of the Tangential Velocity Component Ratios for Three Speeds: Composite of Tests 35, 36, and 37

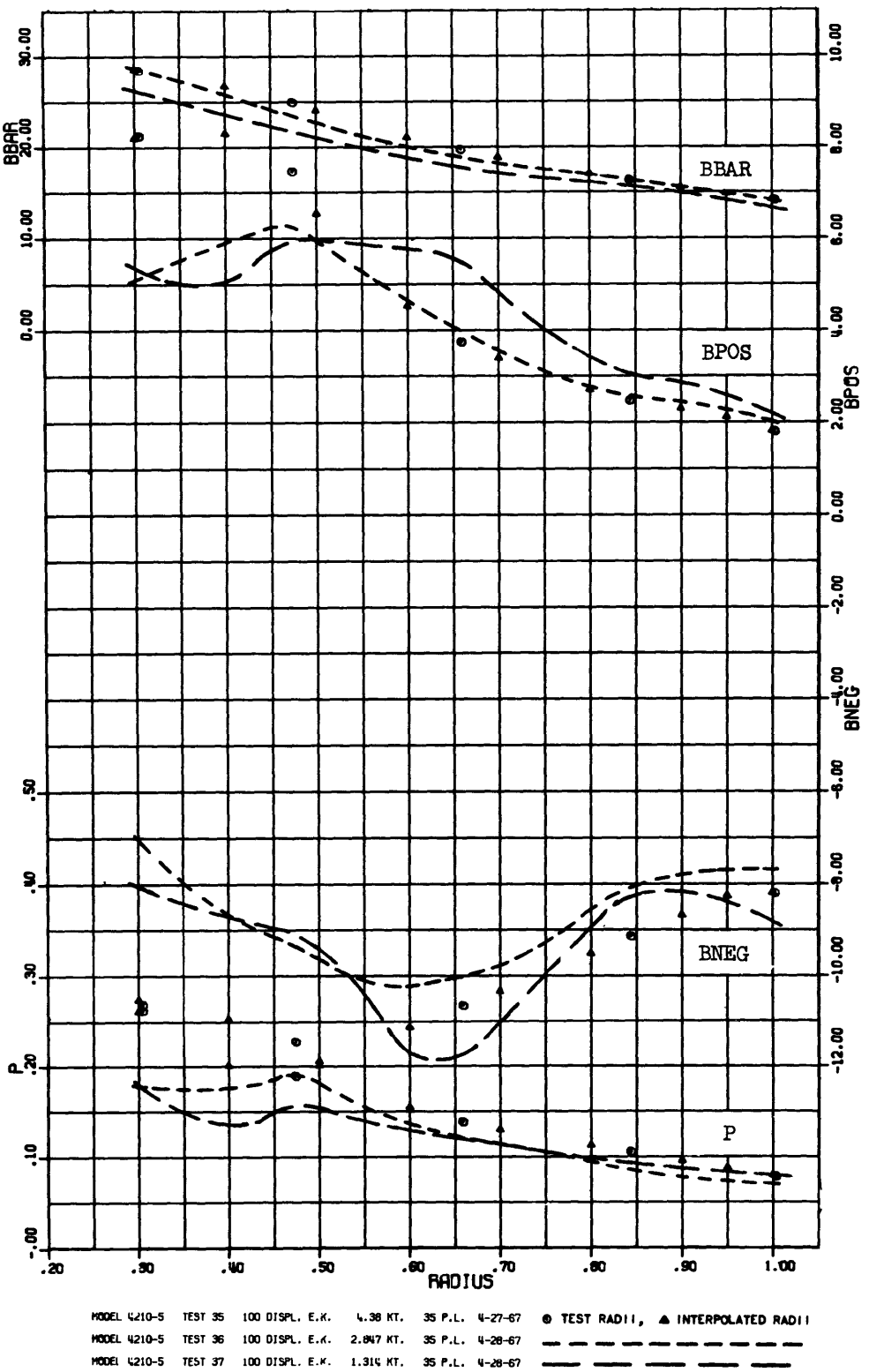

Figure 18 – Radial Distribution of the Mean Advance Angle, the Maximum Variations of the Advance Angle, and the Pressure Factor for Three Speeds: Composite of Tests 35, 36, and 37

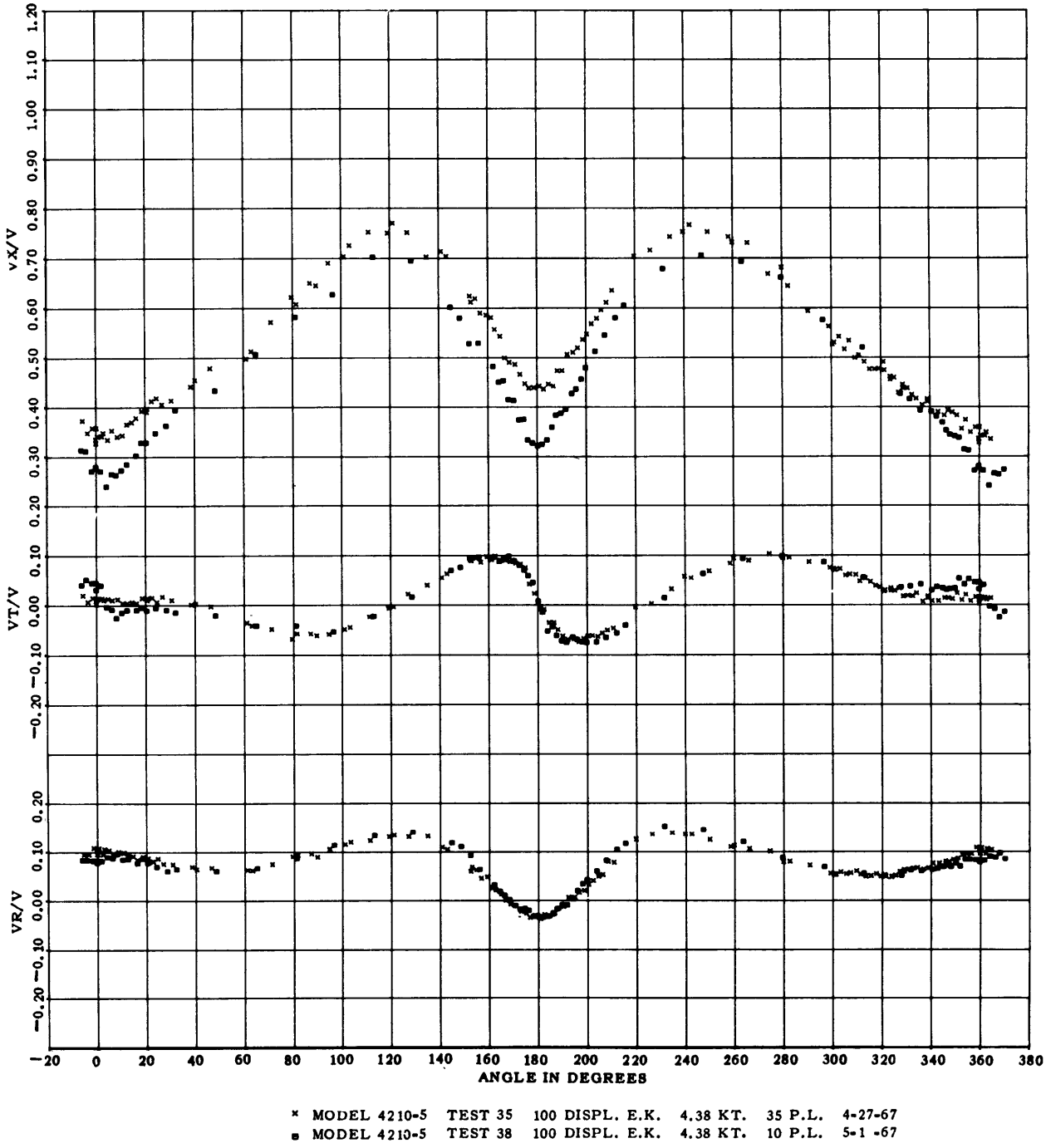

Figure 19 – Circumferential Distribution of Longitudinal, Tangential, and Radial Velocity Component Ratios at a Radius Ratio of 0.305 for Two Propeller Positions: Composite of Tests 35 and 38

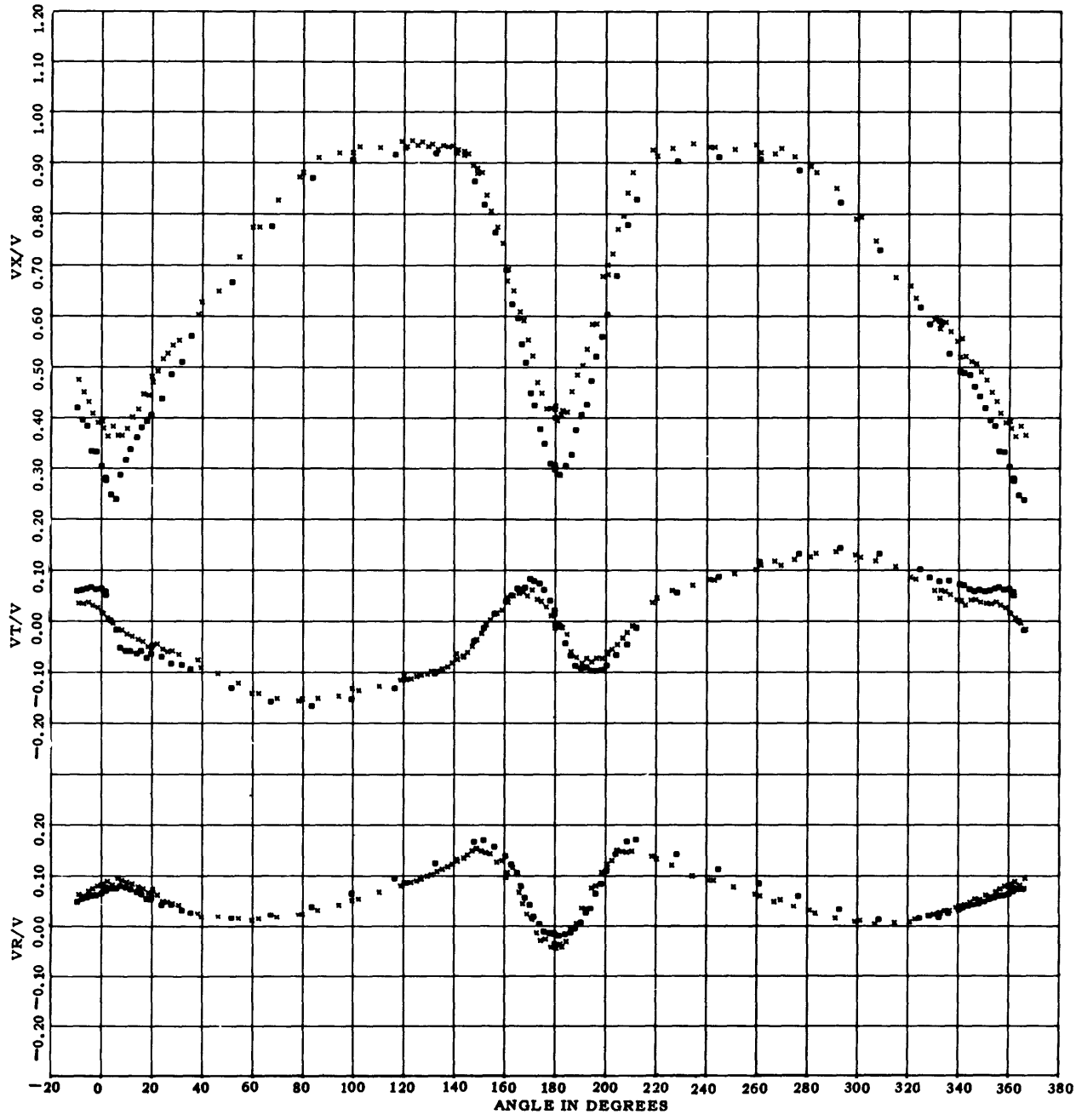

Figure 20 – Circumferential Distribution of Longitudinal, Tangential, and Radial Velocity Component Ratios at a Radius Ratio of 0.474 for Two Propeller Positions: Composite of Tests 35 and 38

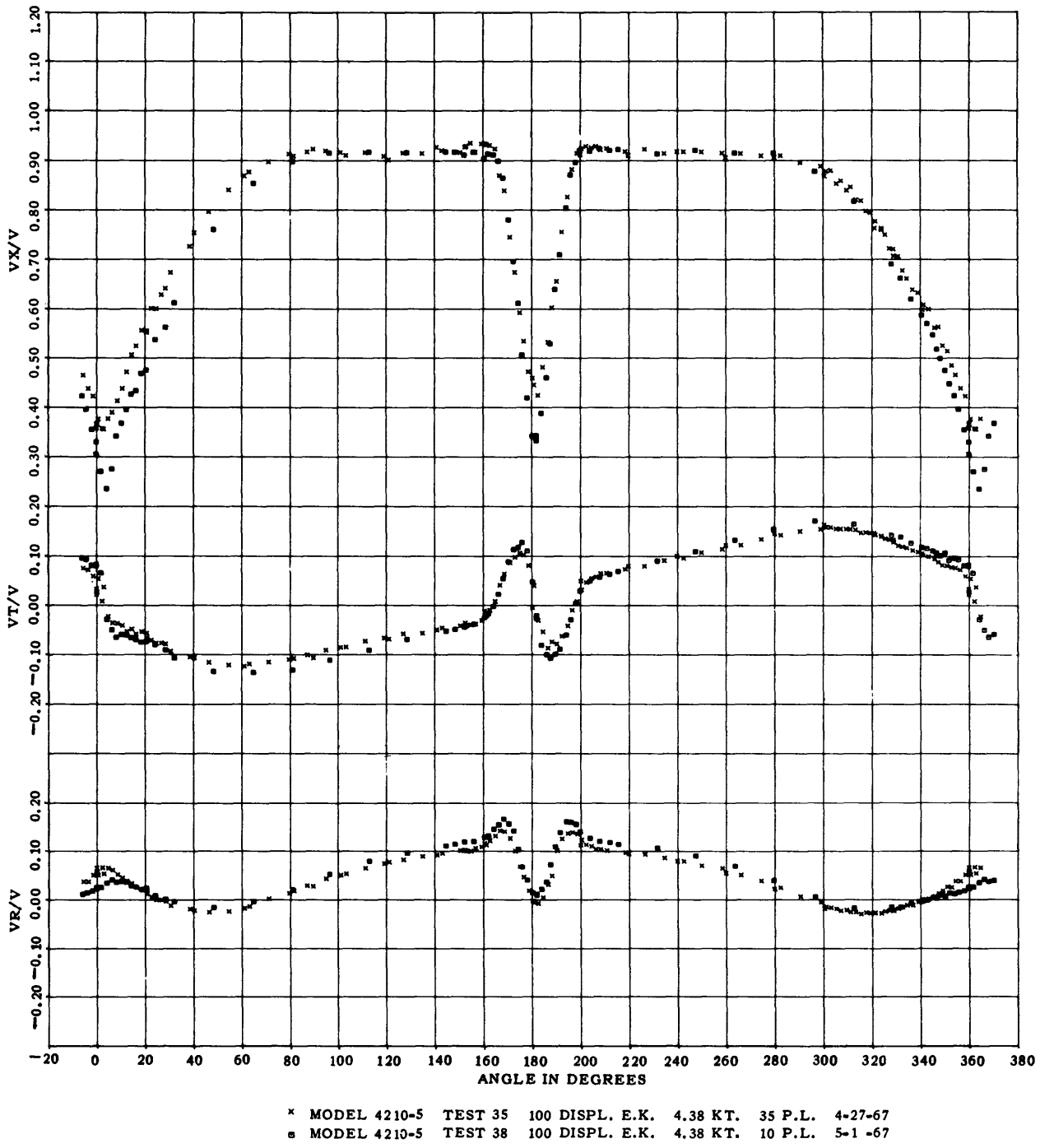

Figure 21 – Circumferential Distribution of Longitudinal, Tangential, and Radial Velocity Component Ratios at a Radius Ratio of 0.659 for Two Propeller Positions: Composite of Tests 35 and 38

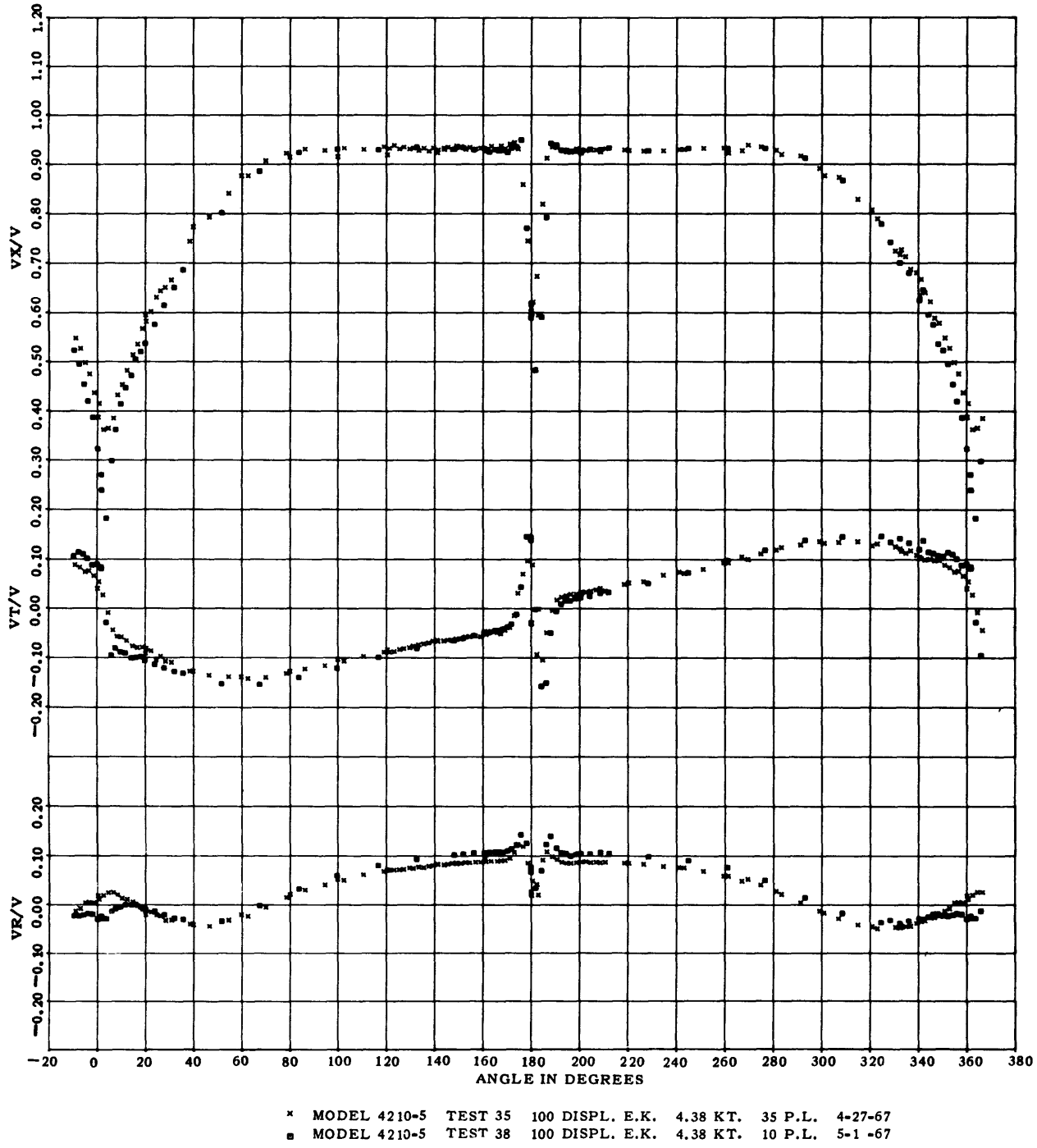

Figure 22 – Circumferential Distribution of Longitudinal, Tangential, and Radial Velocity Component Ratios at a Radius Ratio of 0.844 for Two Propeller Positions: Composite of Tests 35 and 38

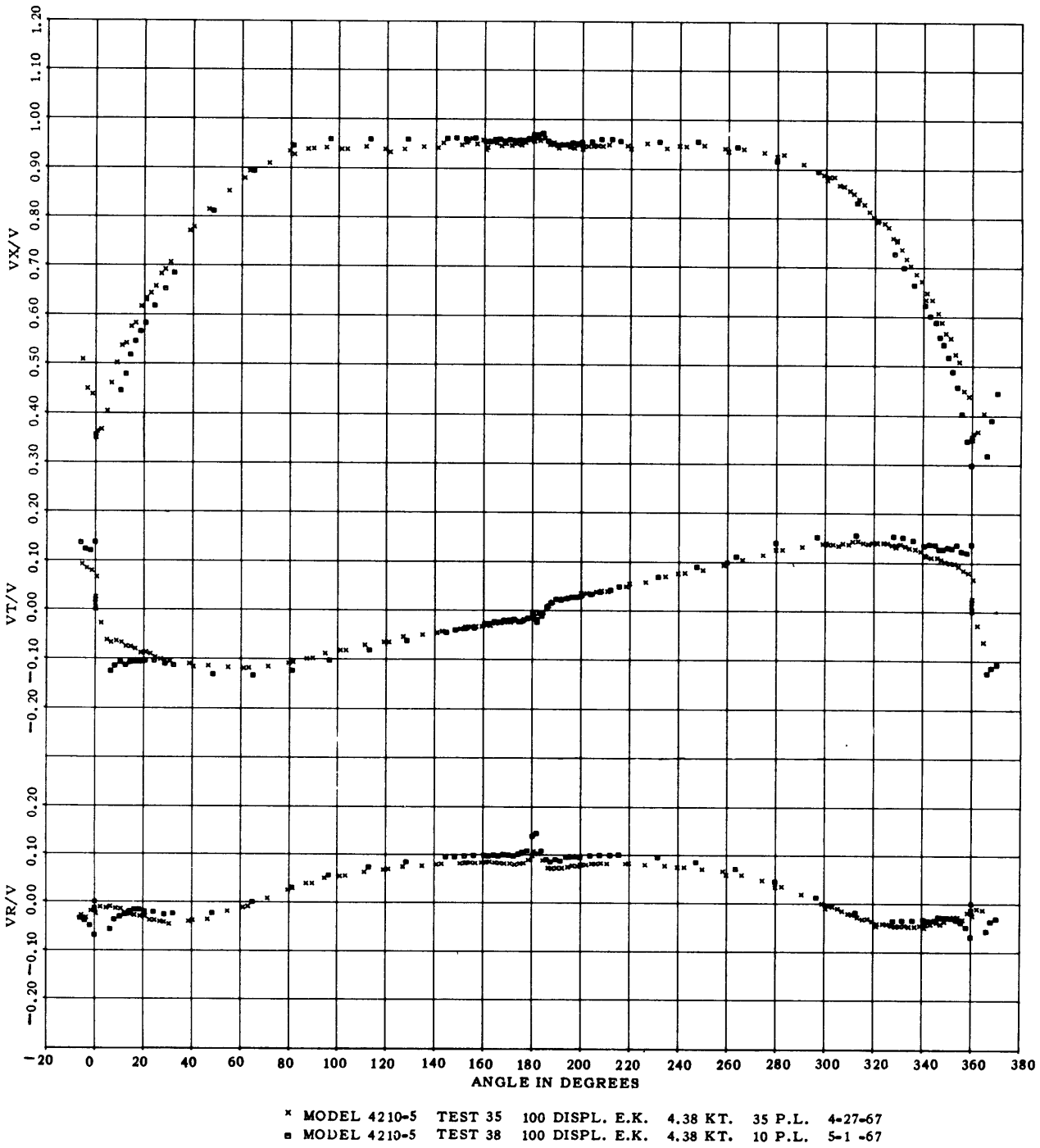

Figure 23 – Circumferential Distribution of Longitudinal, Tangential, and Radial Velocity Component Ratios at a Radius Ratio of 1.003 for Two Propeller Positions: Composite of Tests 35 and 38

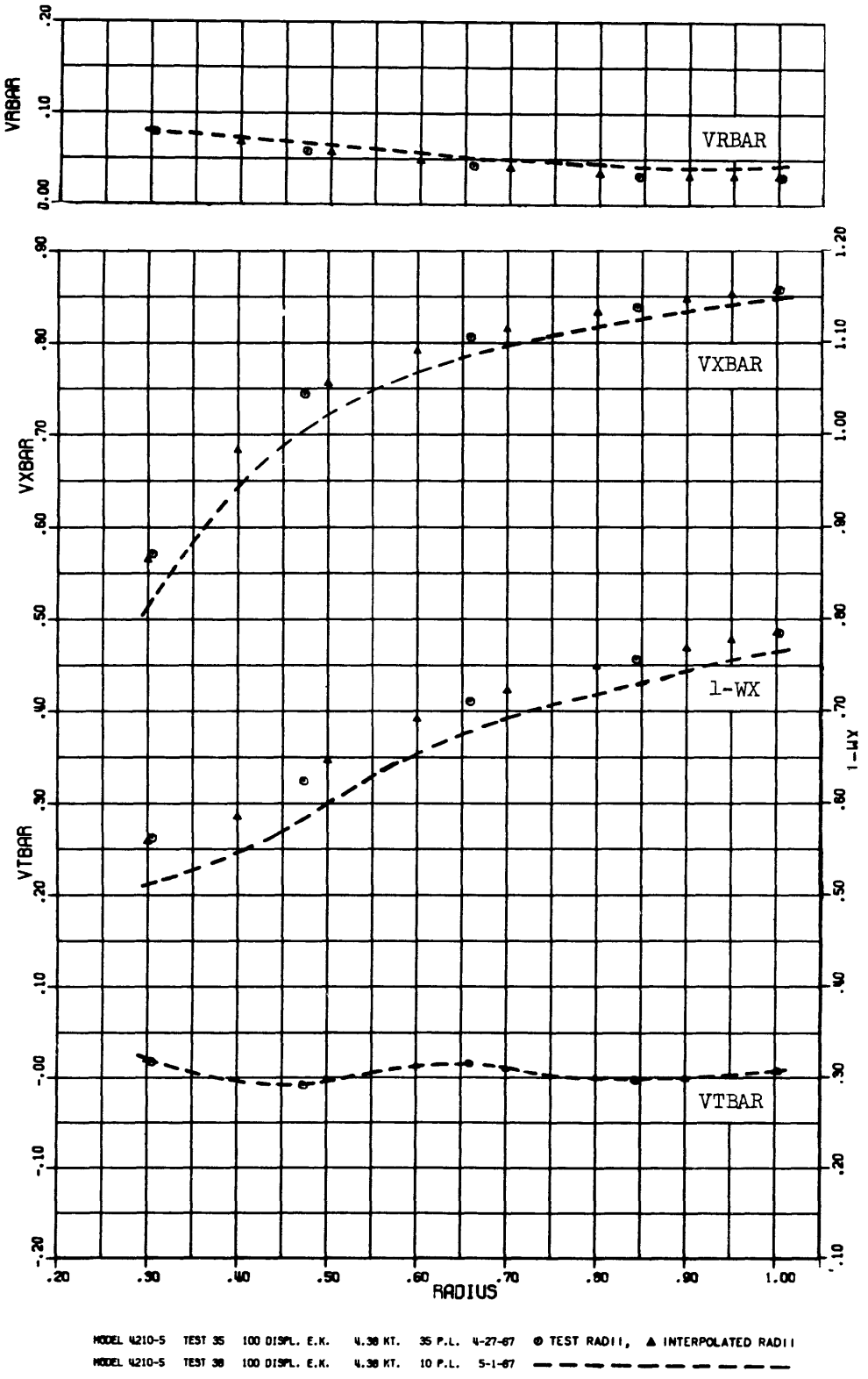

Figure 24 – Radial Distribution of the Volumetric Mean Wake Velocity Component Ratio and of the Mean Longitudinal, Tangential, and Radial Velocity Component Ratios for Two Propeller Positions: Composite of Tests 35 and 38

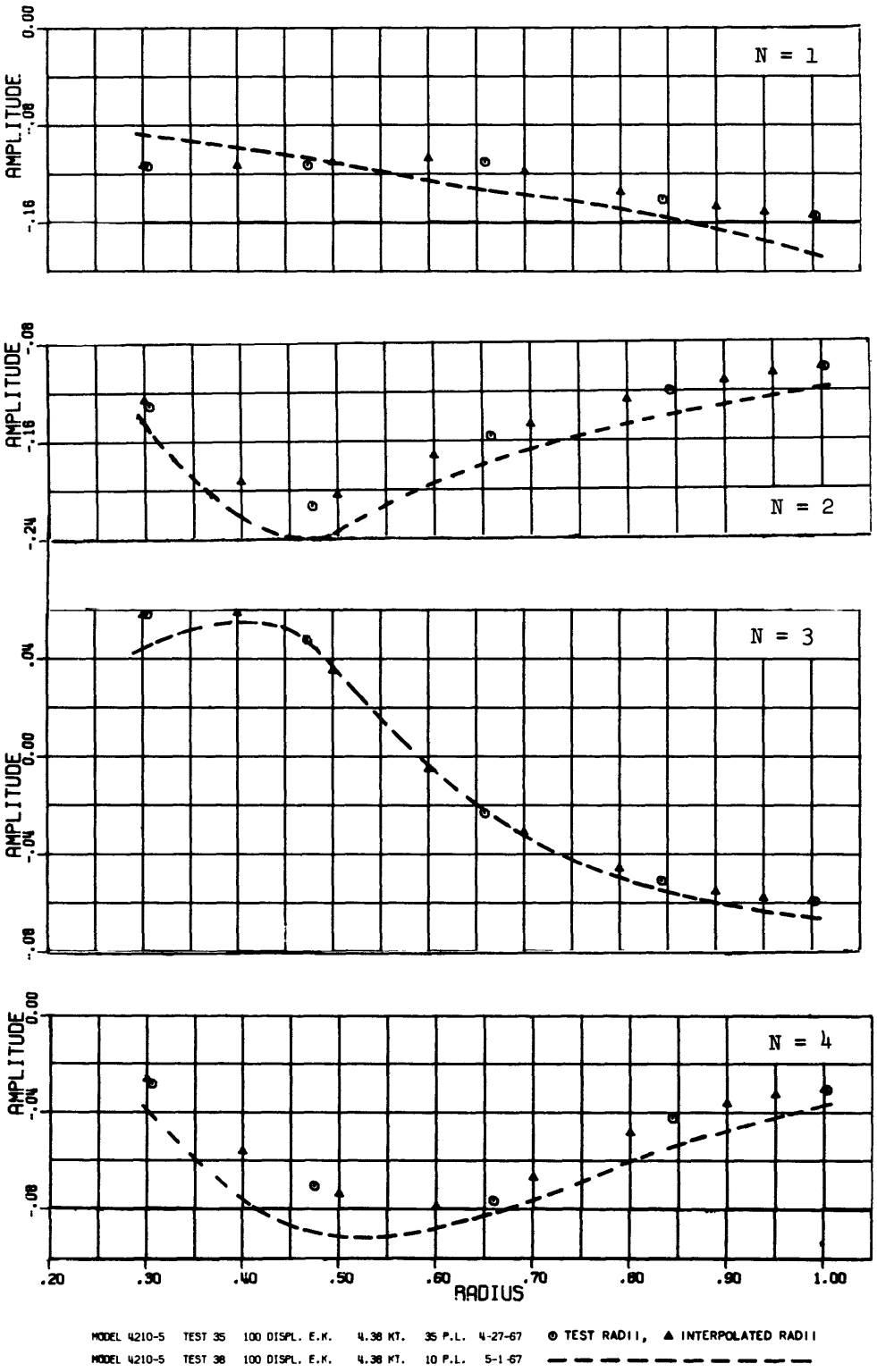

Figure 25 – Radial Distribution of the Amplitudes of the First through the Fourth Harmonic of the Circumferential Distribution of the Longitudinal Velocity Component Ratios for Two Propeller Positions: Composite of Tests 35 and 38

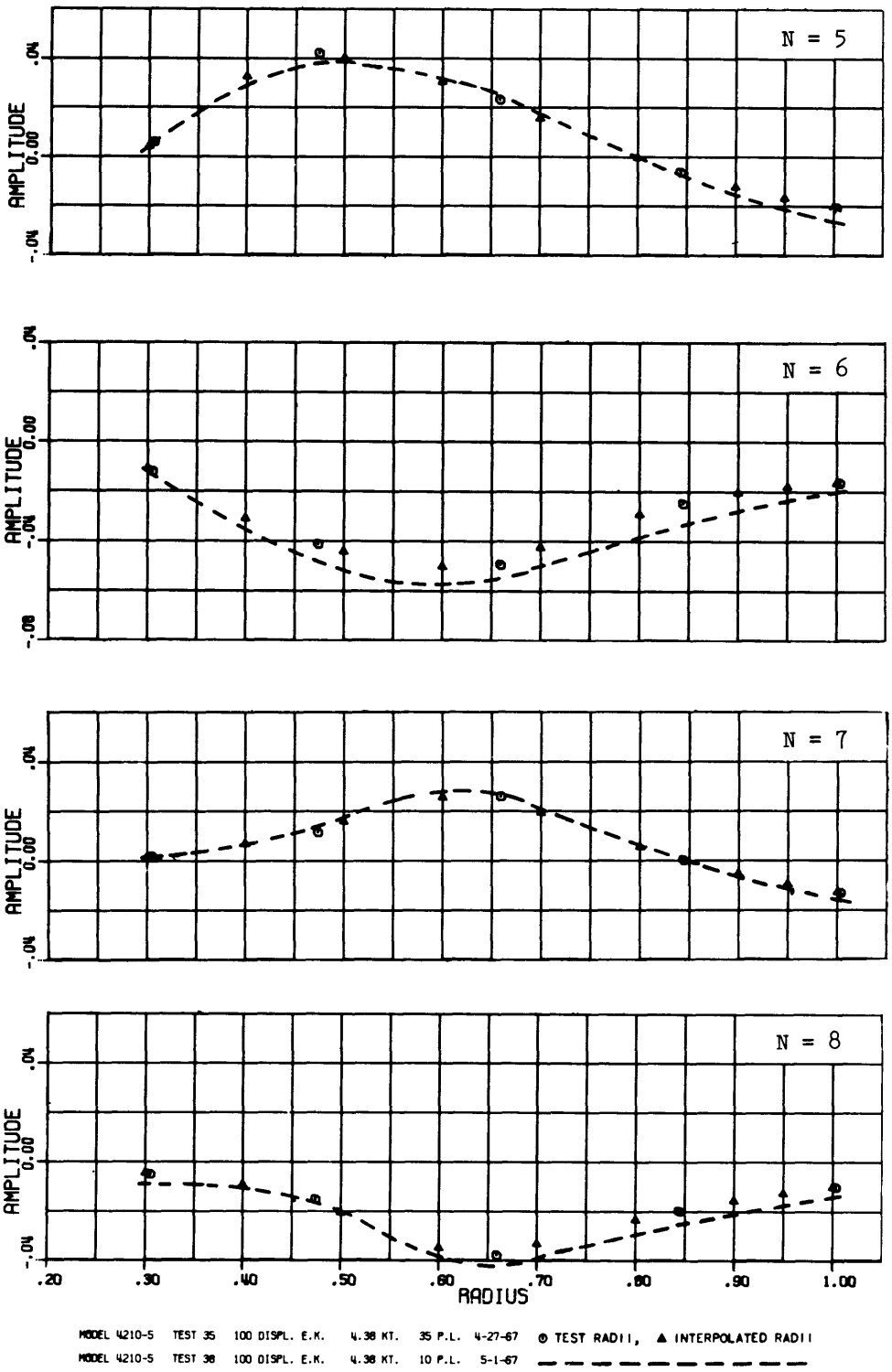

Figure 26 – Radial Distribution of the Amplitudes of the Fifth through the Eighth Harmonic of the Circumferential Distribution of the Longitudinal Velocity Component Ratios for Two Propeller Positions: Composite of Tests 35 and 38

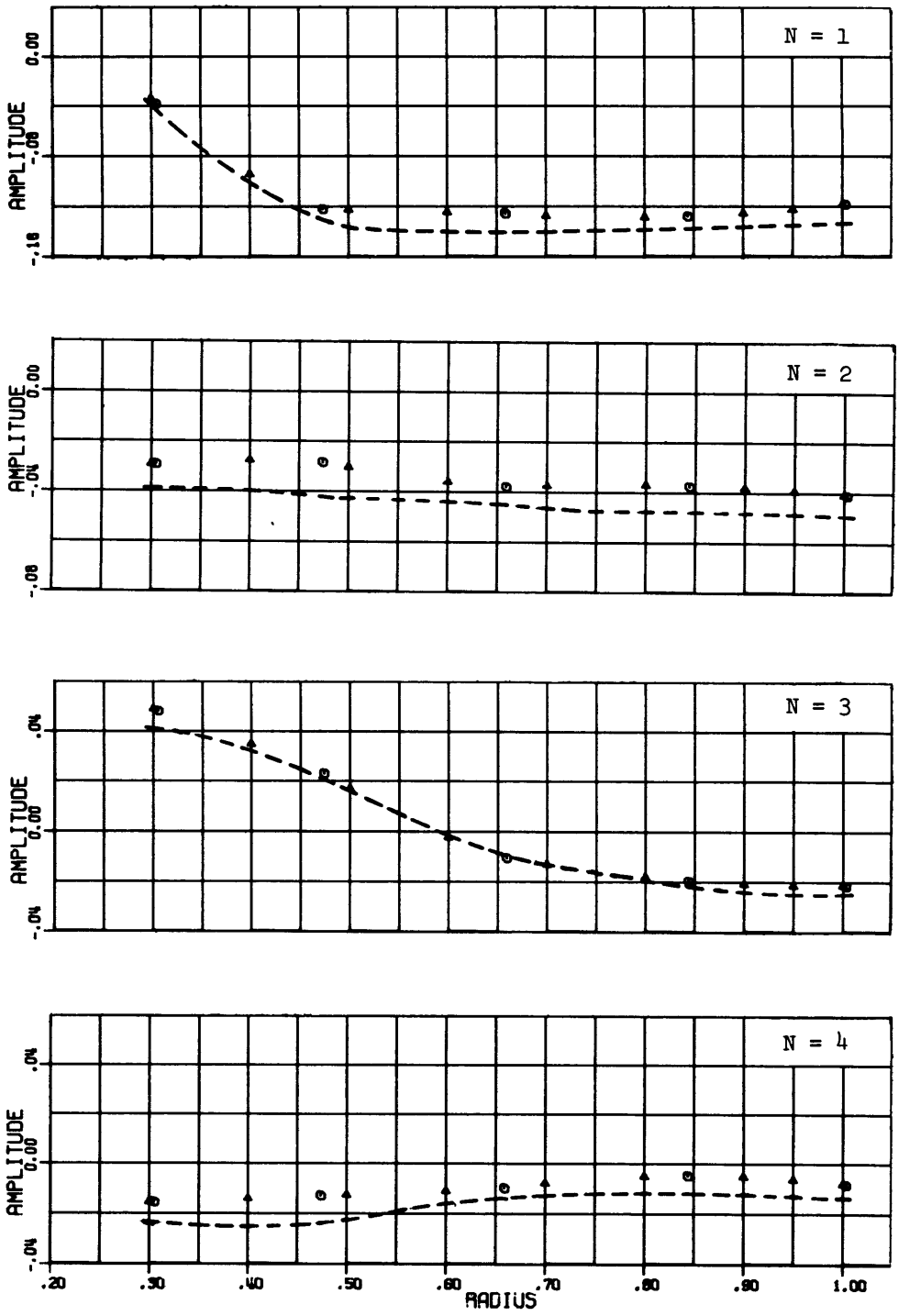

Figure 27 – Radial Distribution of the Amplitudes of the First through the Fourth Harmonic of the Circumferential Distribution of the Tangential Velocity Component Ratios for Two Propeller Positions: Composite of Tests 35 and 38

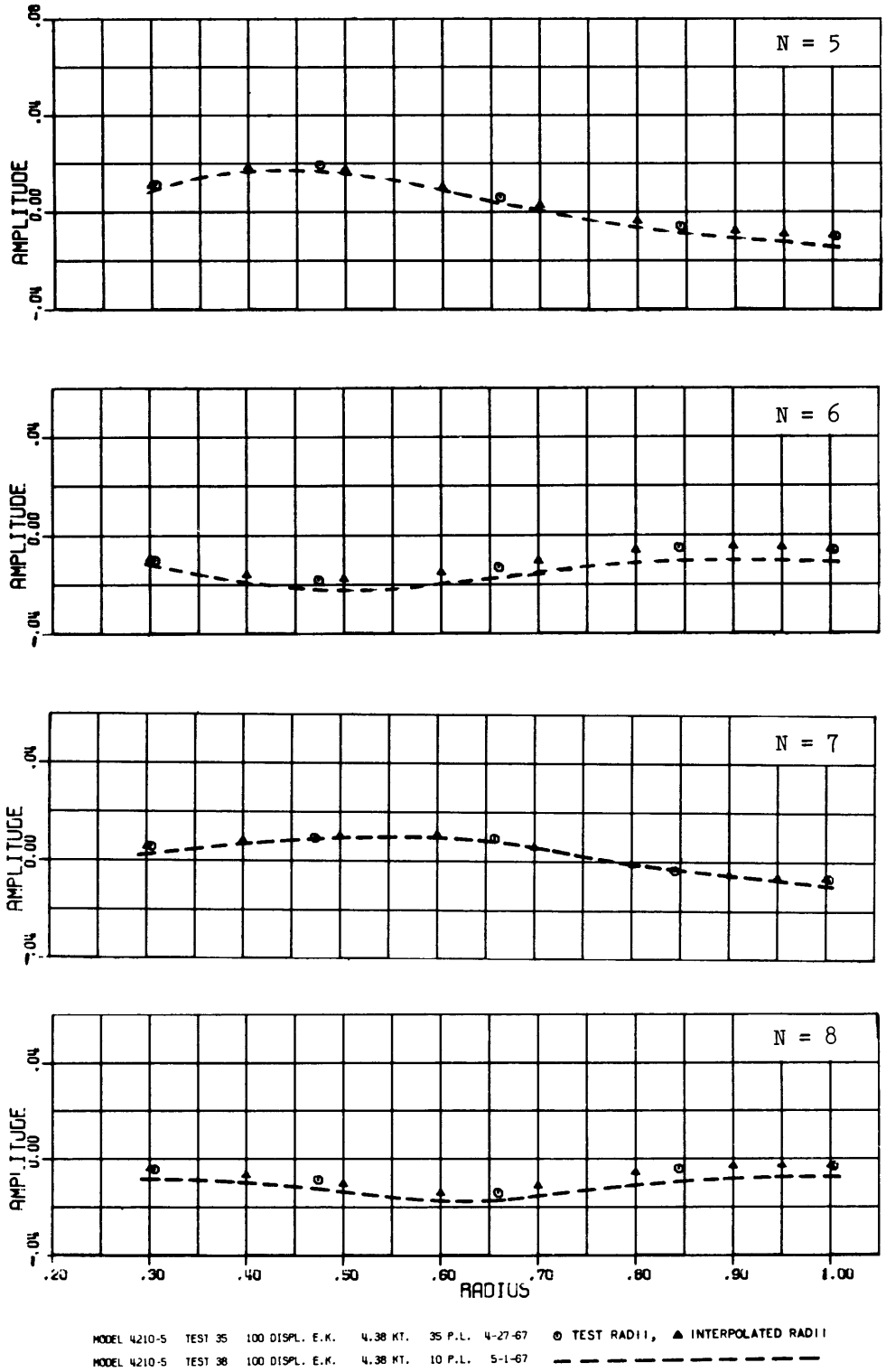

Figure 28 – Radial Distribution of the Amplitudes of the Fifth through the Eighth Harmonic of the Circumferential Distribution of the Tangential Velocity Component Ratios for Two Propeller Positions: Composite of Tests 35 and 38

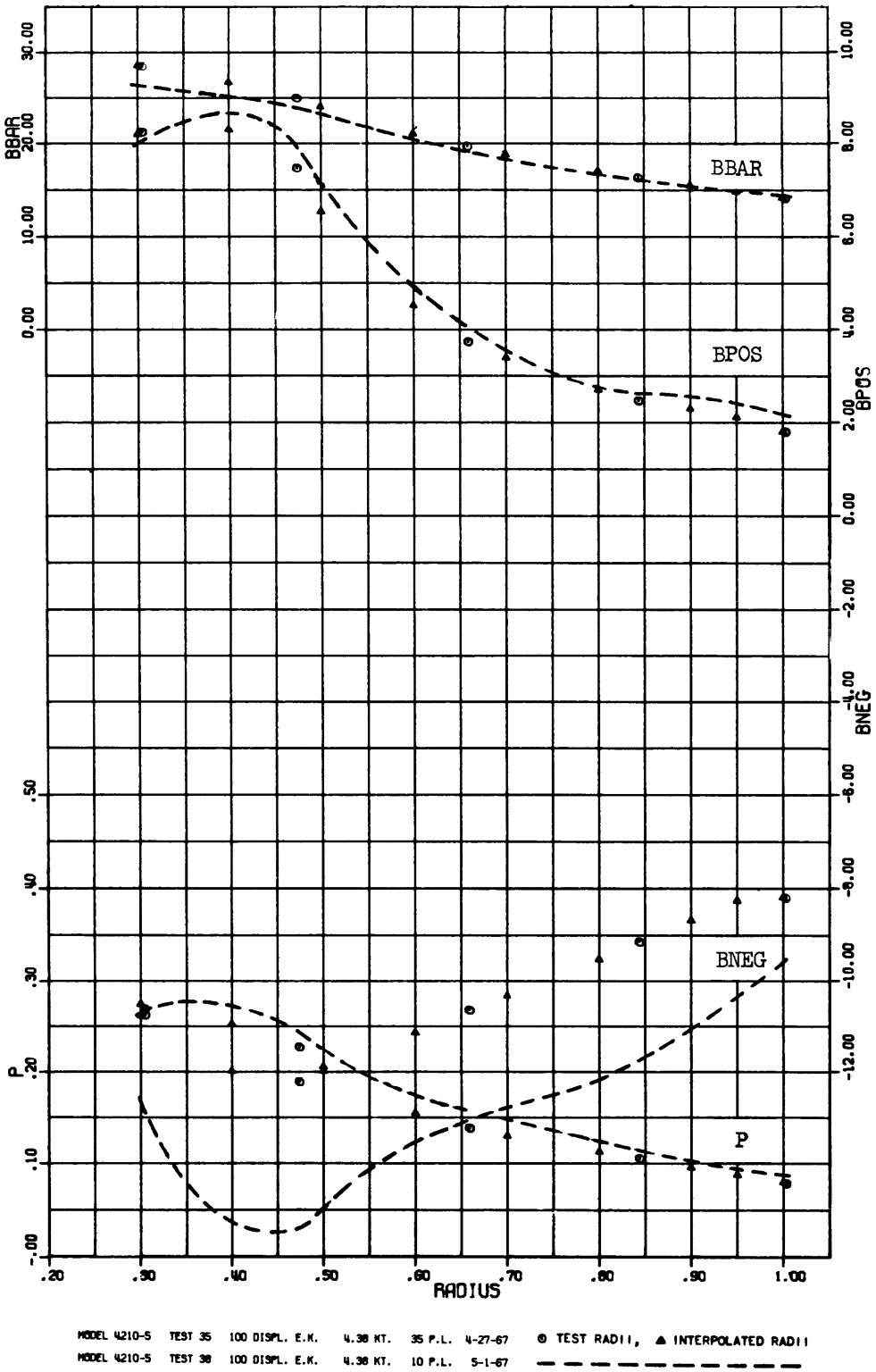

Figure 29 – Radial Distribution of the Mean Advance Angle, the Maximum Variations of the Advance Angle, and the Pressure Factor for Two Propeller Positions: Composite of Tests 35 and 38

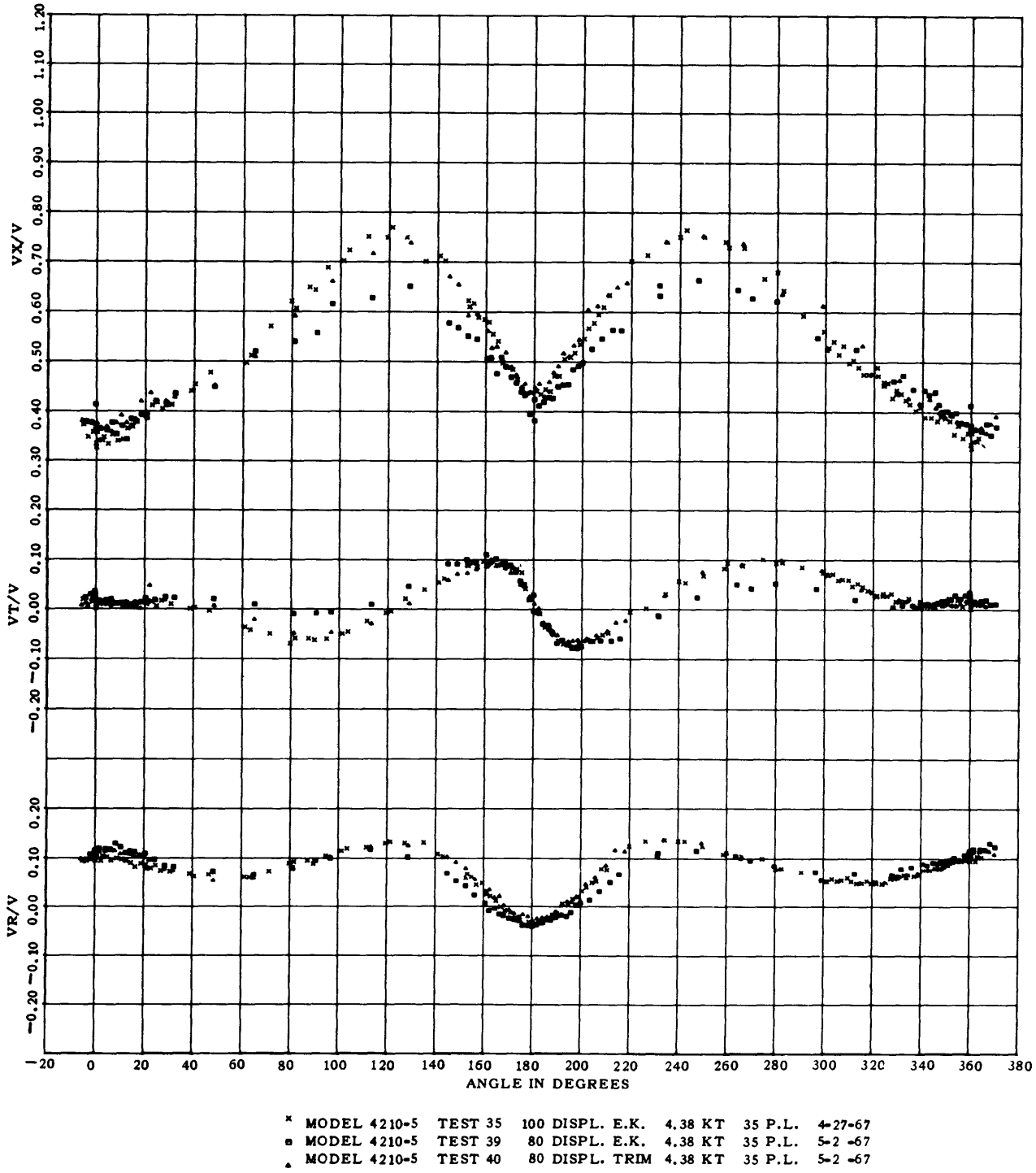

Figure 30 – Circumferential Distribution of Longitudinal, Tangential, and Radial Velocity Component Ratios at a Radius Ratio of 0.305 for Two Displacements and a Trimmed Condition: Composite of Tests 35, 39, and 40

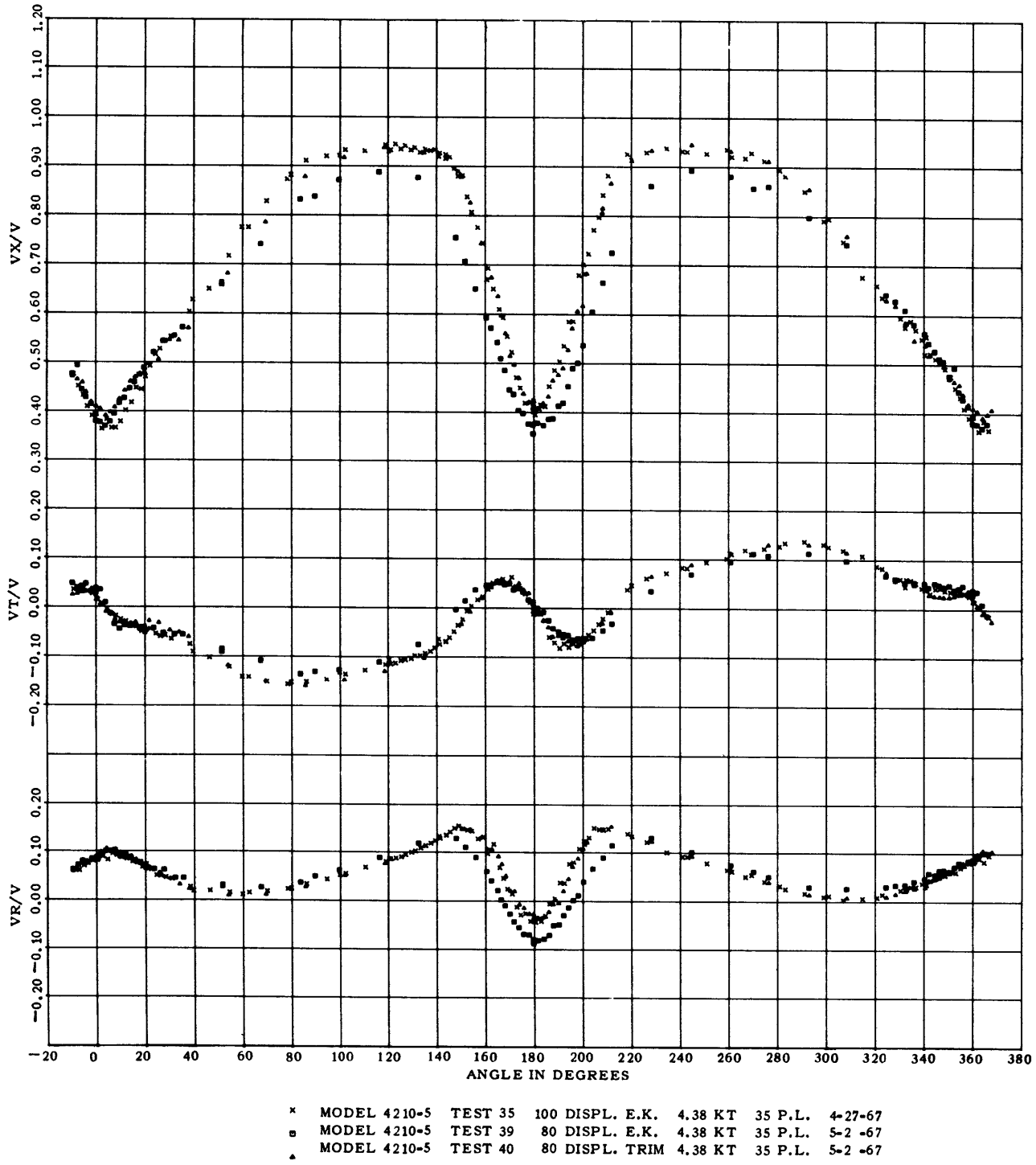

Figure 31 – Circumferential Distribution of Longitudinal, Tangential, and Radial Velocity Component Ratios at a Radius Ratio of 0.474 for Two Displacements and a Trimmed Condition: Composite of Tests 35, 39, and 40

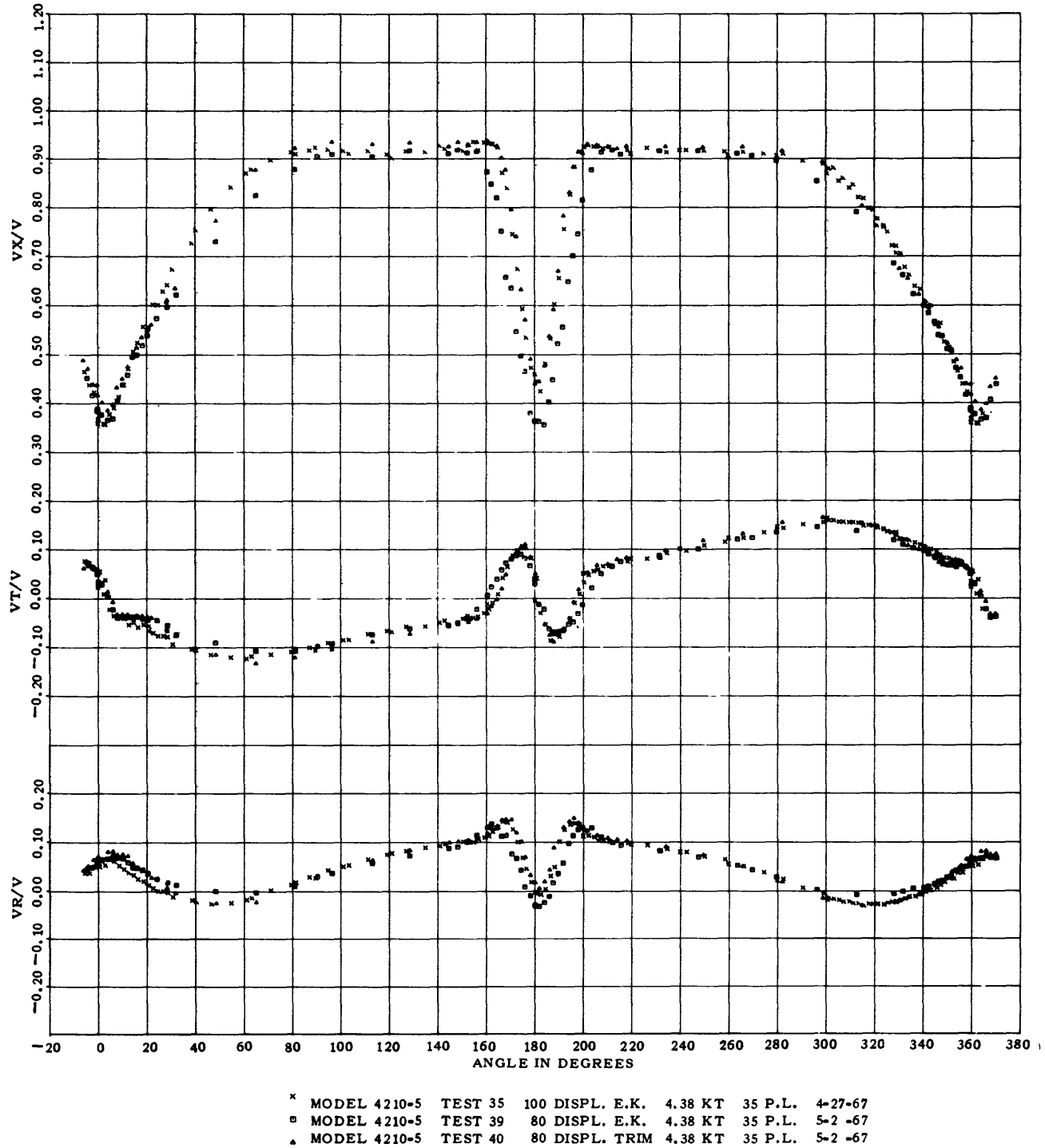

Figure 32 – Circumferential Distribution of Longitudinal, Tangential, and Radial Velocity Component Ratios at a Radius Ratio of 0.659 for Two Displacements and a Trimmed Condition: Composite of Tests 35, 39, and 40

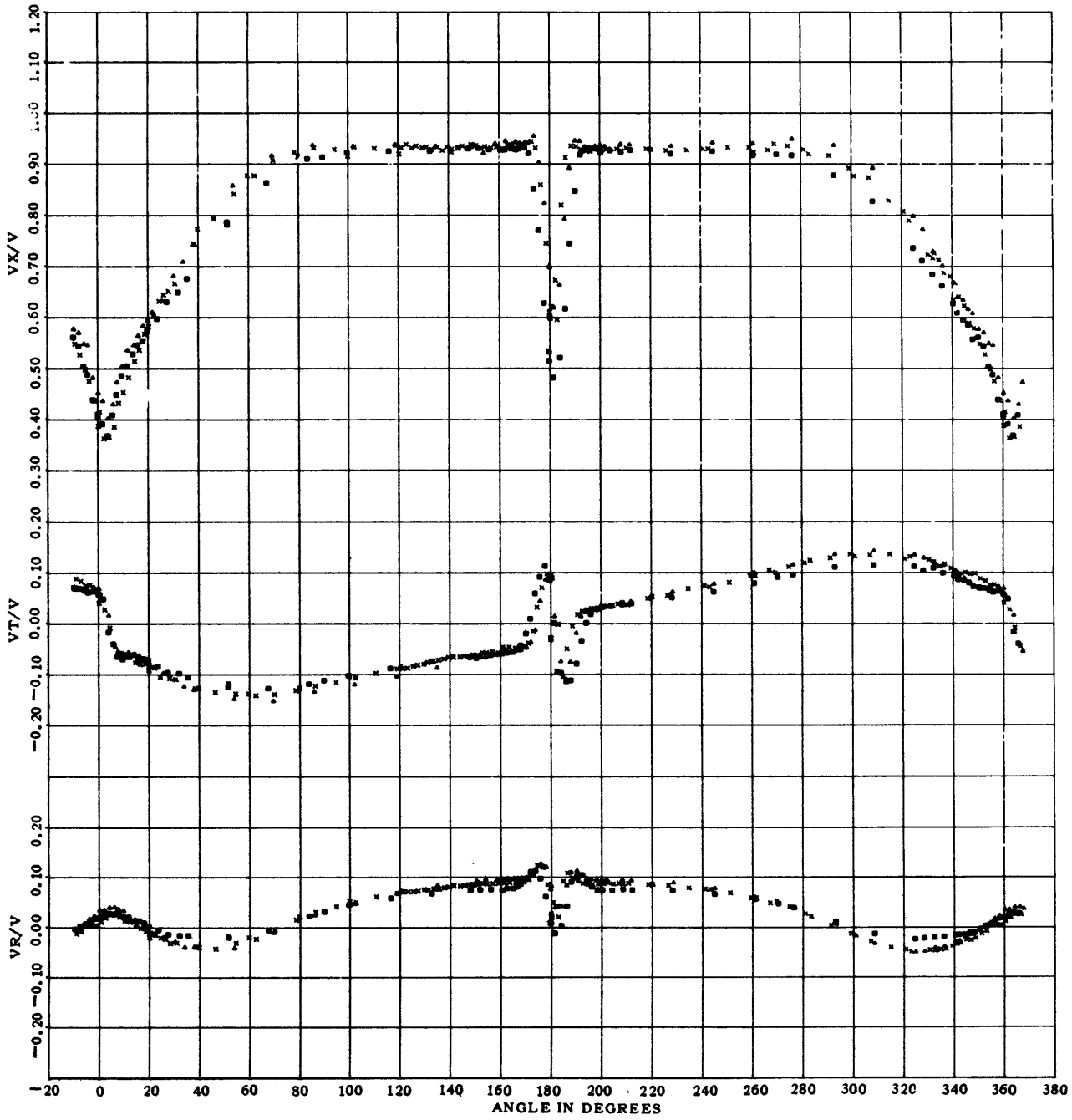

Figure 33 – Circumferential Distribution of Longitudinal, Tangential, and Radial Velocity Component Ratios at a Radius Ratio of 0.844 for Two Displacements and a Trimmed Condition: Composite of Tests 35, 39, and 40

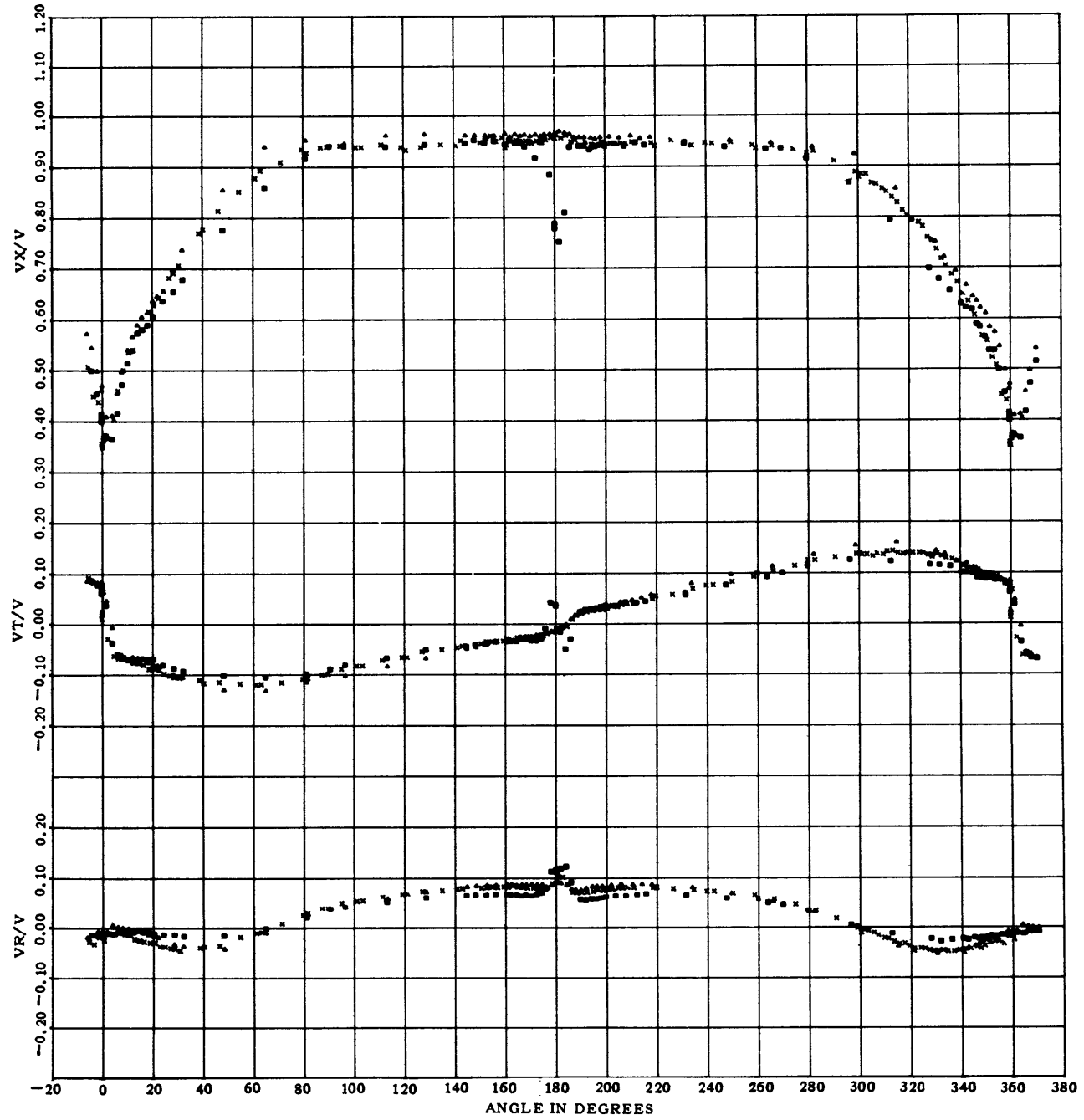

Figure 34 – Circumferential Distribution of Longitudinal, Tangential, and Radial Velocity Component Ratios at a Radius Ratio of 1.003 for Two Displacements and a Trimmed Condition: Composite of Tests 35, 39, and 40

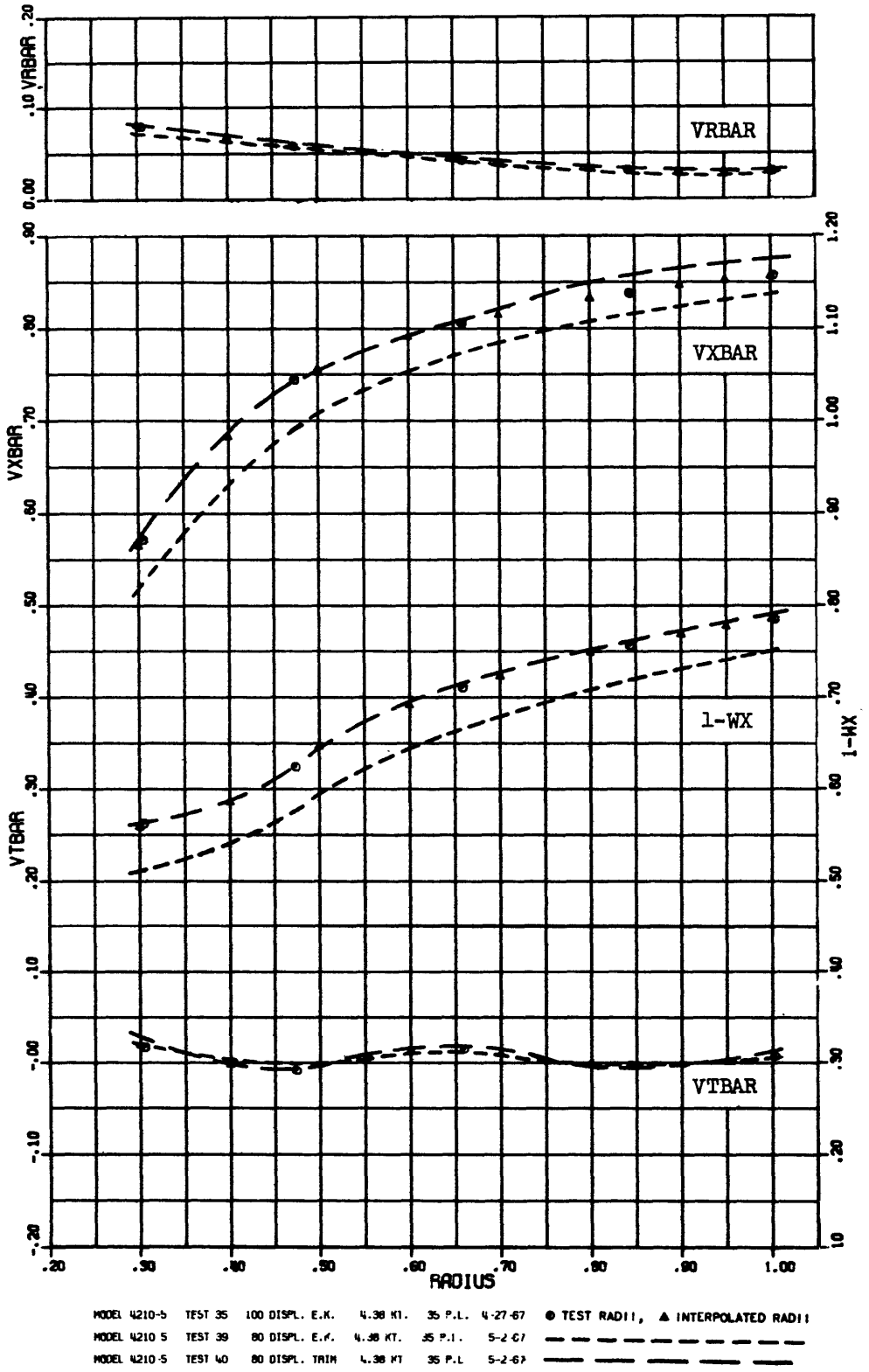

Figure 35 – Radial Distribution of the Volumetric Mean Wake Velocity Component Ratio and of the Mean Longitudinal, Tangential, and Radial Velocity Component Ratios for Two Displacements and a Trimmed Condition: Composite of Tests 35, 39, and 40

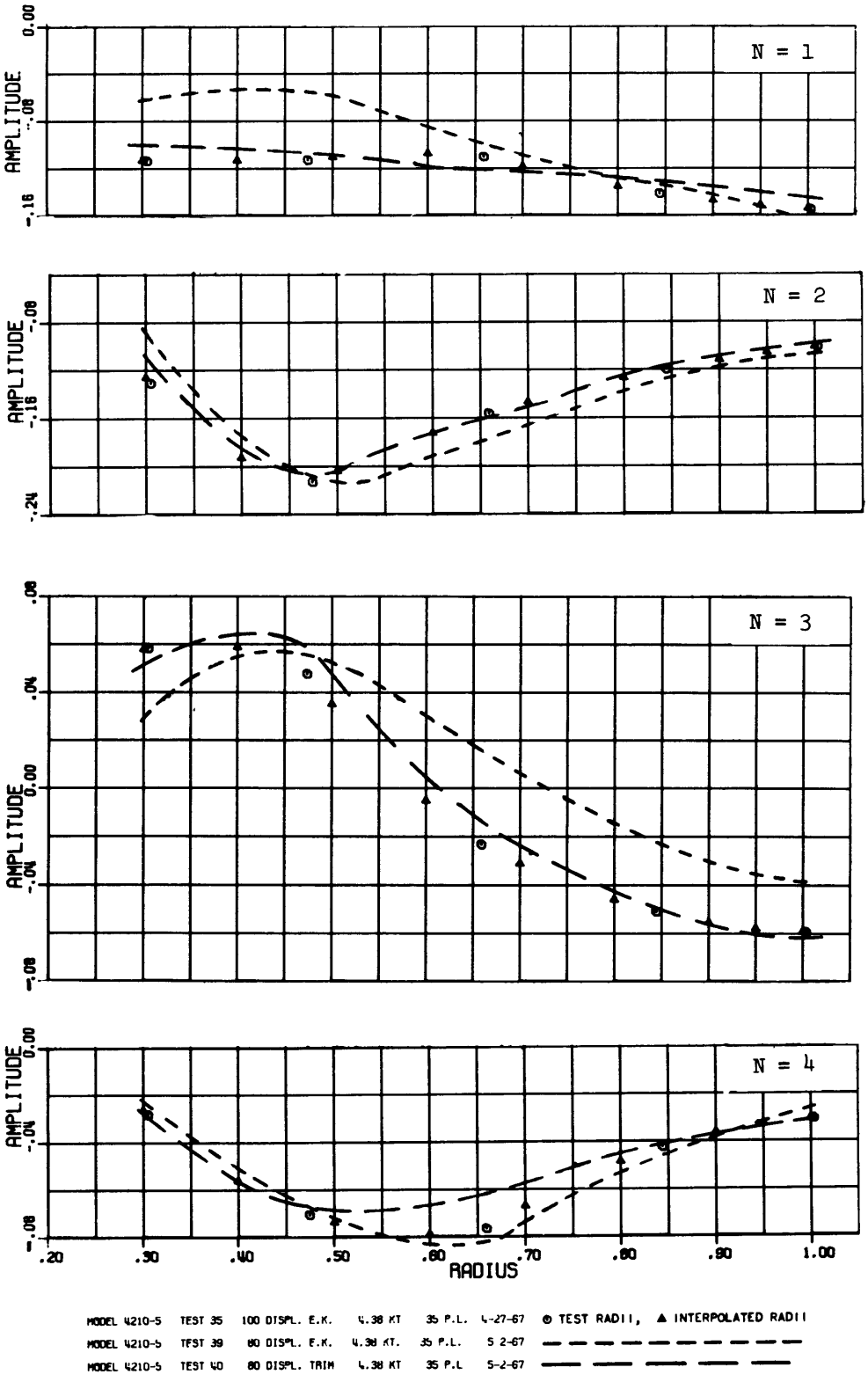

Figure 36 – Radial Distribution of the Amplitudes of the First through the Fourth Harmonic of the Circumferential Distribution of the Longitudinal Velocity Component Ratios for Two Displacements and a Trimmed Condition: Composite of Tests 35, 39, and 40

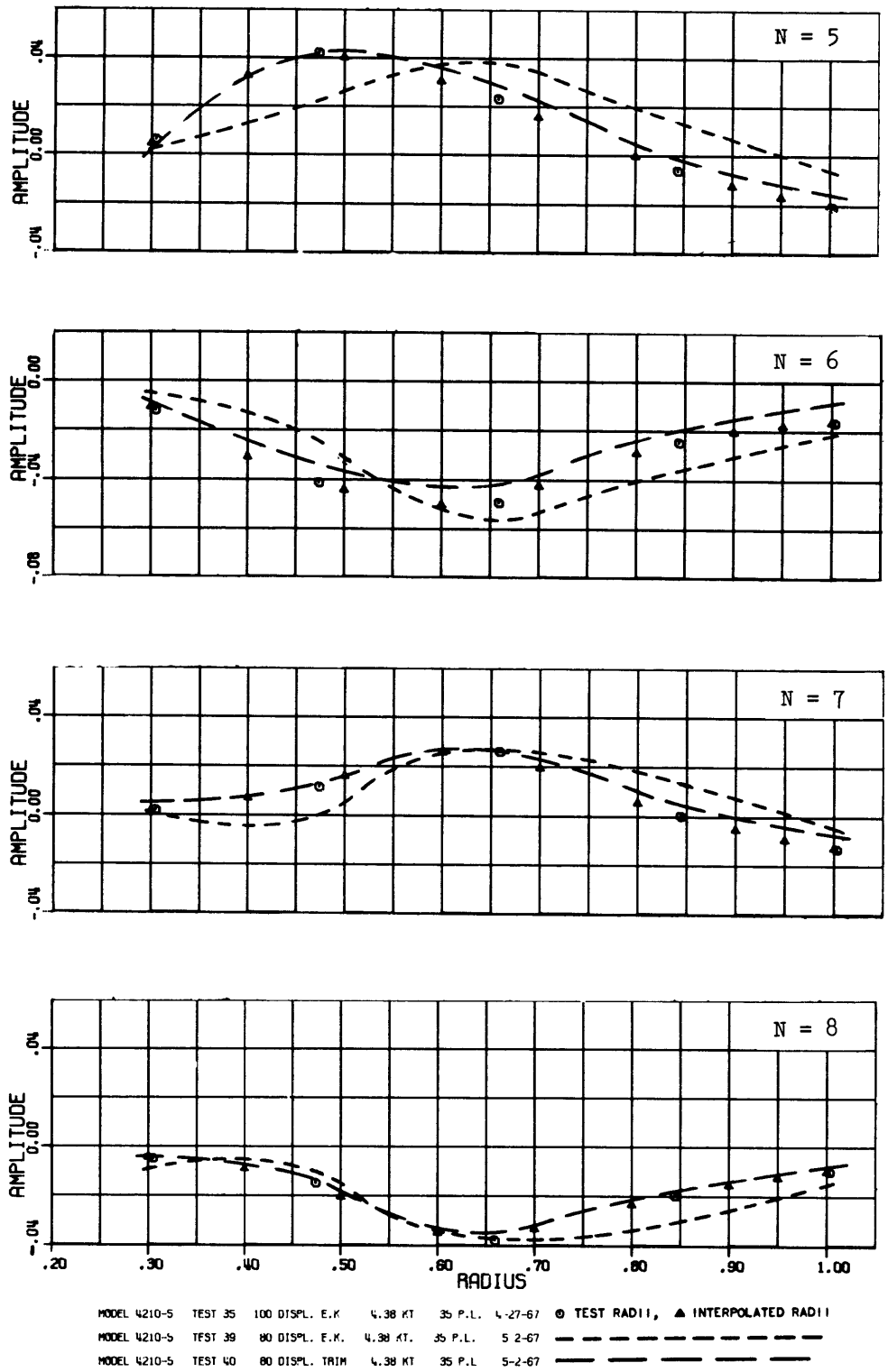

Figure 37 – Radial Distribution of the Amplitudes of the Fifth through the Eighth Harmonic of the Circumferential Distribution of the Longitudinal Velocity Component Ratios for Two Displacements and a Trimmed Condition: Composite of Tests 35, 39, and 40

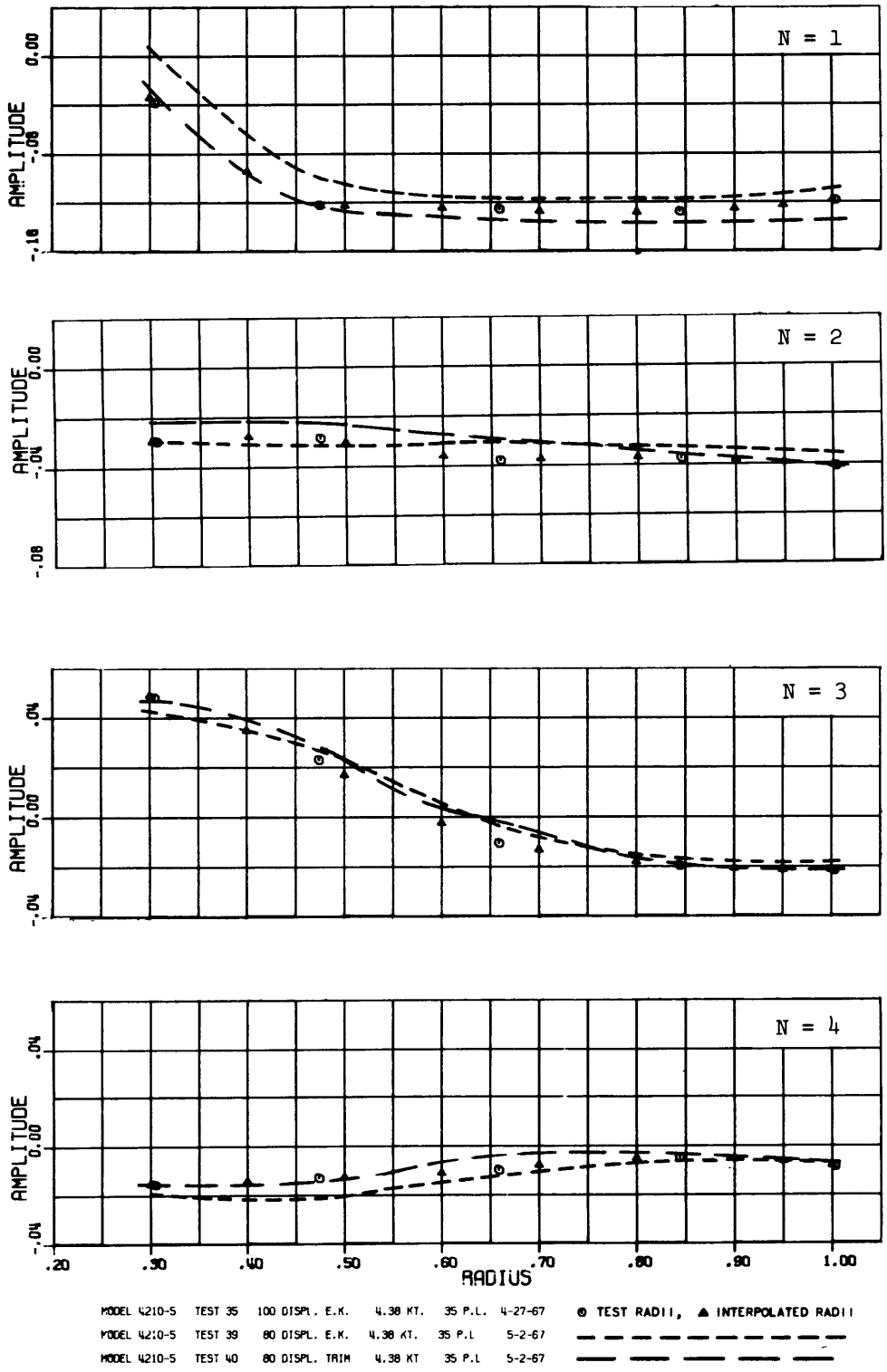

Figure 38 – Radial Distribution of the Amplitudes of the First through the Fourth Harmonic of the Circumferential Distribution of the Tangential Velocity Component Ratios for Two Displacements and a Trimmed Condition: Composite of Tests 35, 39, and 40

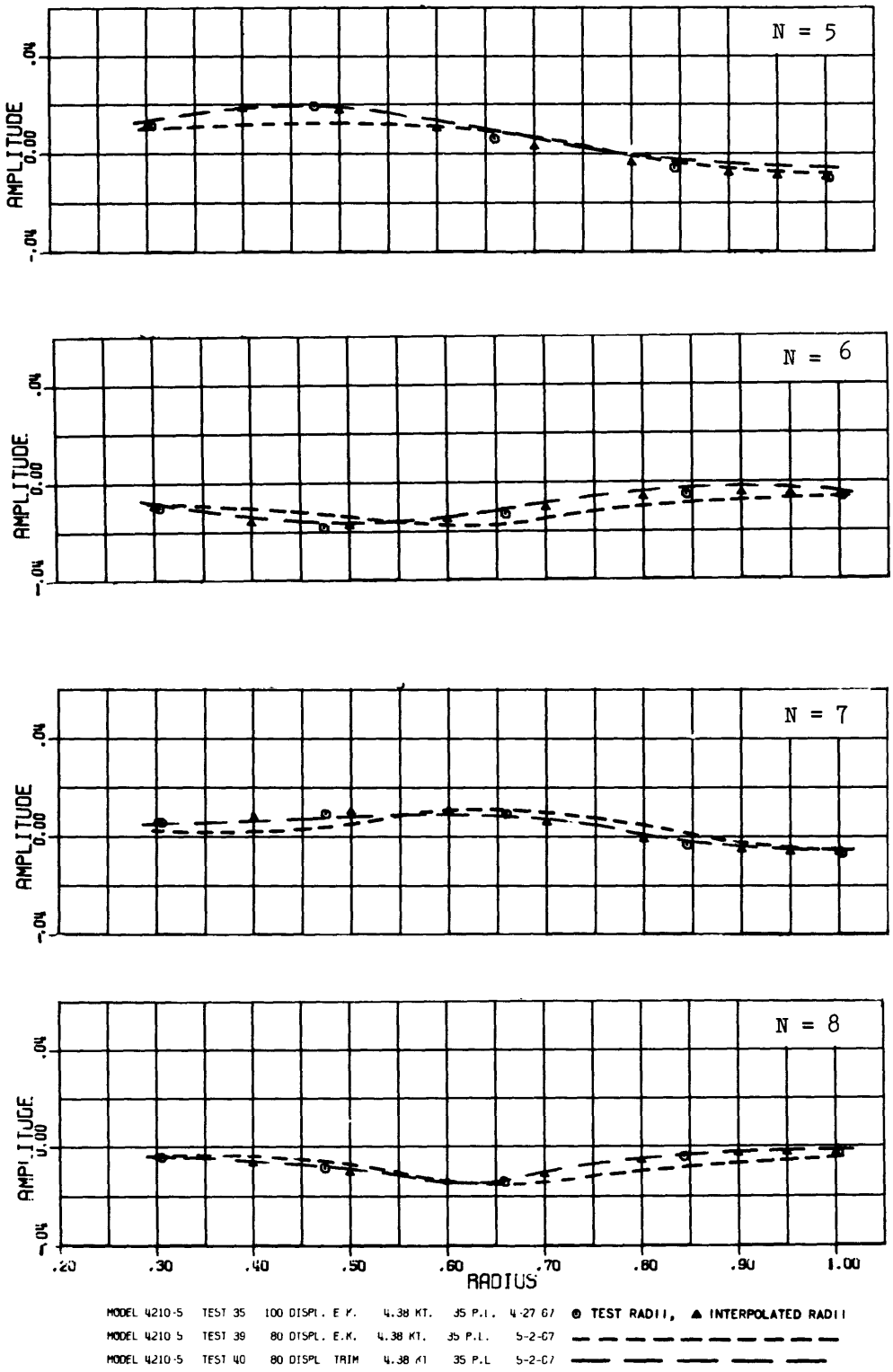

Figure 39 – Radial Distribution of the Amplitudes of the Fifth through the Eighth Harmonic of the Circumferential Distribution of the Tangential Velocity Component Ratios for Two Displacements and a Trimmed Condition: Composite of Tests 35, 39, and 40

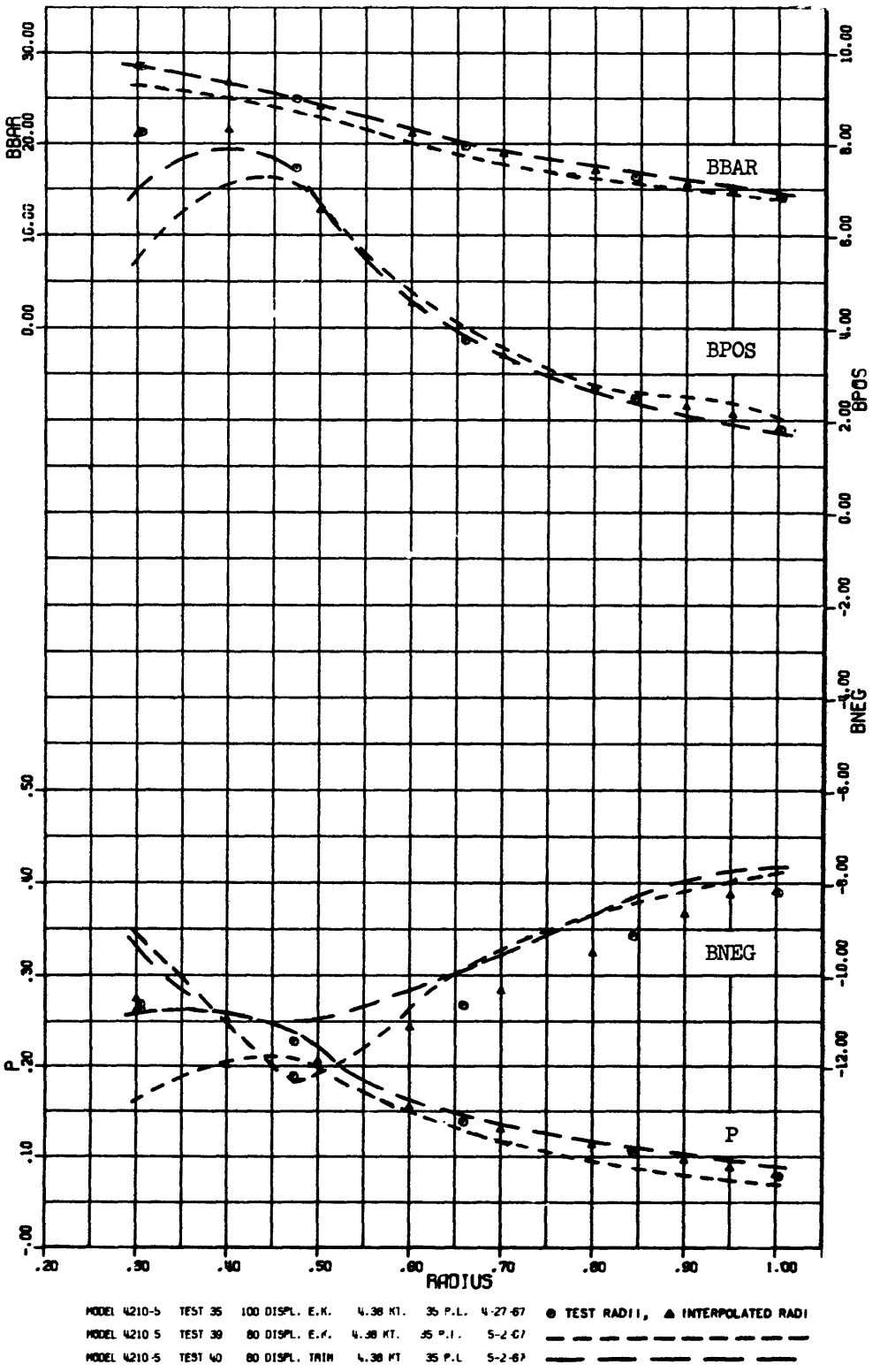

Figure 40 – Radial Distribution of the Mean Advance Angle, the Maximum Variations of the Advance Angle, and the Pressure Factor for Two Displacements and a Trimmed Condition: Composite of Tests 35, 39, and 40

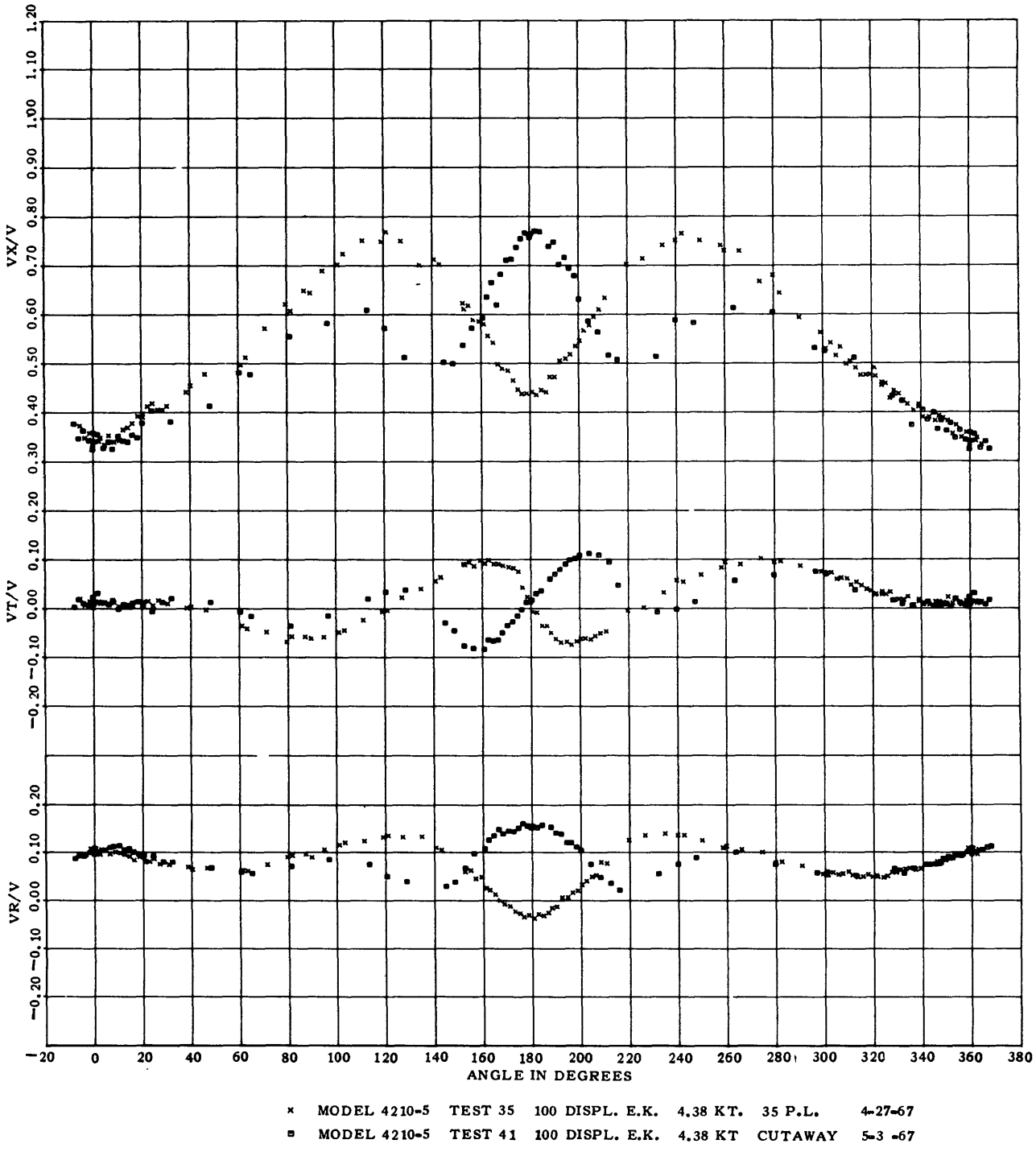

Figure 41 – Circumferential Distribution of Longitudinal, Tangential, and Radial Velocity Component Ratios at a Radius Ratio of 0.305 for Two Deadwood Conditions: Composite of Tests 35 and 41

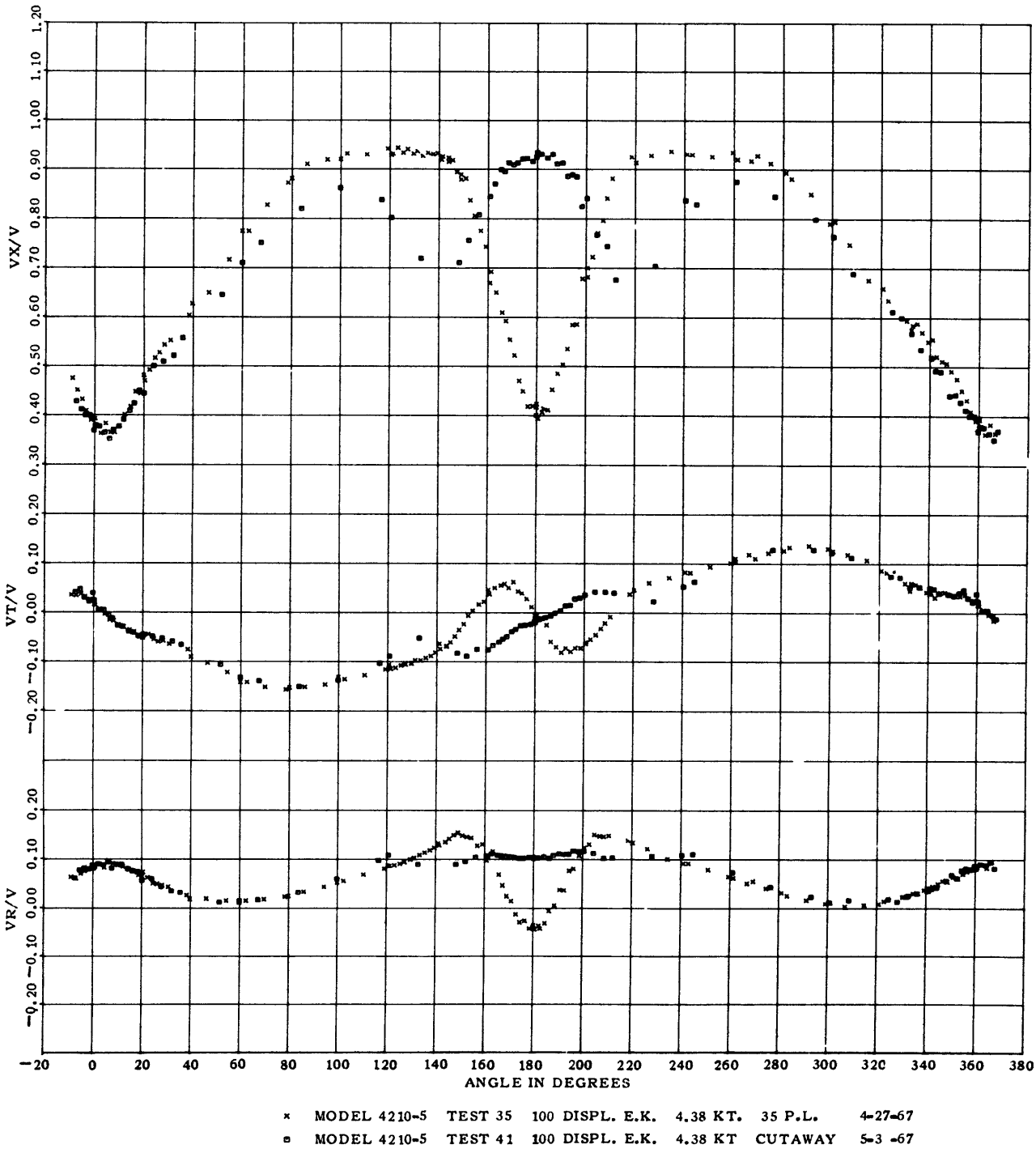

Figure 42 – Circumferential Distribution of Longitudinal, Tangential, and Radial Velocity Component Ratios at a Radius Ratio of 0.474 for Two Deadwood Conditions: Composite of Tests 35 and 41

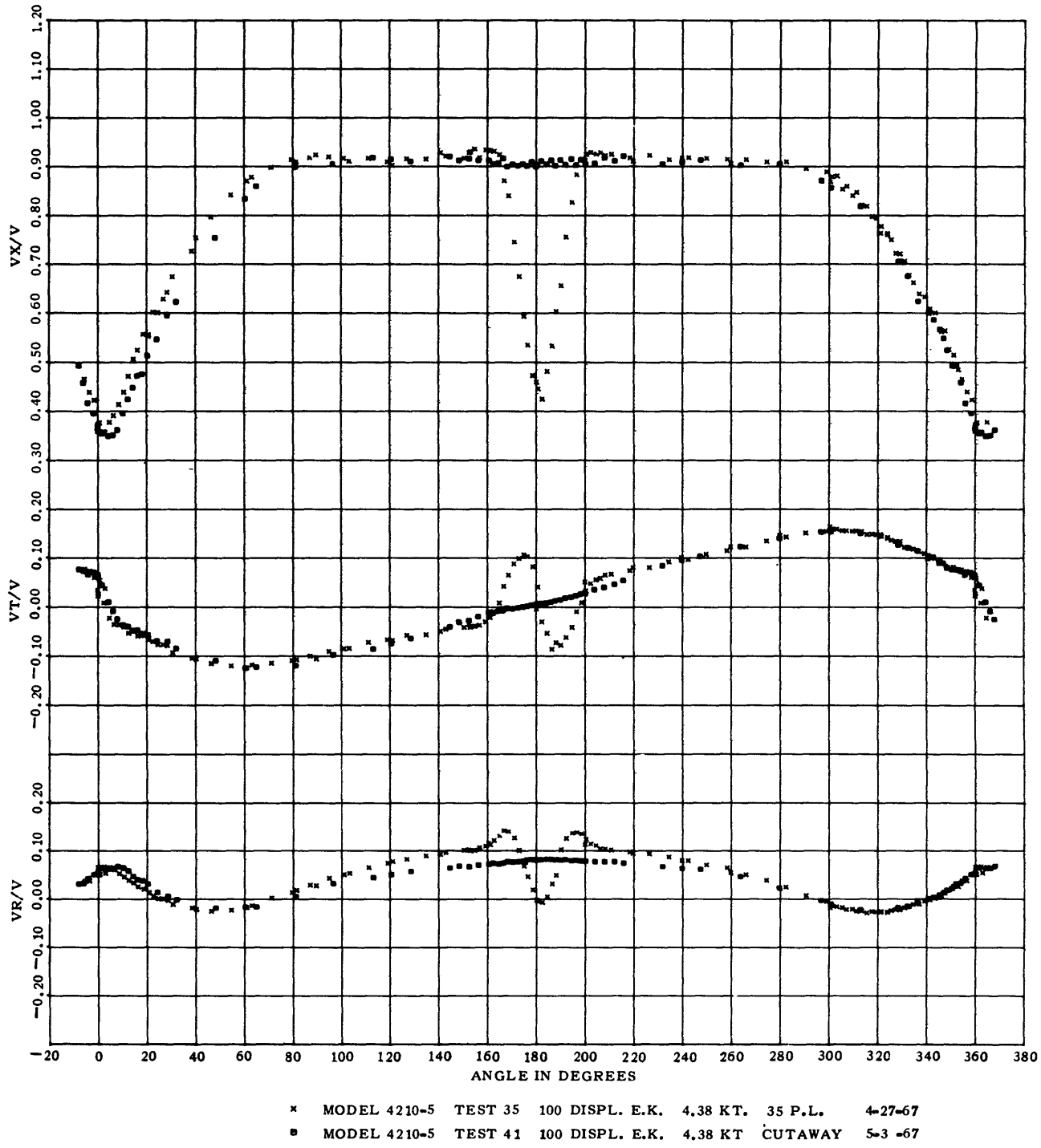

Figure 43 – Circumferential Distribution of Longitudinal, Tangential, and Radial Velocit Component Ratios at a Radius Ratio of 0.659 for Two Deadwood Conditions: Composite of Tests 35 and 41

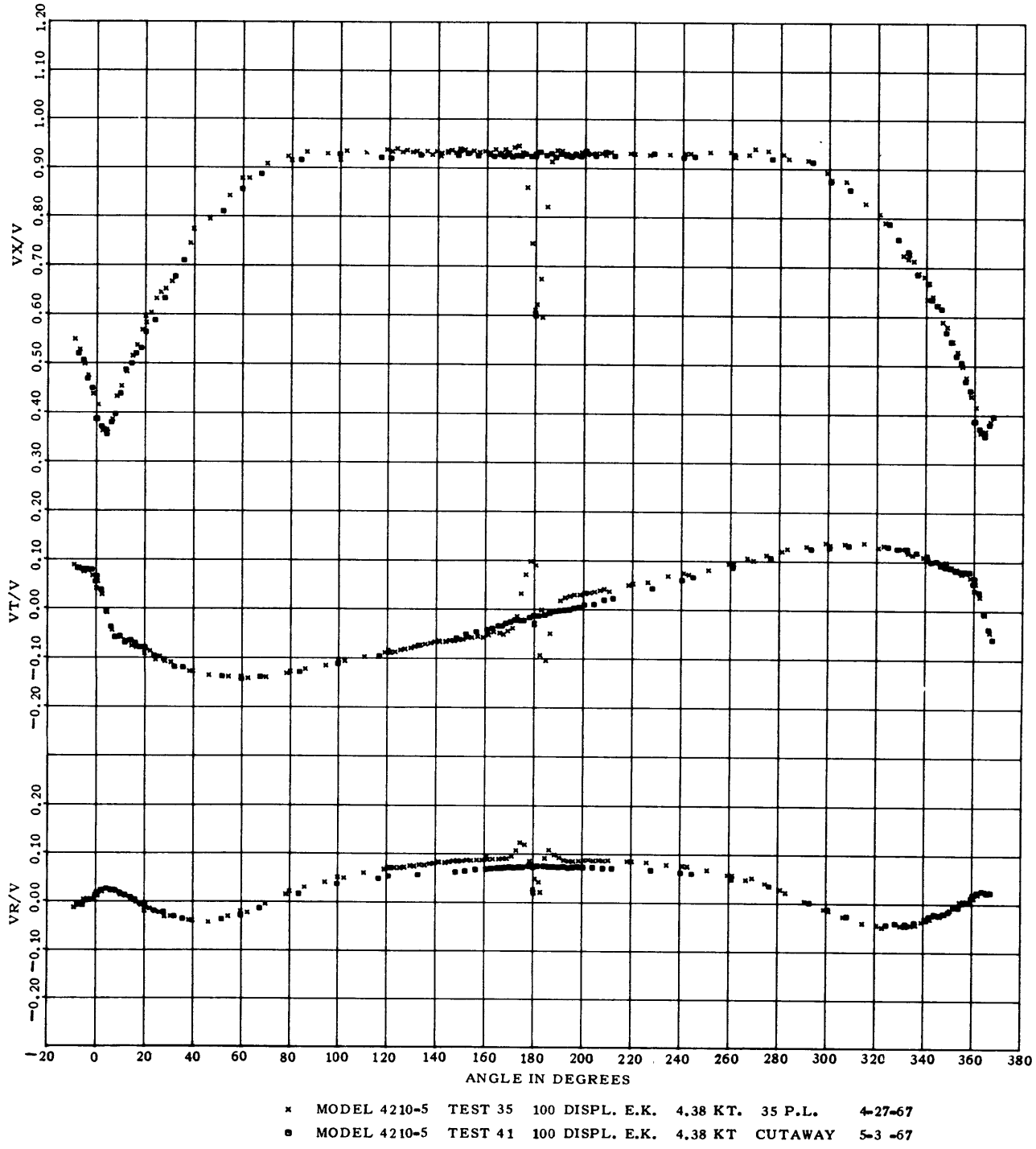

Figure 44 – Circumferential Distribution of Longitudinal, Tangential, and Radial Velocity Component Ratios at a Radius Ratio of 0.844 for Two Deadwood Conditions: Composite of Tests 35 and 41

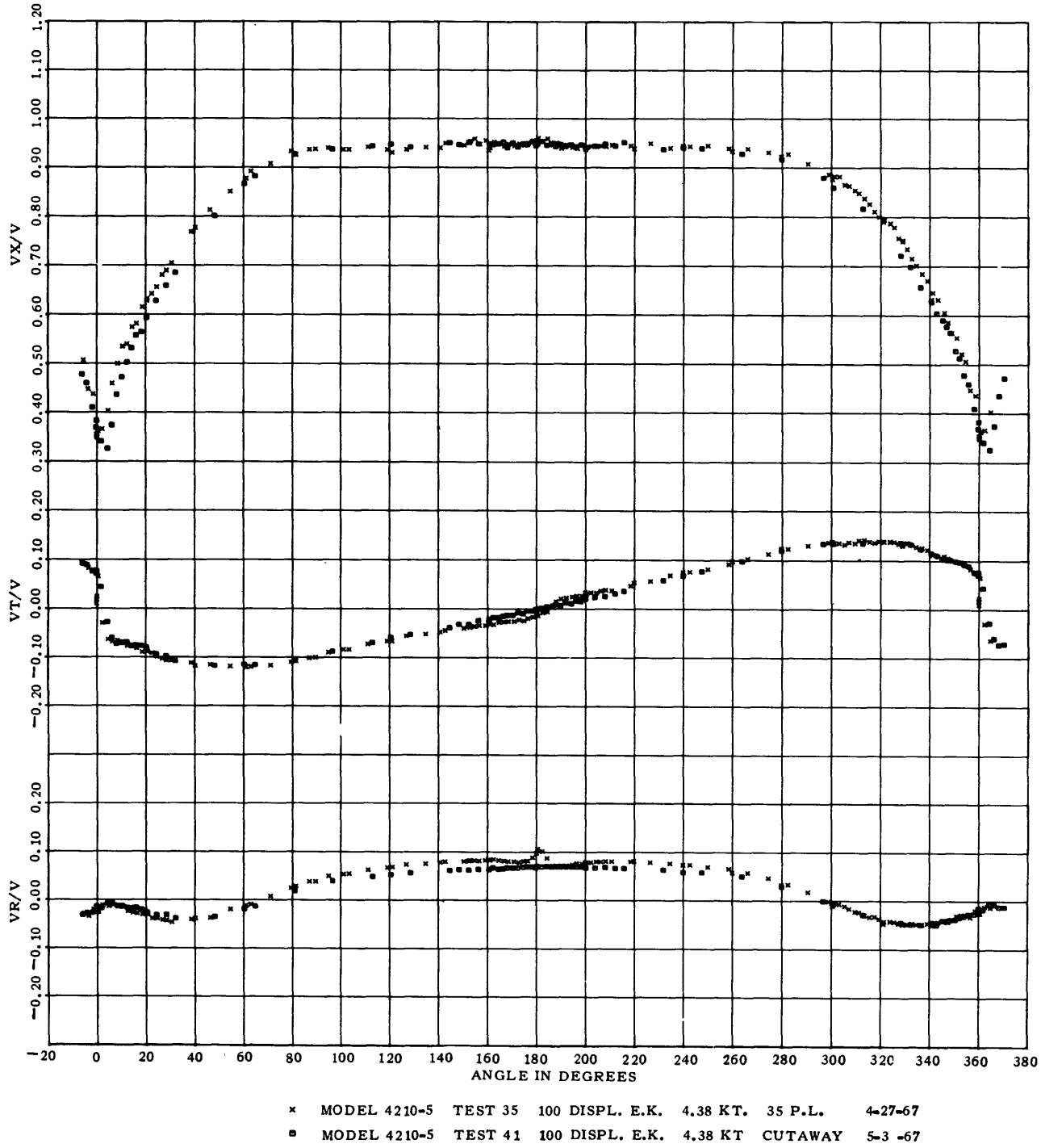

Figure 45 – Circumferential Distribution of Longitudinal, Tangential, and Radial Velocity Component Ratios at a Radius Ratio of 1.003 for Two Deadwood Conditions: Composite of Tests 35 and 41

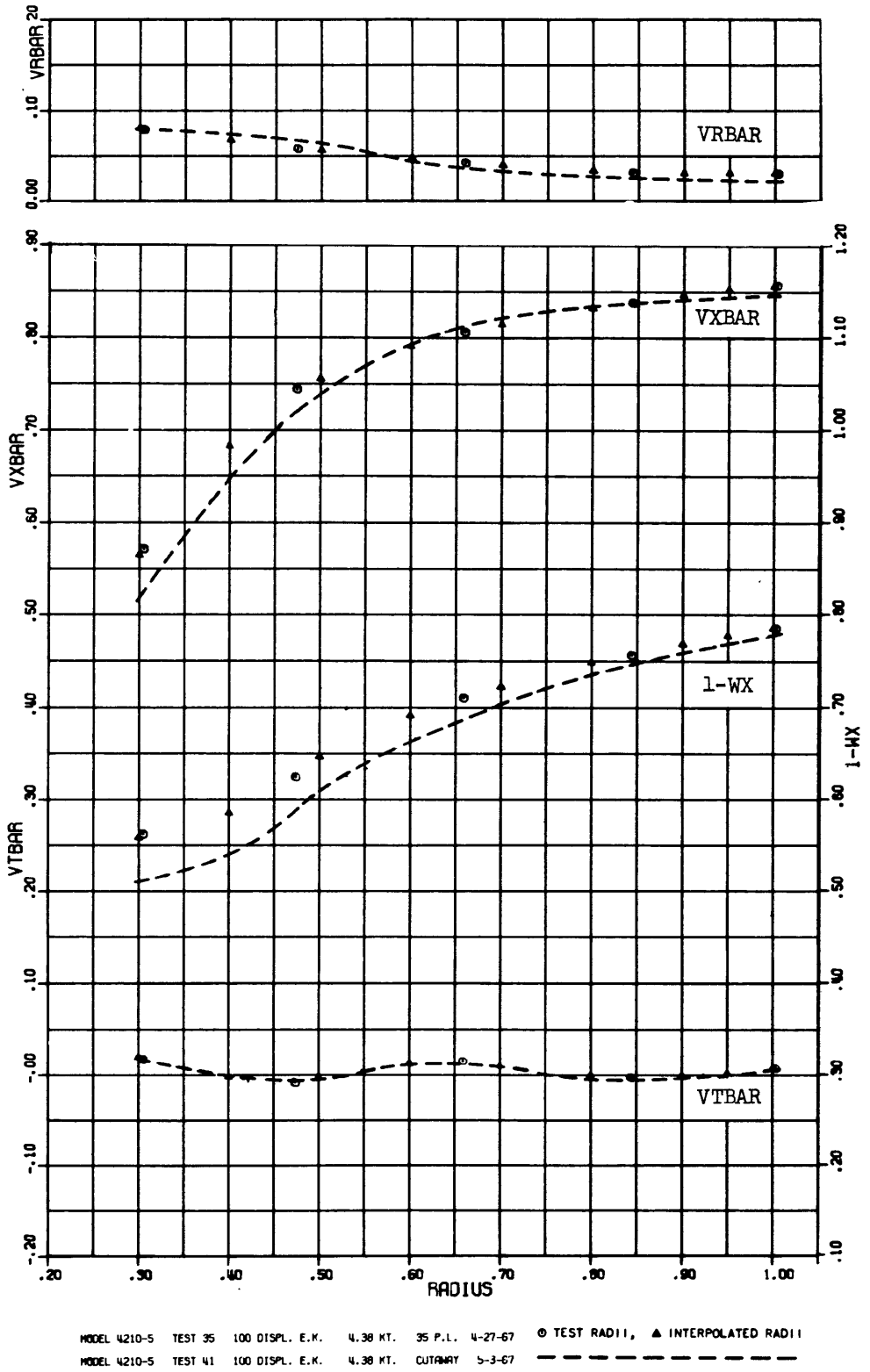

Figure 46 – Radial Distribution of the Volumetric Mean Wake Velocity Component Ratio and of the Mean Longitudinal, Tangential, and Radial Velocity Component Ratios for Two Deadwood Conditions: Composite of Tests 35 and 41

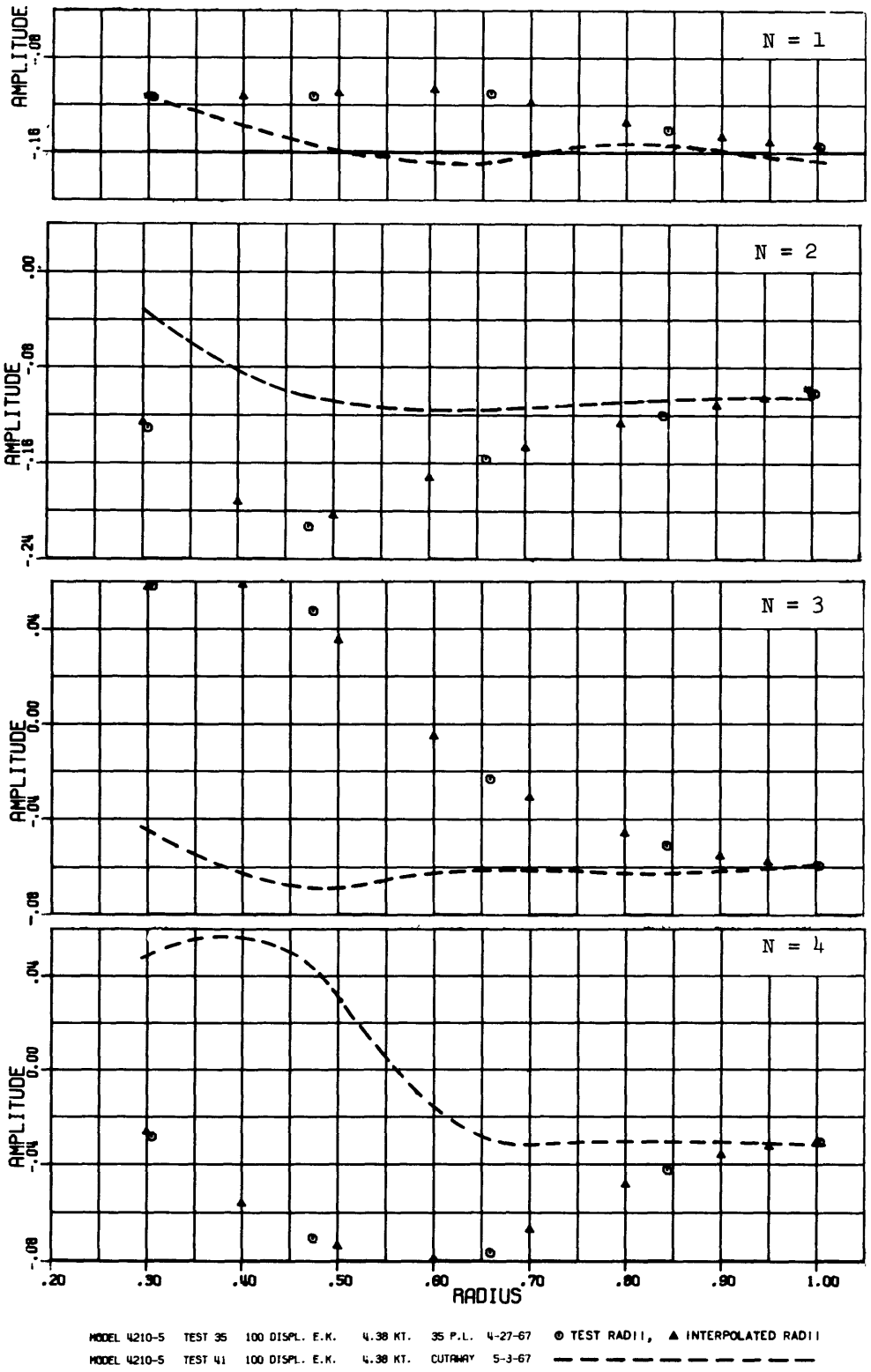

Figure 47 – Radial Distribution of the Amplitudes of the First through the Fourth Harmonic of the Circumferential Distribution of the Longitudinal Velocity Component Ratios for Two Deadwood Conditions: Composite of Tests 35 and 41

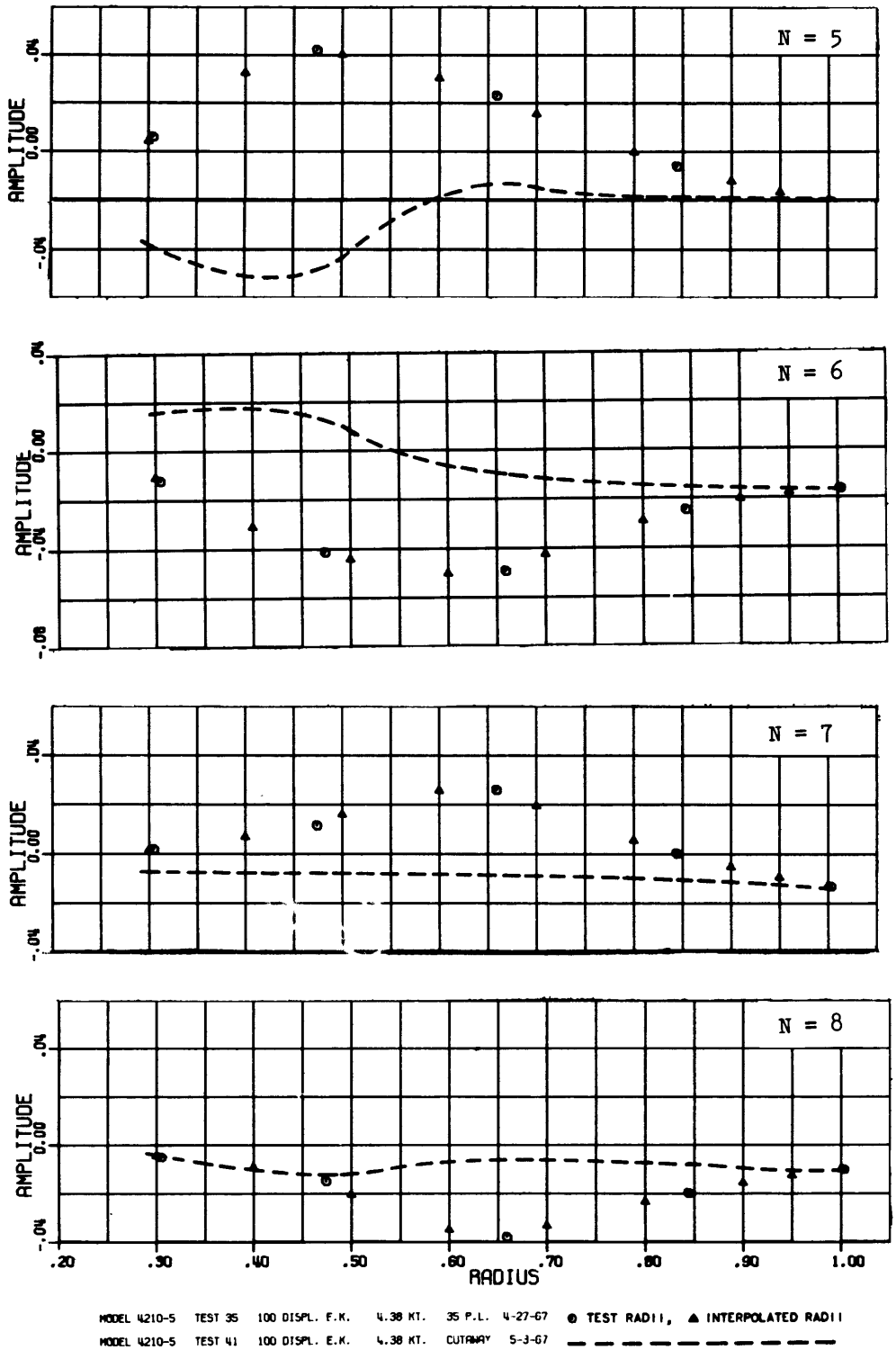

Figure 48 – Radial Distribution of the Amplitudes of the Fifth through the Eighth Harmonic of the Circumferential Distribution of the Longitudinal Velocity Component Ratios for Two Deadwood Conditions: Composite of Tests 35 and 41

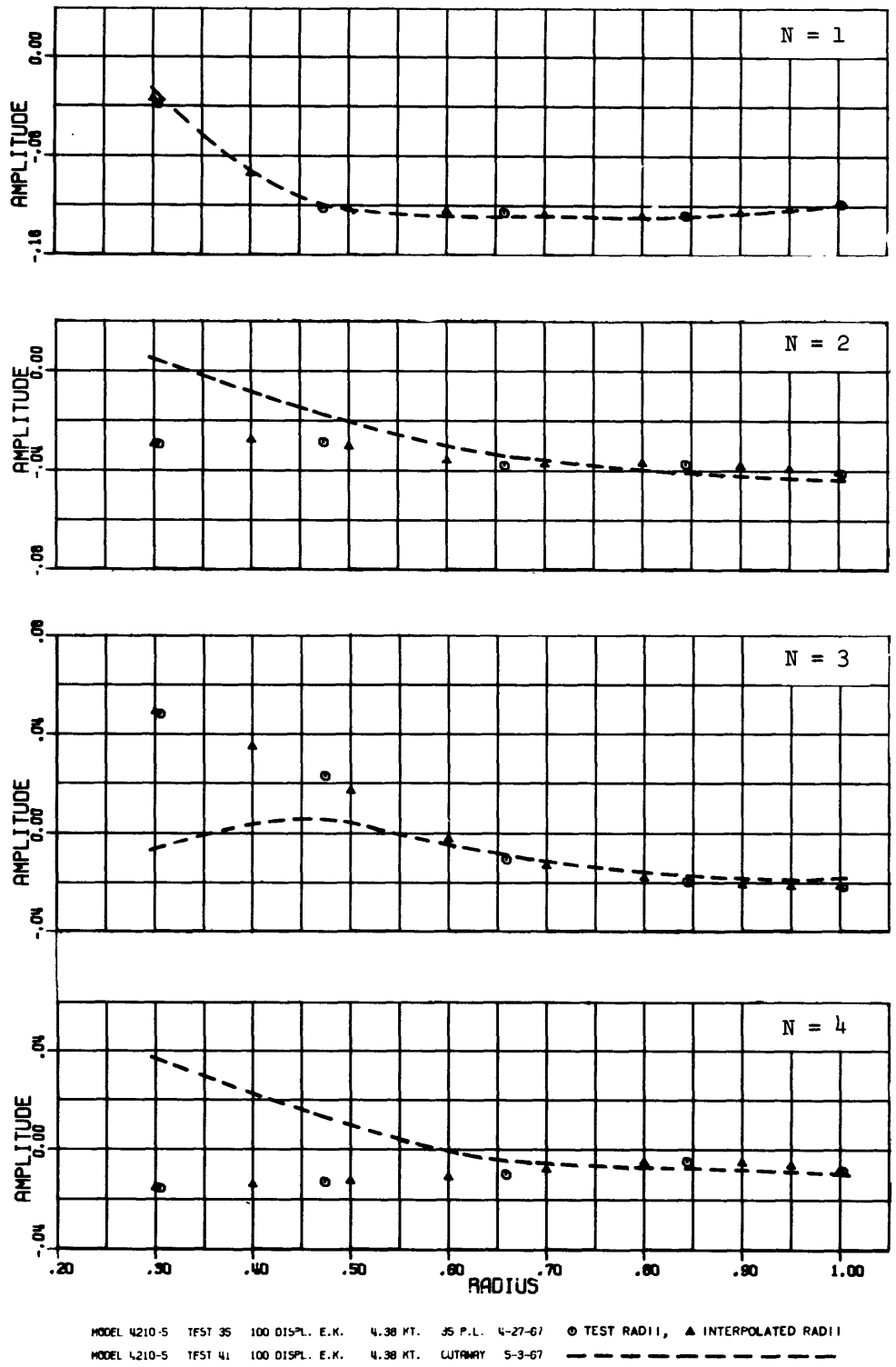

Figure 49 – Radial Distribution of the Amplitudes of the First through the Fourth Harmonic of the Circumferential Distribution of the Tangential Velocity Component Ratios for Two Deadwood Conditions: Composite of Tests 35 and 41

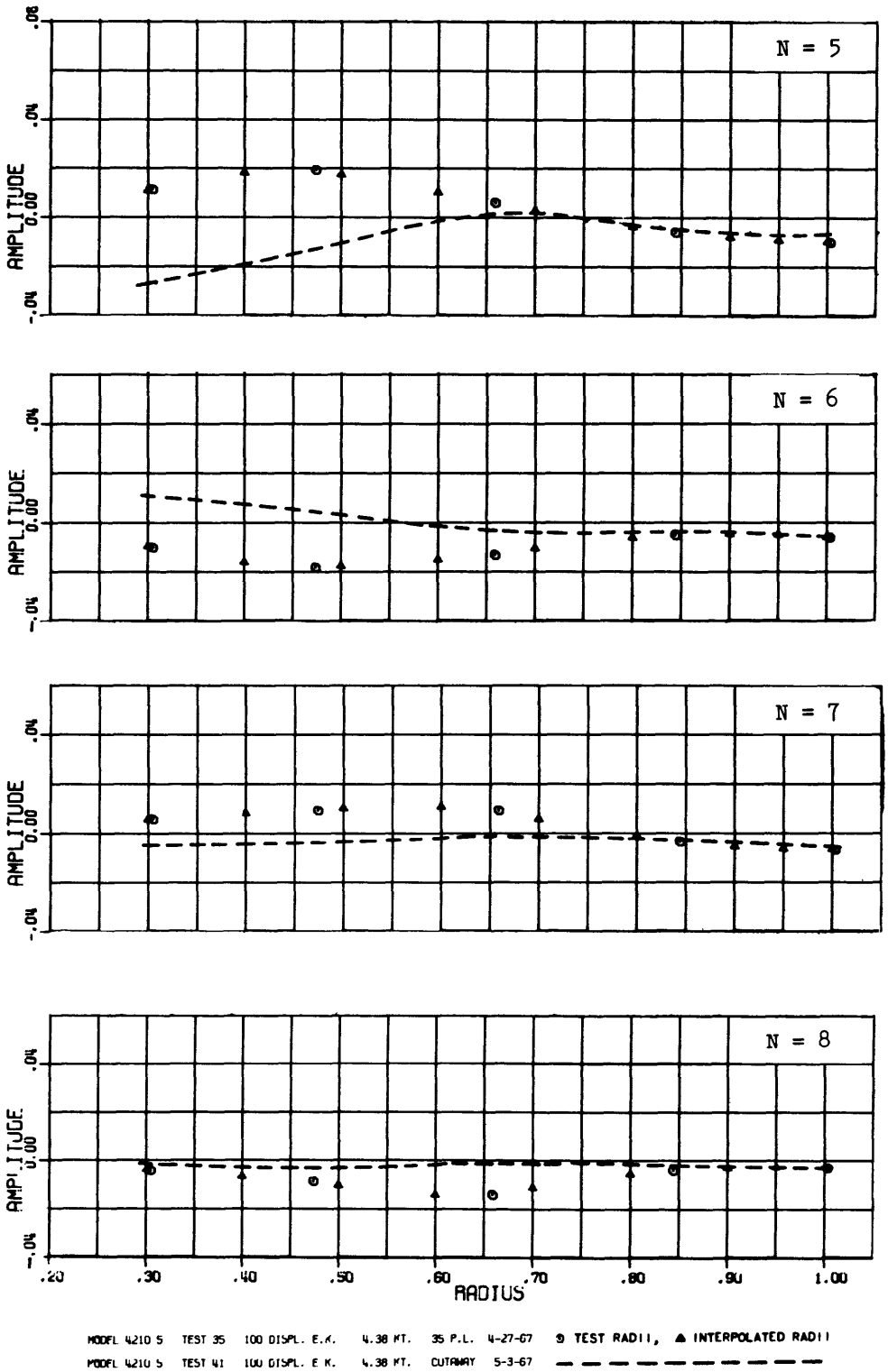

Figure 50 – Radial Distribution of the Amplitudes of the Fifth through the Eighth Harmonic of the Circumferential Distribution of the Tangential Velocity Component Ratios for Two Deadwood Conditions: Composite of Tests 35 and 41

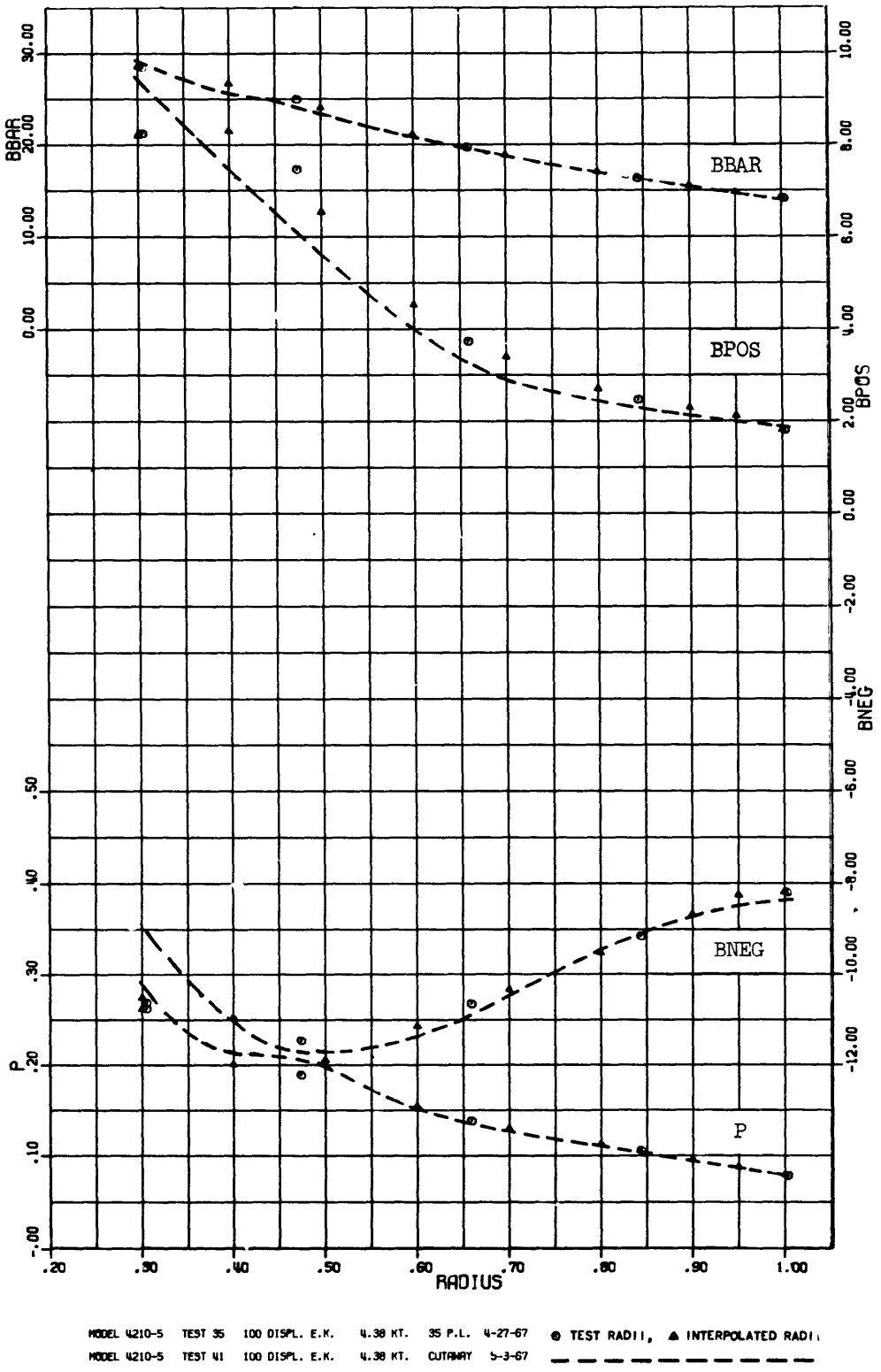

Figure 51 – Radial Distribution of the Mean Advance Angle, the Maximum Variations of the Advance Angle, and the Pressure Factor for Two Deadwood Conditions: Composite of Tests 35 and 41

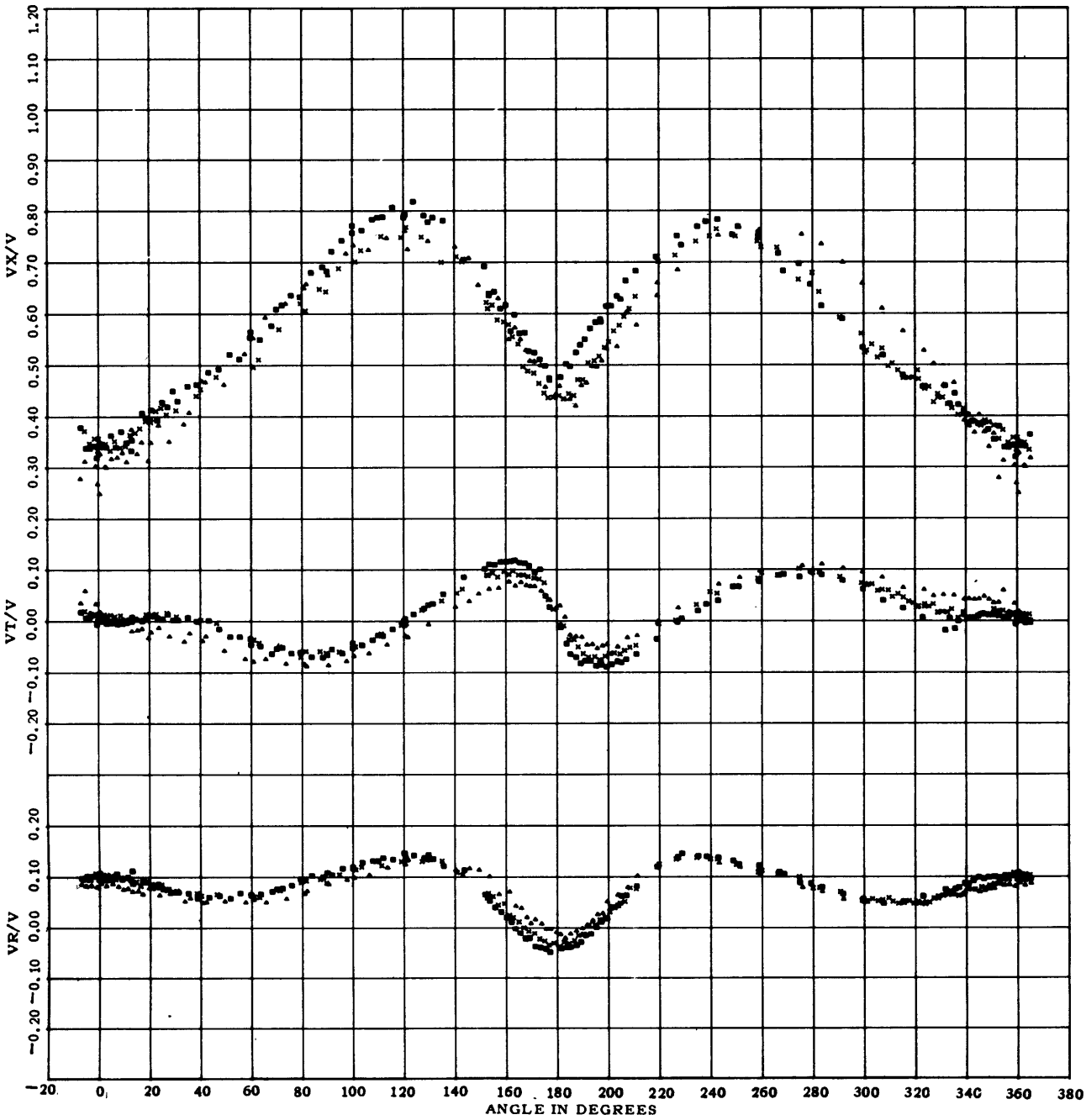

Figure 52 – Circumferential Distribution of Longitudinal, Tangential, and Radial Velocity Component Ratios at a Radius Ratio of 0.305 for Three Stern Section Shapes: Composite of Tests 35, 42, and 43

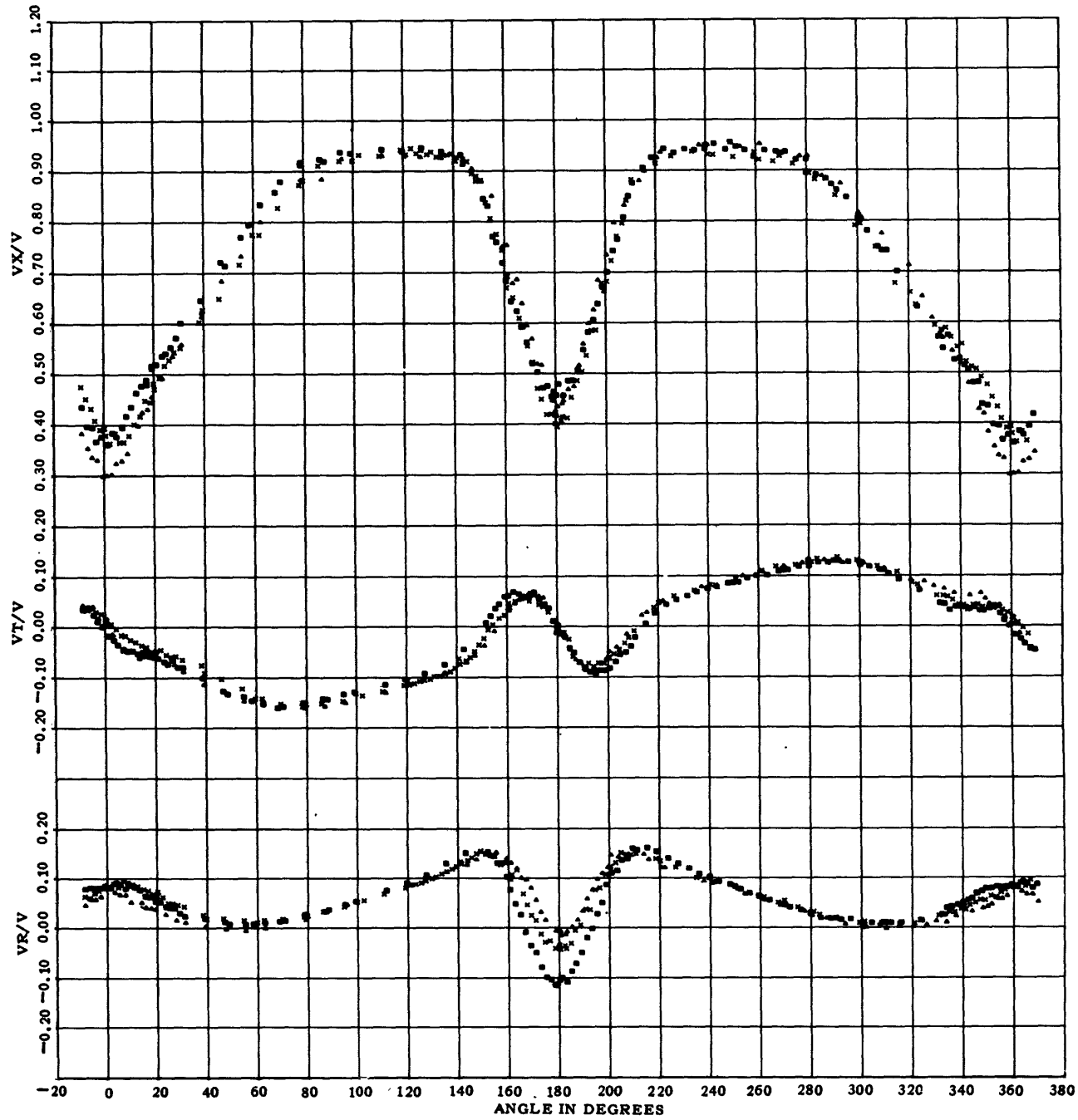

Figure 53 – Circumferential Distribution of Longitudinal, Tangential, and Radial Velocity Component Ratios at a Radius Ratio of of 0.474 Three Stern Section Shapes: Composite of Tests 35, 42, and 43

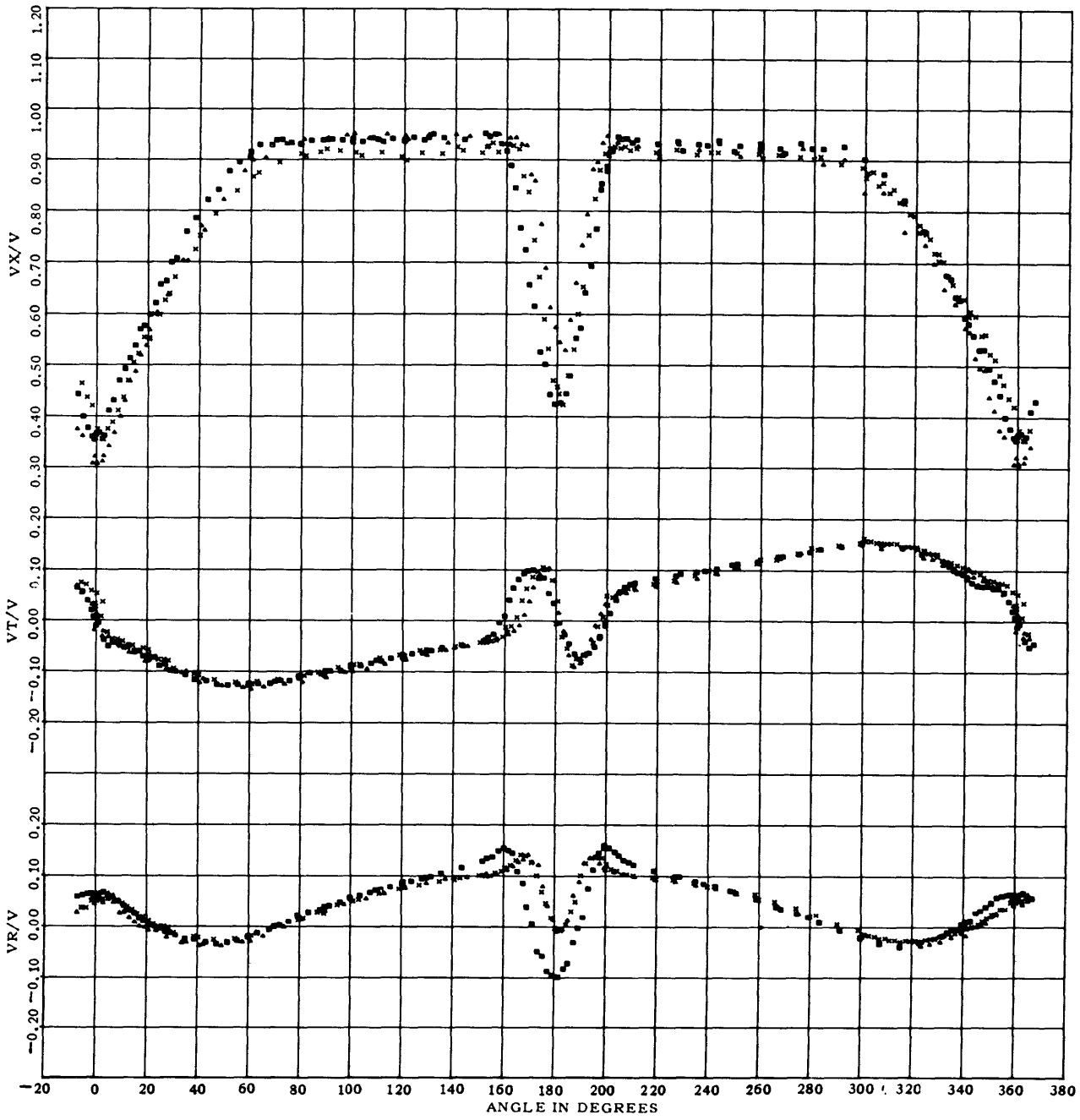

Figure 54 – Circumferential Distribution of Longitudinal, Tangential, and Radial Velocity Component Ratios at a Radius Ratio of 0.659 for Three Stern Section Shapes: Composite of Tests 35, 42, and 43

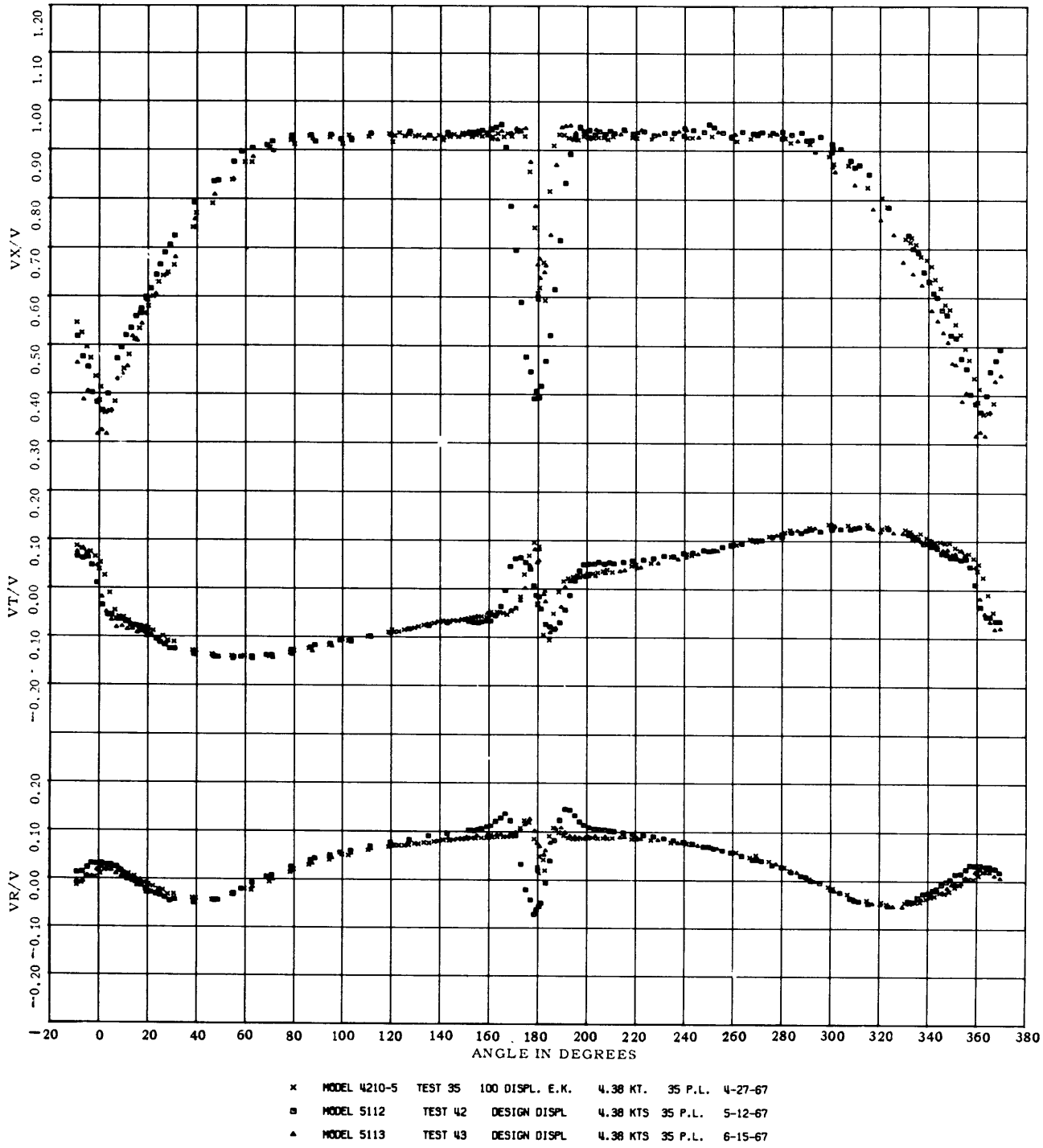

Figure 55 – Circumferential Distribution of Longitudinal, Tangential, and Radial Velocity Component Ratios at a Radius Ratio of 0.844 for Two Displacements and a Trimmed Condition: Composite of Tests 35, 39, and 40

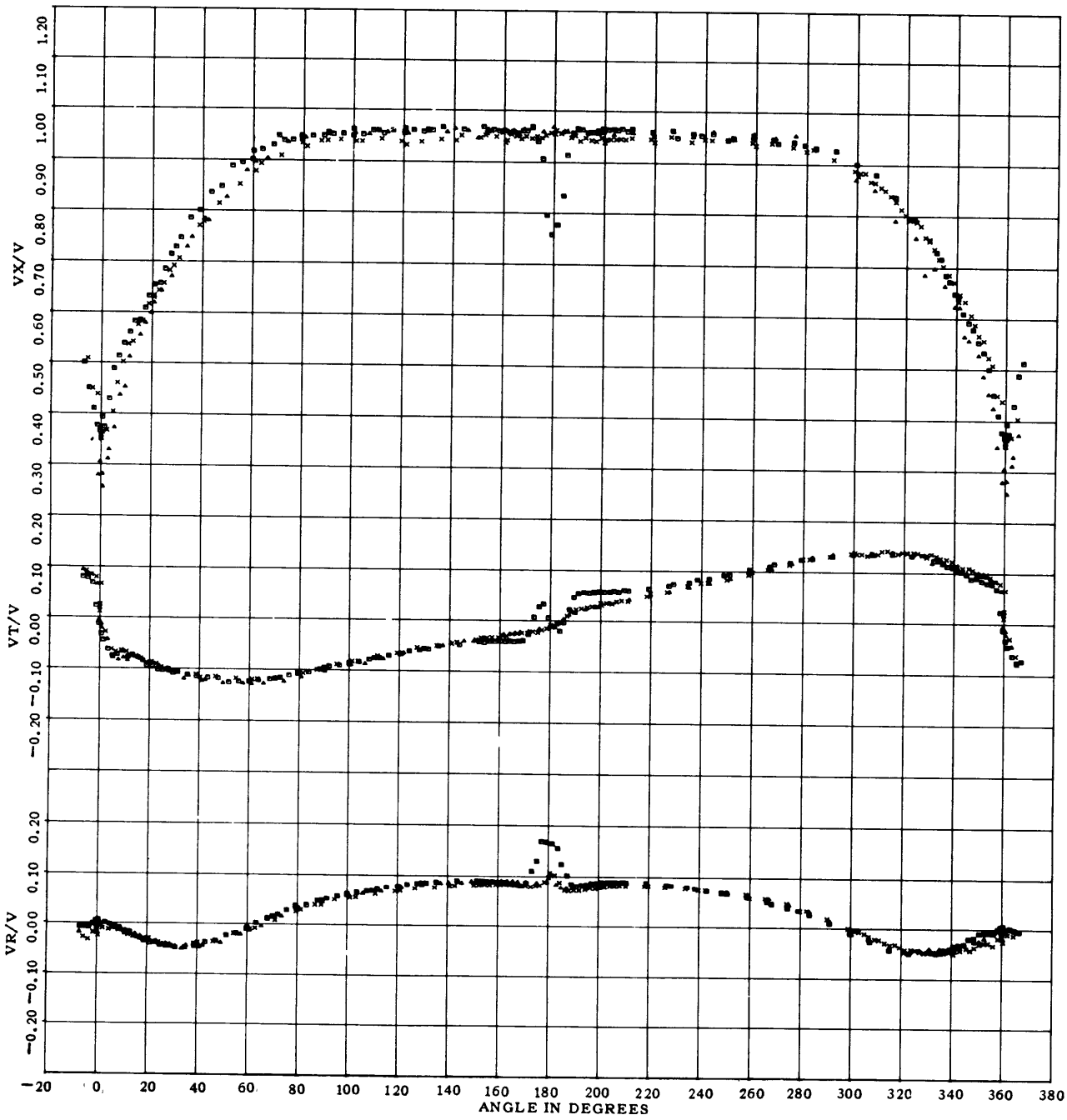

Figure 56 – Circumferential Distribution of Longitudinal, Tangential, and Radial Velocity Component Ratios at a Radius Ratio of 1.003 for Three Stern Section Shapes: Composite of Tests 35, 42, and 43

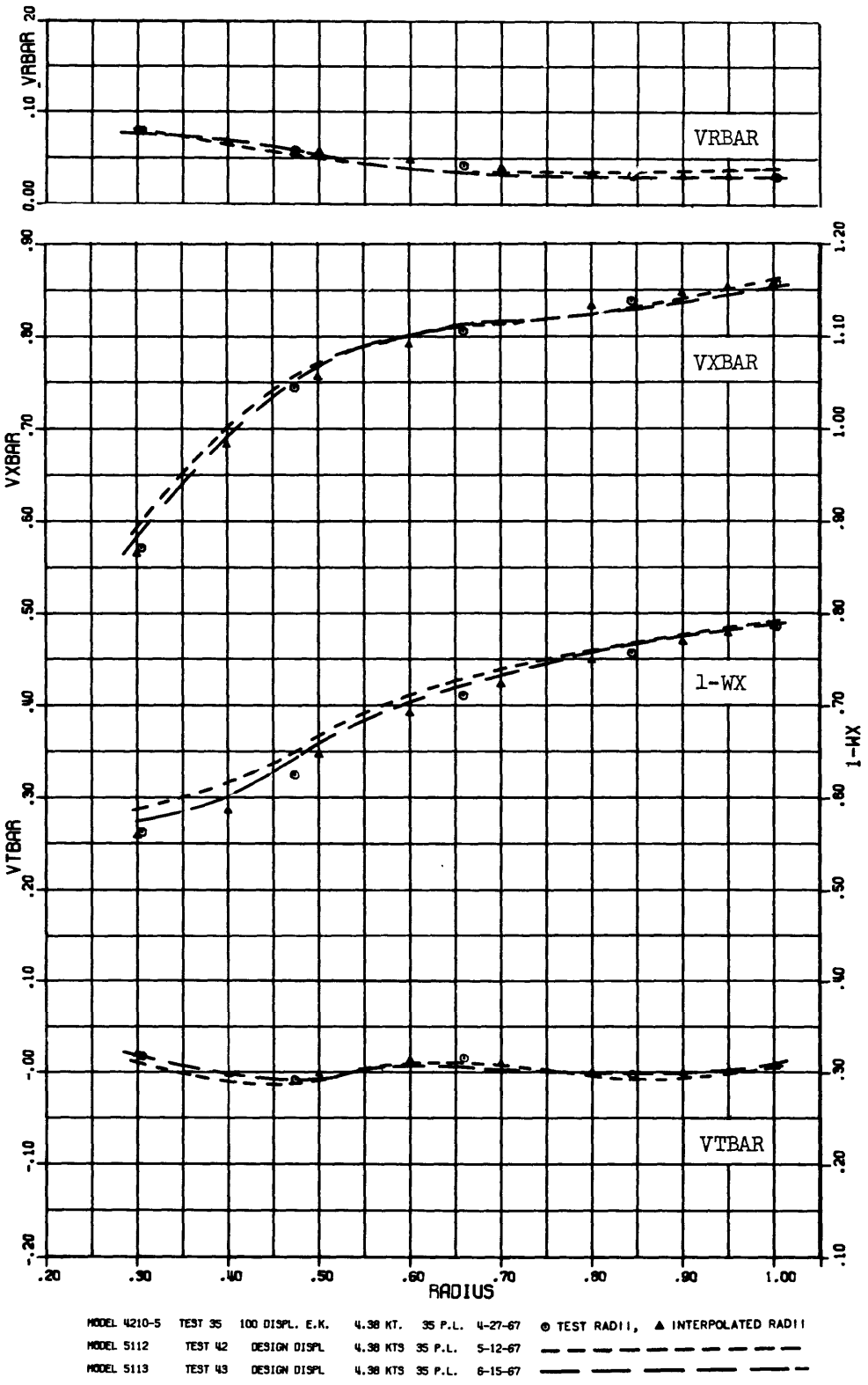

Figure 57 – Radial Distribution of the Volumetric Mean Wake Velocity Component Ratio and of the Mean Longitudinal, Tangential, and Radial Velocity Component Ratios for Three Stern Section Shapes: Composite of Tests 35, 42, and 43

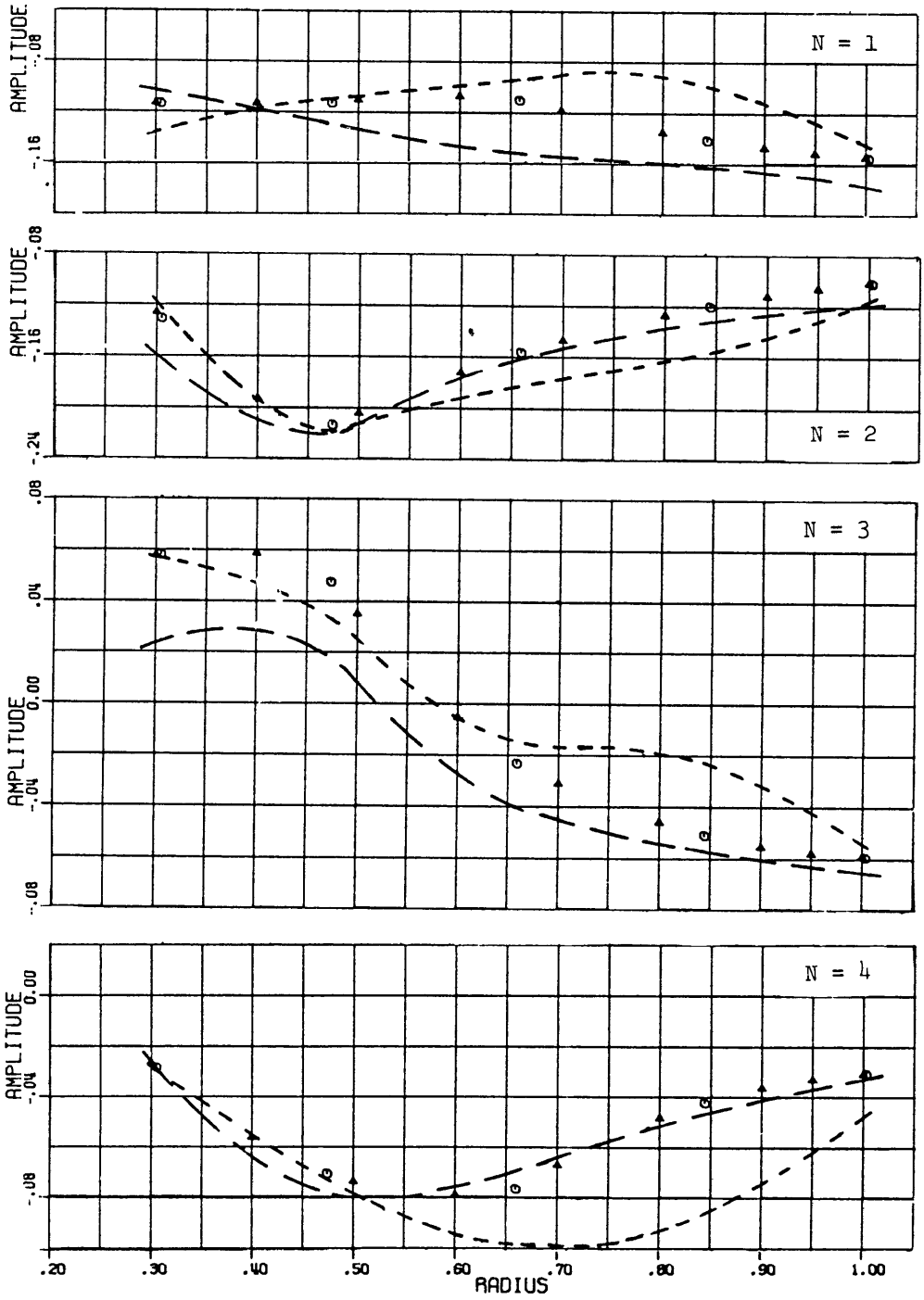

Figure 58 – Radial Distribution of the Amplitudes of the First through the Fourth Harmonic of the Circumferential Distribution of the Longitudinal Velocity Component Ratios for Three Stern Section Shapes: Composite of Tests 35, 42, and 43

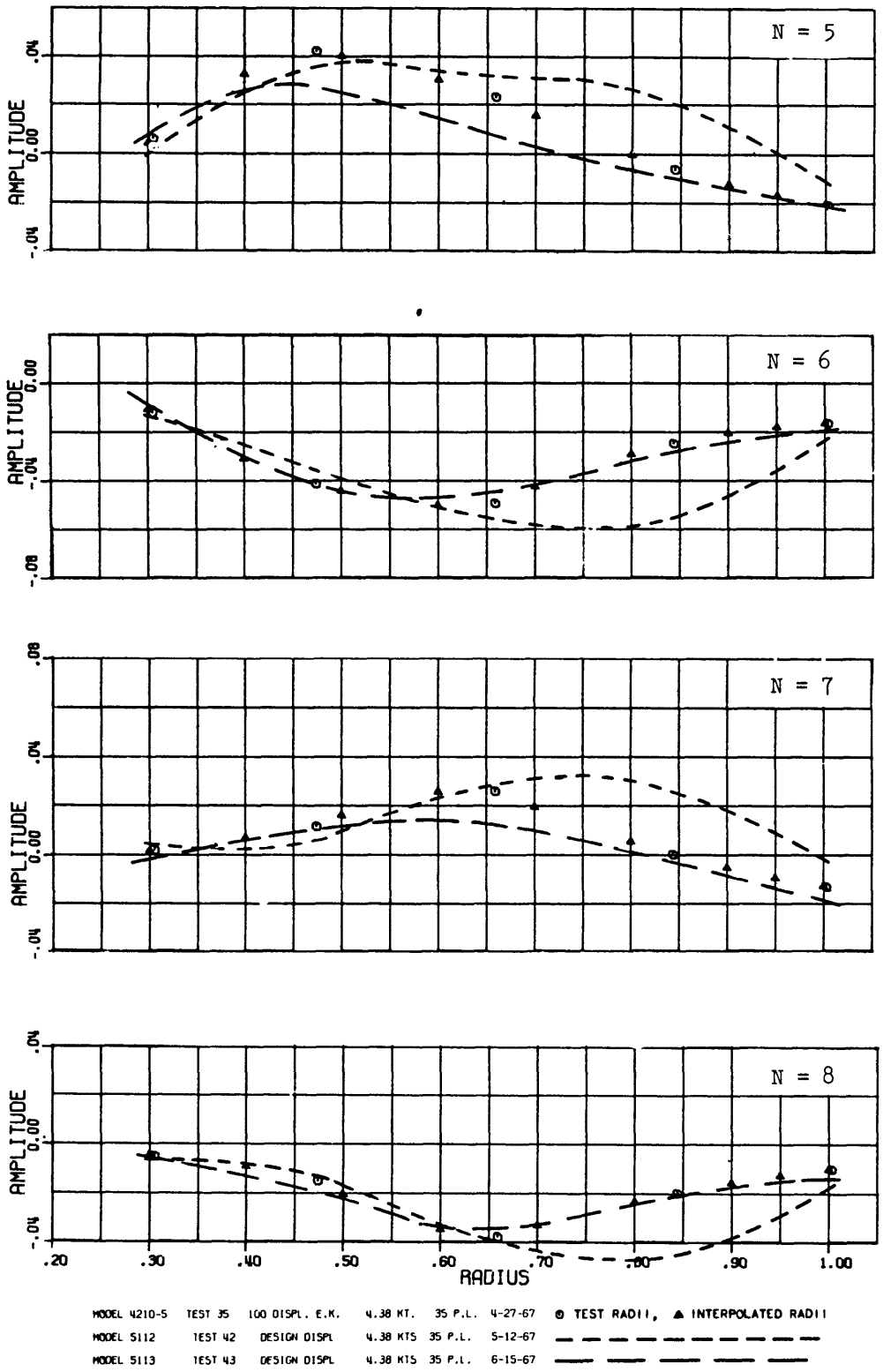

Figure 59 – Radial Distribution of the Amplitudes of the Fifth through the Eighth Harmonic of the Circumferential Distribution of the Longitudinal Velocity Component Ratios for Three Stern Section Shapes: Composite of Tests 35, 42, and 43

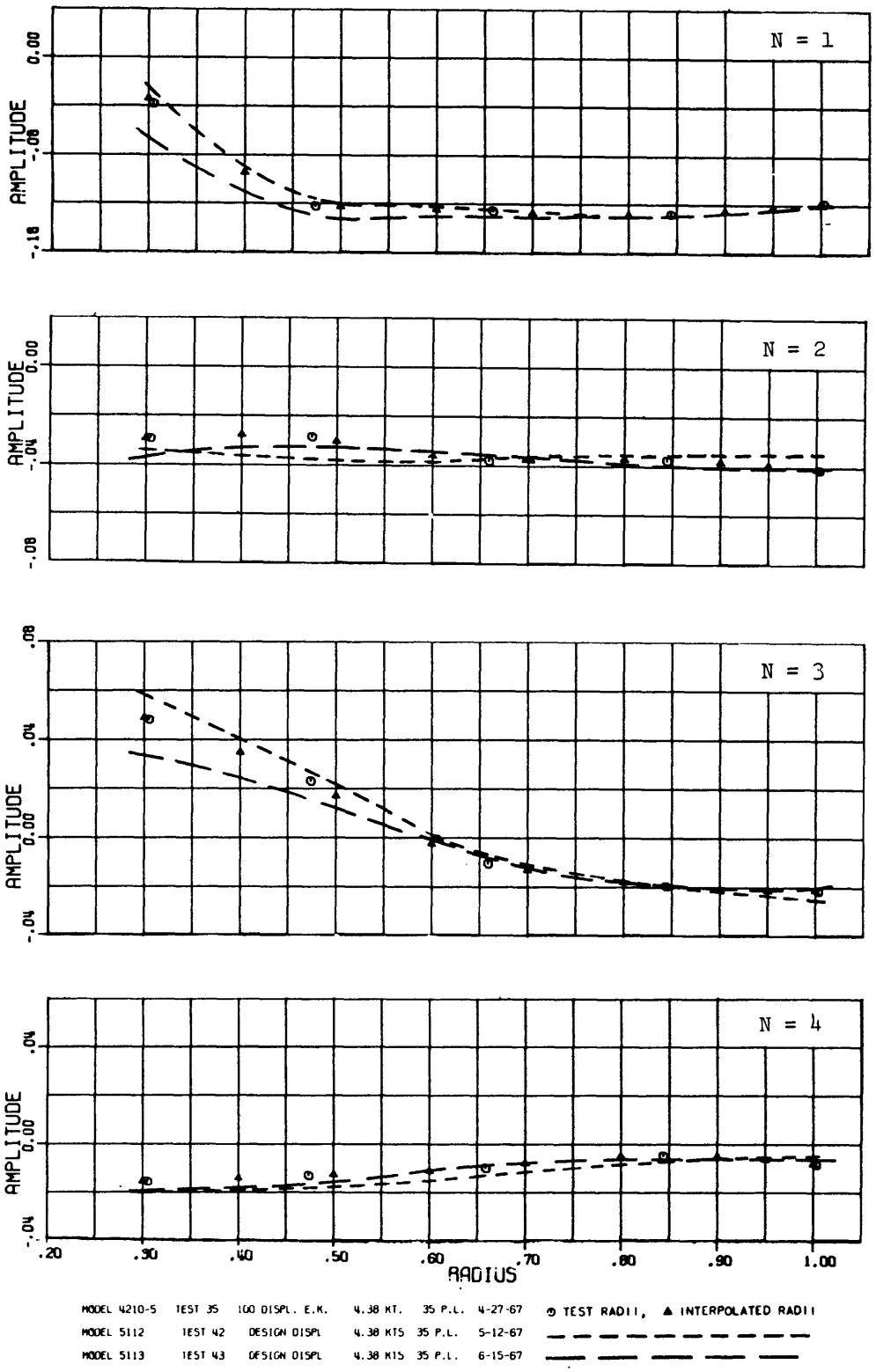

Figure 60 – Radial Distribution of the Amplitudes of the First through the Fourth Harmonic of the Circumferential Distribution of the Tangential Velocity Component Ratios for Three Stern Section Shapes: Composite of Tests 35, 42, and 43

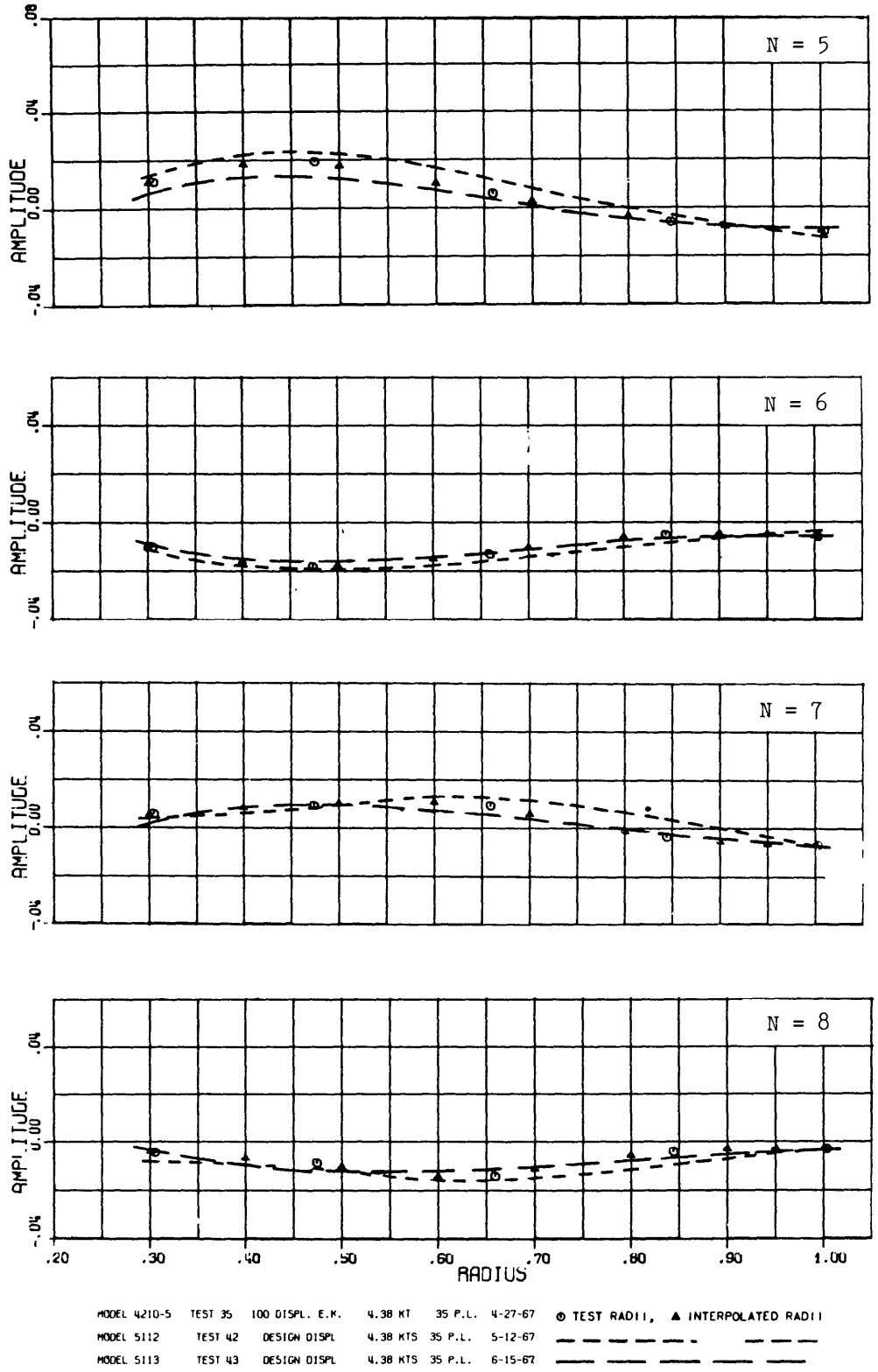

Figure 61 – Radial Distribution of the Amplitudes of the Fifth through the Eighth Harmonic of the Circumferential Distribution of the Tangential Velocity Component Ratios for Three Stern Section Shapes: Composite of Tests 35, 42, and 43

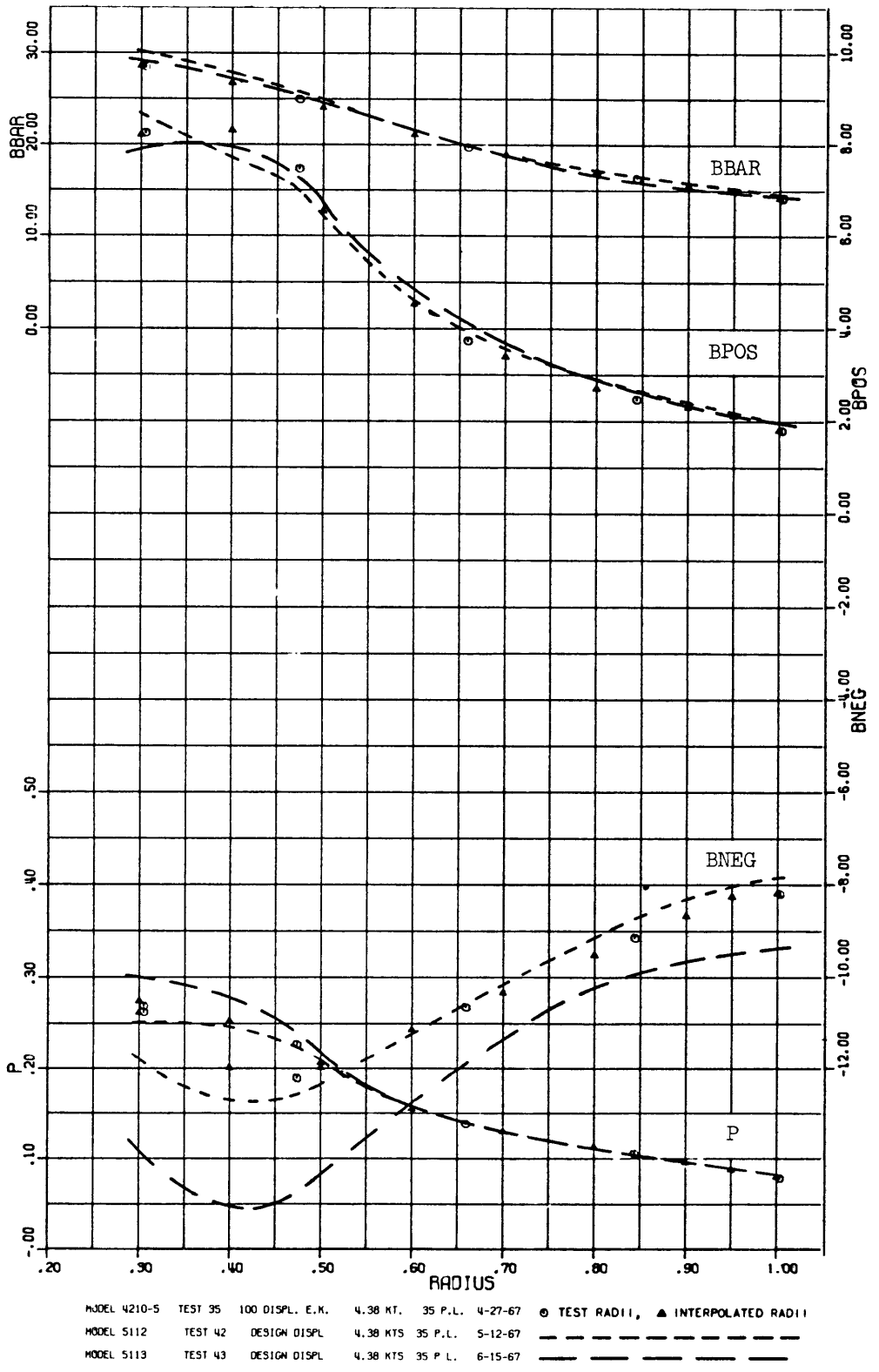

Figure 62 - Radial Distribution of the Mean Advance Angle, the Maximum Variations of the Advance Angle, and the Pressure Factor for Three Stern Section Shapes: Composite of Tests 35, 42, and 43

BLANK

APPENDIX A

WAKE SURVEY APPARATUS

This appendix describes in some detail the testing apparatus currently used in conducting wake surveys at this Center. In the description of this equipment, experimental procedures are briefly considered. Essentially, the testing apparatus consists of the following components:

1. A rake of five spherically headed pitot tubes.
2. A hydraulic system to connect the pitot tubes to the instrumentation.
3. An indexing mechanism and a position encoder to facilitate the angular positioning of the rake.
4. A data acquisition system consisting of pressure transducers and electronic measurement/recording devices.

The wake surveys are presently conducted using the rake of five spherically headed pitot-tubes of the five-hole type[7] inserted into the shaft bossing so that the rake can be rotated by an indexer-encoder in the plane of measurement. Twenty-five small pressure transmitting tubes, five for each pitot tube, which are contained within the rake shaft, are connected to the hydraulic system which links the pressures on the spherical surfaces to differential pressure transducers. The hydraulic system is linked with the pressure transducers such that four differential pressures are measured for each pitot tube.

The electronic measurement/recording devices consist of control units, voltmeters, scanners, and printers, etc. The digital voltmeters, which are coupled to the pressure transducers through control units, sample and integrate the signals from the pressure transducers during a 5-sec time interval. After the readout units scan the voltmeters and other electronic apparatus, the required data are printed out and are encoded on paper punch tape. These data are then processed with established NSRDC computer programs; see Appendix D.

THE PITOT TUBE RAKE

The rake consists of five spherically headed pitot tubes mounted on an aerofoil-shaped section which is affixed to a drive shaft. The pitot tubes are spaced along the foil so that velocity samplings can be taken at five radii in the propeller disk. Each pitot tube consists of a spherical head and a support tube. The spherical head is 3/8 in. in diameter and has five holes drilled in the upstream hemisphere, as shown in Figure A-1. The center hole is axially aligned with the support tube. The other four holes are spaced 90 deg apart and 20 deg from the center hole. Two holes are aligned radially and two others are aligned

tangentially with the propeller disk. When the holes are placed in this manner, the longitudinal, tangential, and radial velocity components of the wake can be determined directly by measuring the differential pressure between the center hole and each of the outer holes.

THE HYDRAULIC SYSTEM

The purpose of the hydraulic system (Figure A-2) is to connect the pitot tubes to the pressure transducers and facilitate the purging of air from the system. Small stainless steel tubes, which emerge from the forward end of the rake drive shaft, are connected to the pressure transducers by flexible plastic tubing. The remainder of the system is used for purging air from the gages, the manifolds, and the tubing.

ANGULAR POSITIONING OF THE RAKE ASSEMBLY

The pitot tube rake assembly must be rotated through an arc of 360 deg in order to sample the entire wake in the propeller disk. This is accomplished by a stepping motor which rotates the rake to the desired position and then holds the shaft steady during the data sampling.

A shaft position encoder is linked to the rake assembly by a cog belt. This makes visual readout of the rake position available to the operator. It also makes it possible to position the rake assembly by remote control.

DATA ACQUISITION SYSTEM

A block diagram of the instrumentation used for wake measurement is presented in Figure A-3. The pressure differentials are converted to voltages by Pace differential pressure transducers. A 0.1-psi diaphragm is used in the transducers for wake measurements. The system resolution is better than three hundredths of an inch of water and the system drift is less than three hundredths of an inch of water during a test run.

NSRDC Type 200 control units are used to adjust the sensitivity of the instruments. A schematic diagram of one channel of a control unit is presented in Figure A-4. The signals from each pitot tube individually are scanned so that the data from one pitot tube can be displayed on four integrating digital voltmeters. The voltmeters along with the rake position indicators, carriage speed counters, and pitot tube numbers are scanned by a second scanner. The data stored therein are recorded by a printer and are also punched onto paper tape. The punched tape is then translated onto IBM punched cards and the data are processed by computers at the Center.

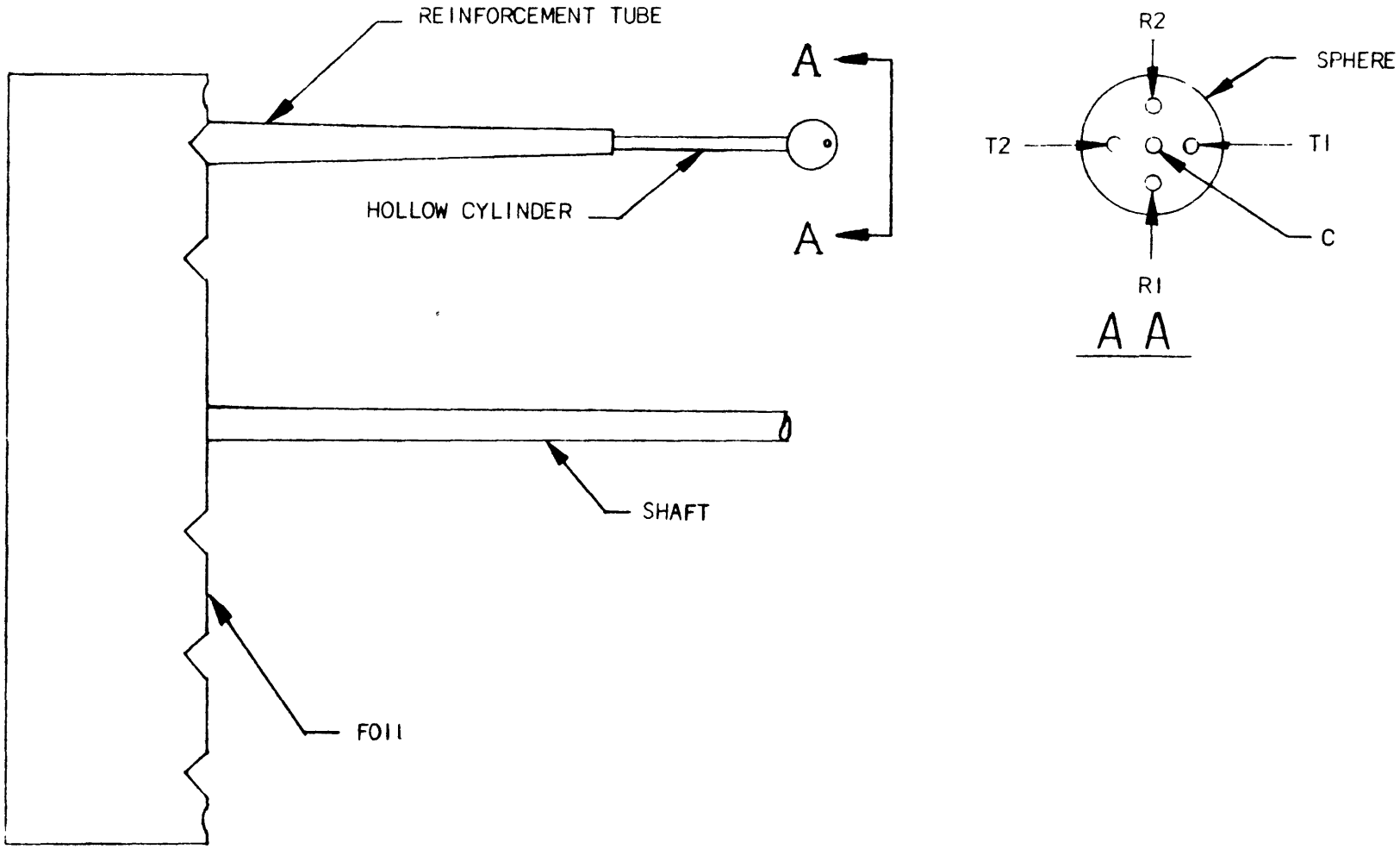

Figure A-1 – Rake Assembly Showing One Spherically Headed Pitot Tube

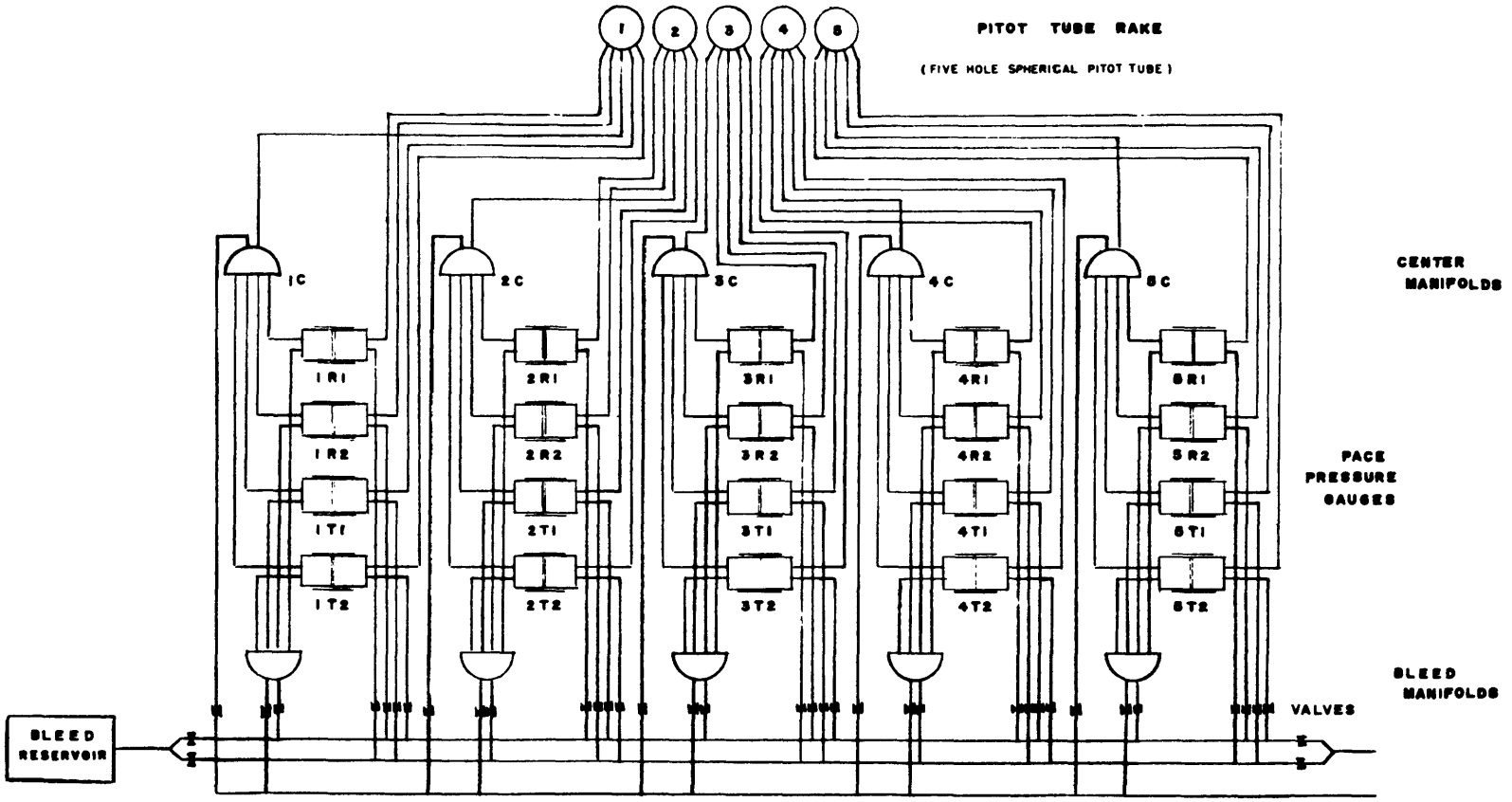

Figure A-2 – The Hydraulic System

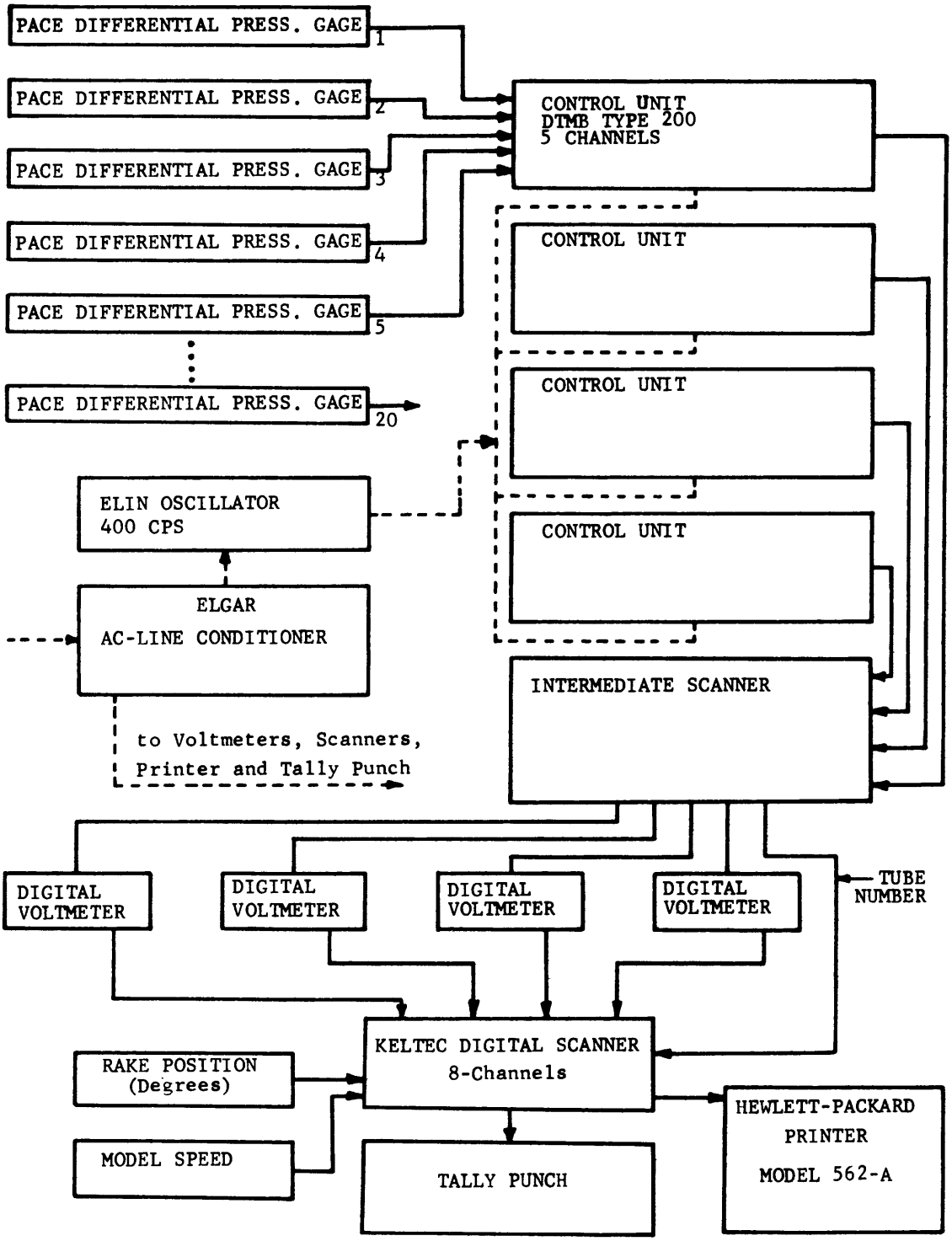

Figure A-3 – Data Acquisition System

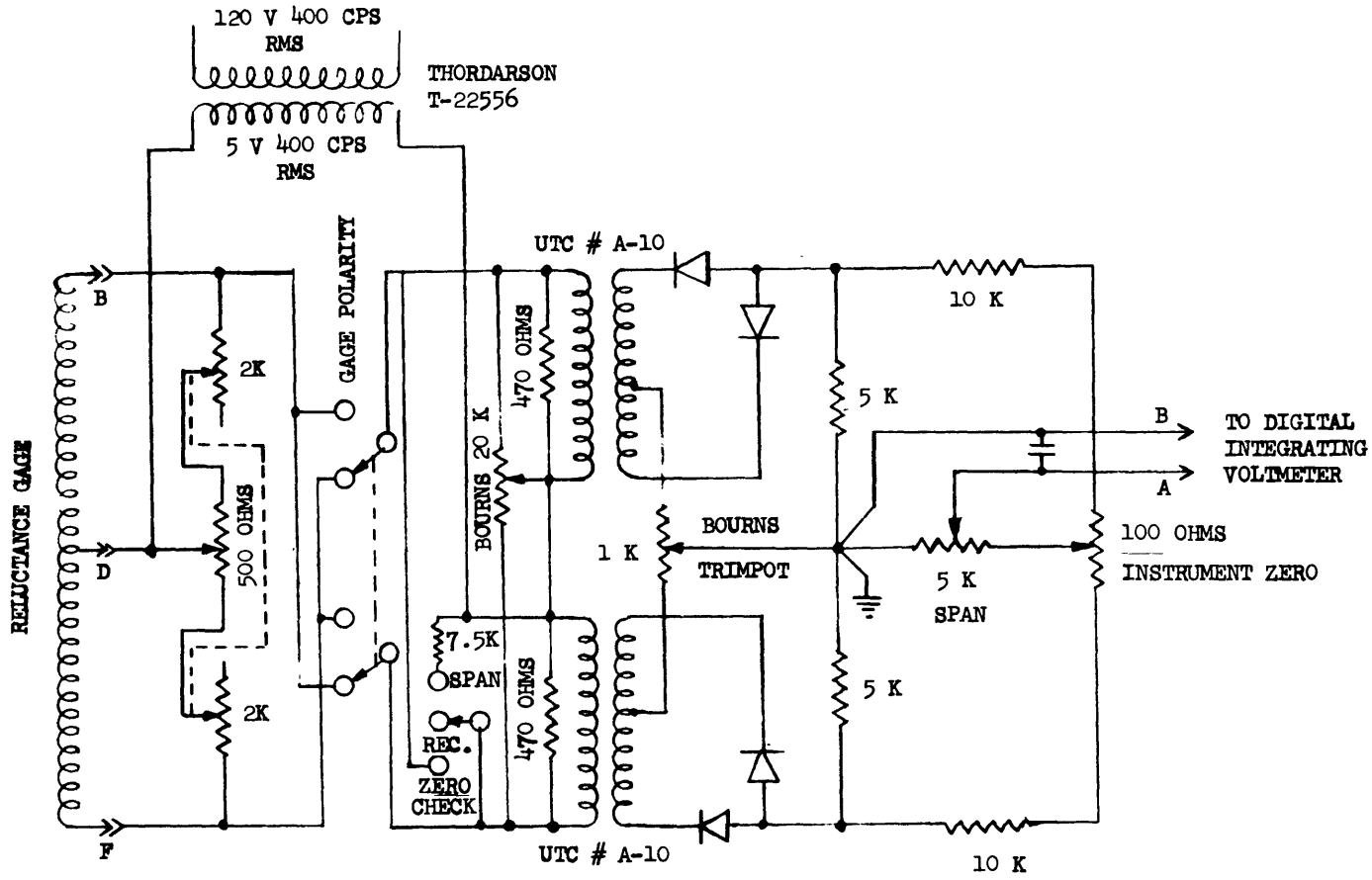

NOTES: (1) Except where marked all potentiometers are Bourns 10 turn
(2) All resistors are Shallcross precission wire wound
(3) Diodes are IN483 Transitron Quad.

Figure A-4 – One Channel of a Control Unit (NSRDC Type 200)

APPENDIX B

SECTION SHAPE COEFFICIENT

This appendix gives the geometrical definition of the section shape coefficient (τ) together with some descriptive terms arbitrarily assigned to certain ranges of the section shape coefficient.

The coefficient (τ) characterizes the shape of the stern at Station 18. Its determination is illustrated in Figure B-1. The construction of a line tangent to Station 18, at a point (B) which is at the same level as the propeller shaft (Point C), creates a right triangle, the legs of which are lines BC and AC. The relationship of these legs is established as a tangent function of the angle that is created by the intersection of the tangent line AB and line AC. The section shape coefficient (τ) is then defined as the tangent of this angle ($\sphericalangle CAB$) or simply as $a \div b$.

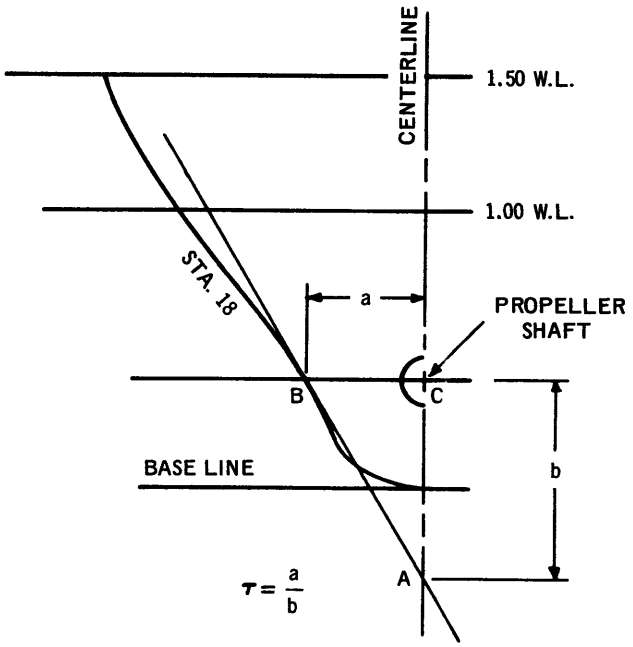

Figure B-1 – Definition of Section Shape Coefficient

It is often desirable in technical discussions to replace a cumbersome descriptive phrase with a one- or two-word descriptive adjective. In this report the terms "U-shaped" and "V-shaped" have been used extensively in this manner. It should be made clear to the

reader that this terminology is completely arbitrary and has been used here solely for the purpose of discussion.* This arbitrary terminology is defined as follows:

Model Number	Section-Shape Coefficient (τ)	Arbitrary Terminology
5112	0.181	U-Shaped
4210-5	0.217	Moderate U-Shaped
5113	0.330	V-Shaped

*It should be noted that the arbitrarily chosen terms used in this report are not necessarily in agreement with those chosen in other publications. The terminology used here is not in complete agreement with that used in Reference 5, nor with that used in Reference 9.

APPENDIX C

RESULTS OF WAKE SURVEY OF MODEL 4287 WITH A MODIFIED BOSSING

A model of the Series 60–0.60 C_B parent hull, designated Model 4287, was modified to accommodate a large, six-component dynamometer. Because of the size and shape of this dynamometer, the stern bossing and the adjacent area had to be enlarged. The body plan in Figure C-11 clearly shows the shape of this modified portion of the hull.

The six-component dynamometer has been used to measure alternating forces and moments transmitted from the model propeller to the shafting and, therefore, to the dynamometer. Since the magnitudes of fluctuating propeller forces and moments are known to be dominated by the wake distribution in the propeller plane, it was decided that a wake survey should be conducted to determine the effects of the bossing modification upon the wake. At the same time it was decided that some further investigation into the effects of propeller position might prove to be fruitful.

As a result, two tests were conducted in June of 1968 on Model 4287 with the modified bossing. These tests, which were designated Tests 44 and 45, were conducted to measure the velocity distribution in the 35- and 45-percent propeller positions, respectively.* In both of these tests, the model was ballasted to its design displacement and was towed at the design speed.

The results of these tests are presented in Figures C-1 through C-10. It can be seen from the comparative plots of the circumferential distribution of longitudinal, tangential, and radial velocity component ratios that the wake was certainly affected by the change in bossing shape. Figure C-5 shows that the effect was greatest at the inner radii. It is quite interesting to observe (Figures C-6 and C-7) that for values of N equal to 2, 4, 6, 7, and 8 the harmonic amplitudes were reduced as a result of the bossing modification.

The slight differences in wake between Tests 44 and 45 were most evident at the innermost radius. The results do, however, illustrate the fact that the wake does become more uniform with increasing distance from the stern frame. The resulting change in the harmonic amplitudes is somewhat negligible.

*The location of the propeller plane, which is expressed as a percentage of the propeller diameter, is measured from the stern frame at the 0.7 propeller radius.

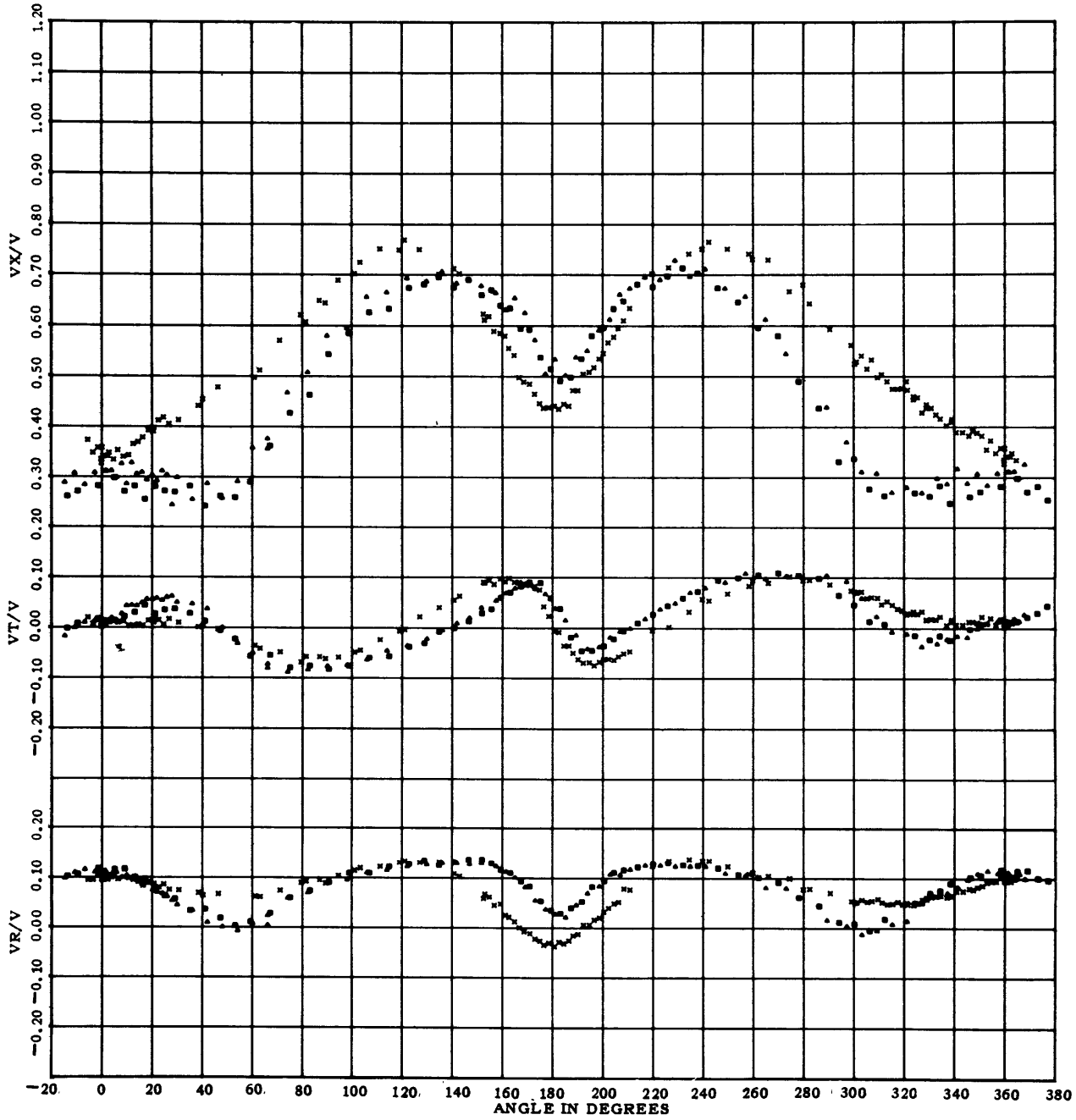

Figure C-1 – Circumferential Distribution of Longitudinal, Tangential, and Radial Velocity Component Ratios at a Radius Ratio of 0.305 for a Modified Bossing at Two Propeller Positions: Composite of Tests 35, 44, and 45

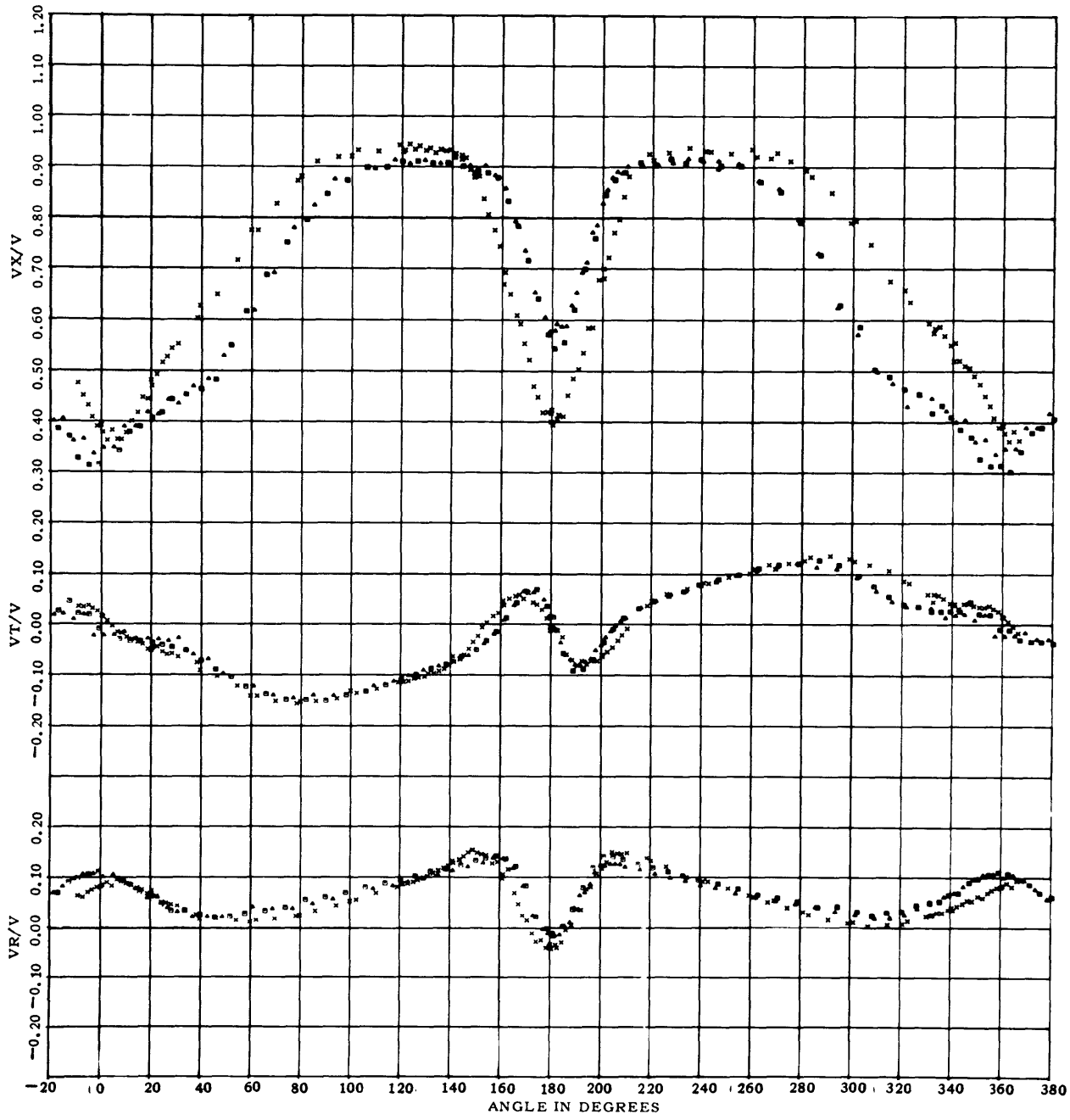

Figure C-2 – Circumferential Distribution of Longitudinal, Tangential, and Radial Velocity Component Ratios at a Radius Ratio of 0.474 for a Modified Bossing at Two Propeller Positions: Composite of Tests 35, 44, and 45

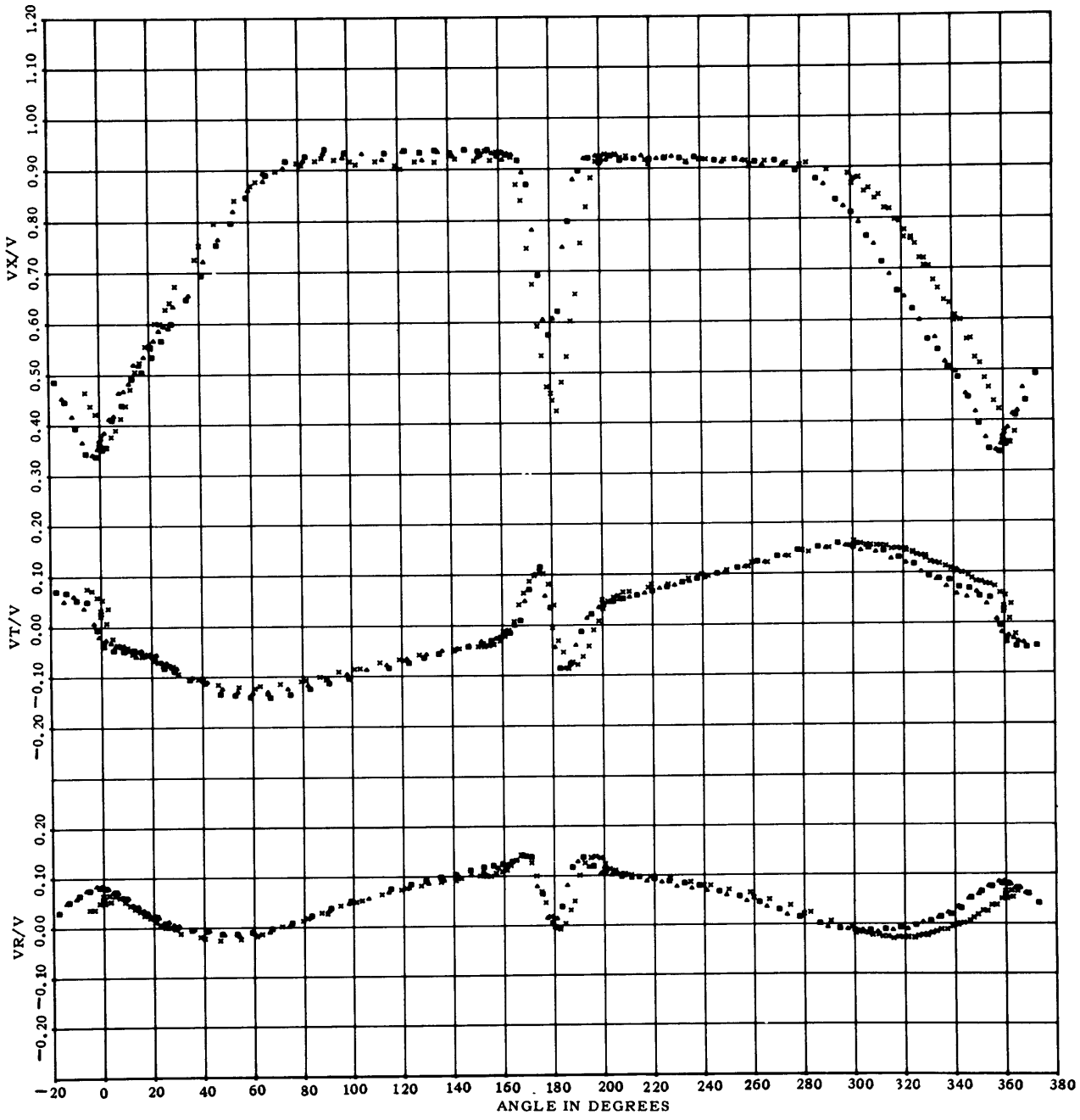

Figure C-3 – Circumferential Distribution of Longitudinal, Tangential, and Radial Velocity Component Ratios at a Radius Ratio of 0.659 for a Modified Bossing at Two Propeller Positions: Composite of Tests 35, 44, and 45

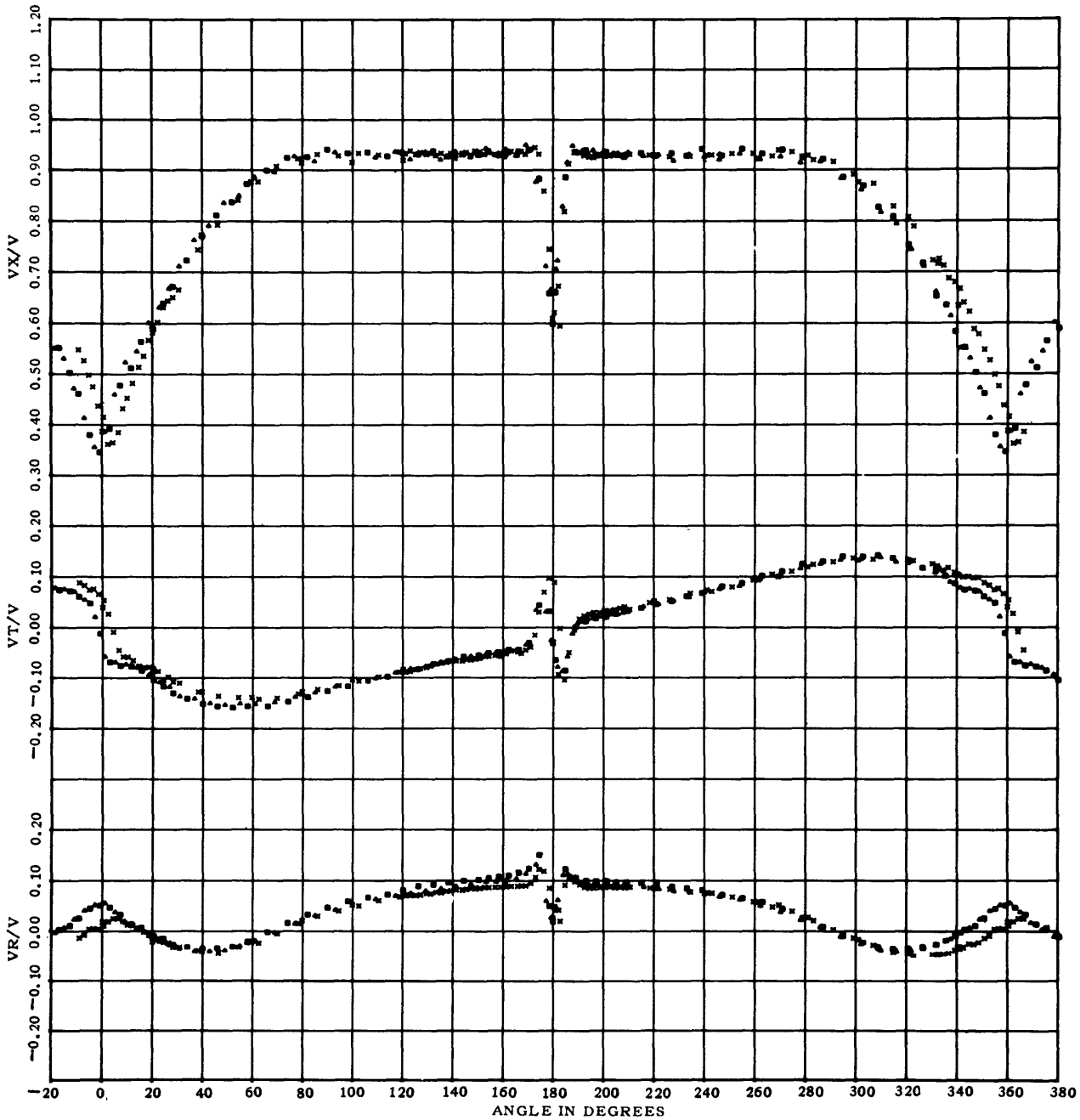

Figure C-4 – Circumferential Distribution of Longitudinal, Tangential, and Radial Velocity Component Ratios at a Radius Ratio of 0.844 for a Modified Bossing at Two Propeller Positions: Composite of Tests 35, 44, and 45

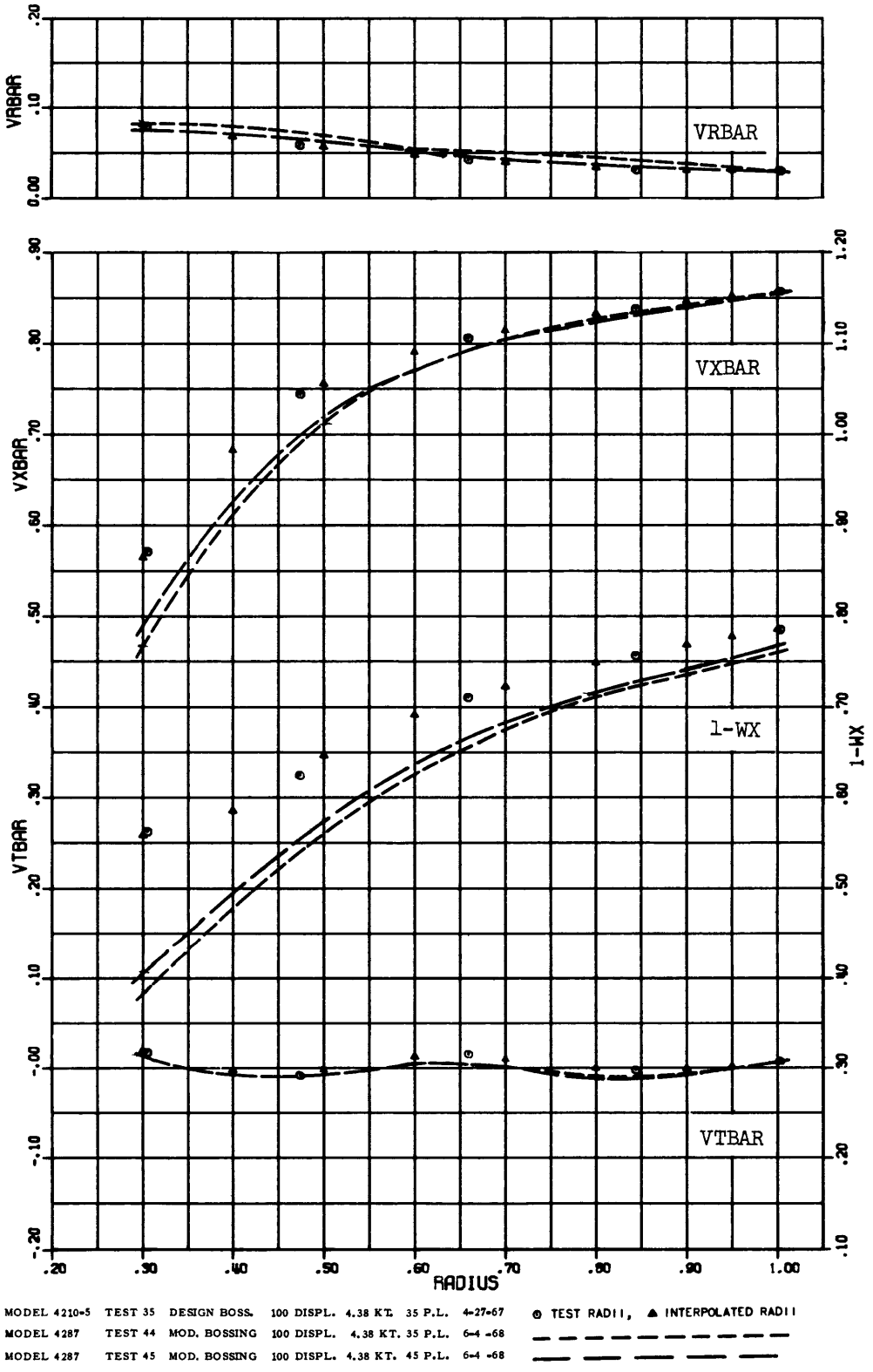

Figure C-5 – Radial Distribution of the Volumetric Mean Wake Velocity Component Ratio and of the Mean Longitudinal, Tangential, and Radial Velocity Component Ratios for a Modified Bossing at Two Propeller Positions: Composite of Tests 35, 44, and 45

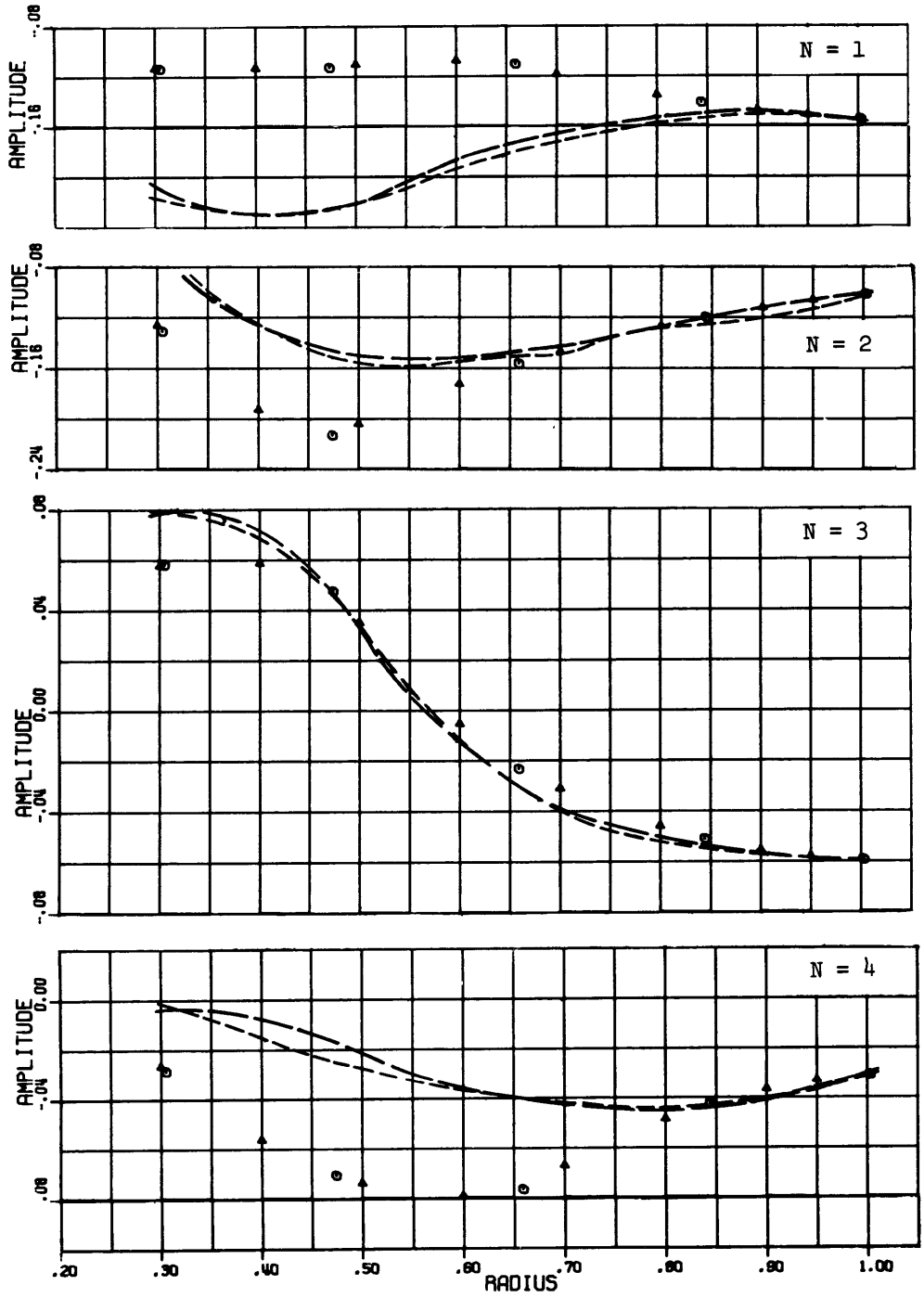

Figure C-6 – Radial Distribution of the Amplitudes of the First through the Fourth Harmonic of the Circumferential Distribution of the Longitudinal Velocity Component Ratios for a Modified Bossing at Two Propeller Positions: Composite of Tests 35, 44, and 45

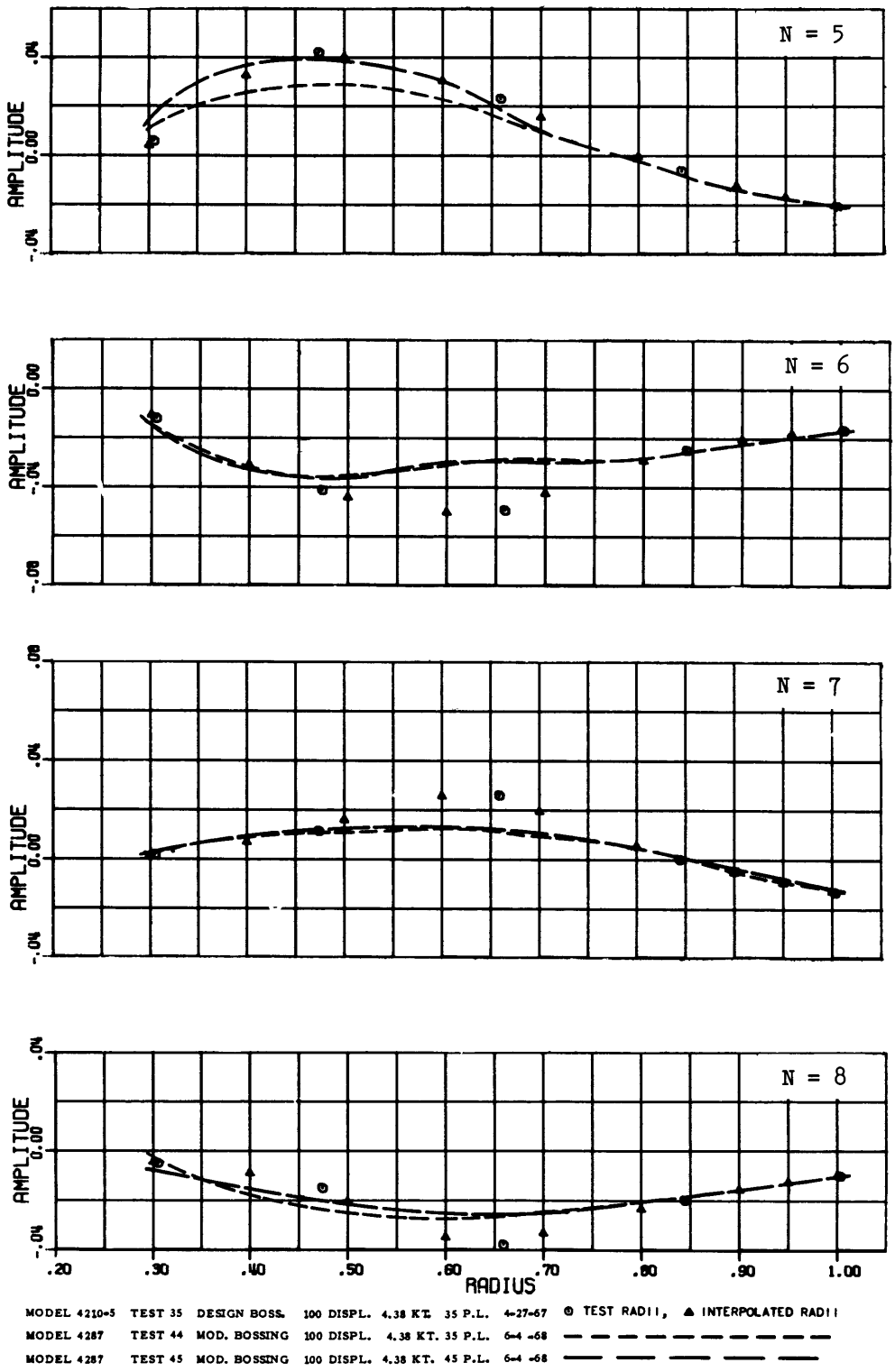

Figure C-7 – Radial Distribution of the Amplitudes of the Fifth through the Eighth Harmonic of the Circumferential Distribution of the Longitudinal Velocity Component Ratios for a Modified Bossing at Two Propeller Positions: Composite of Tests 35, 44, and 45

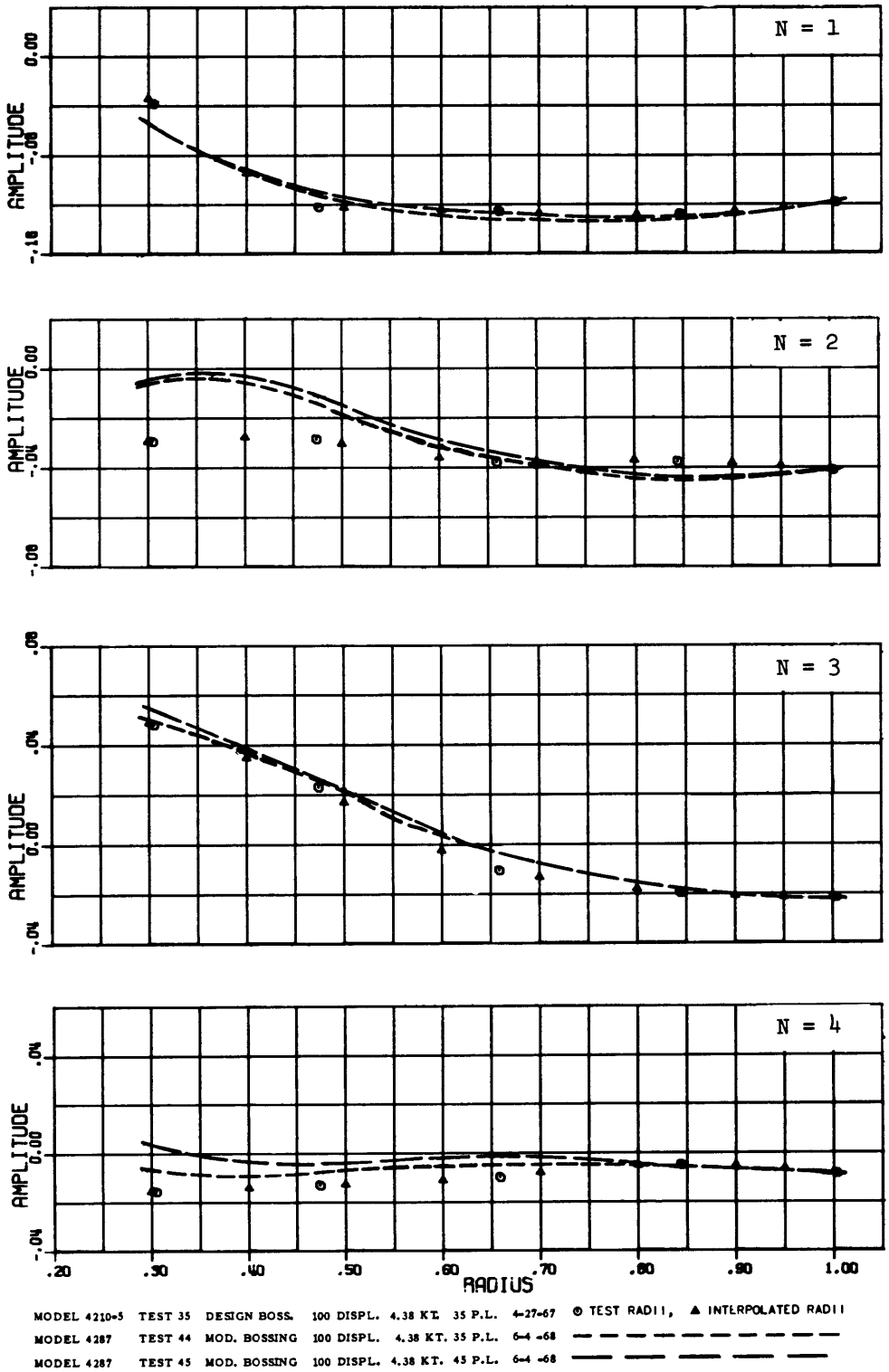

Figure C-8 – Radial Distribution of the Amplitudes of the First through the Fourth Harmonic of the Circumferential Distribution of the Tangential Velocity Component Ratios for a Modified Bossing at Two Propeller Positions: Composite of Tests 35, 44, and 45

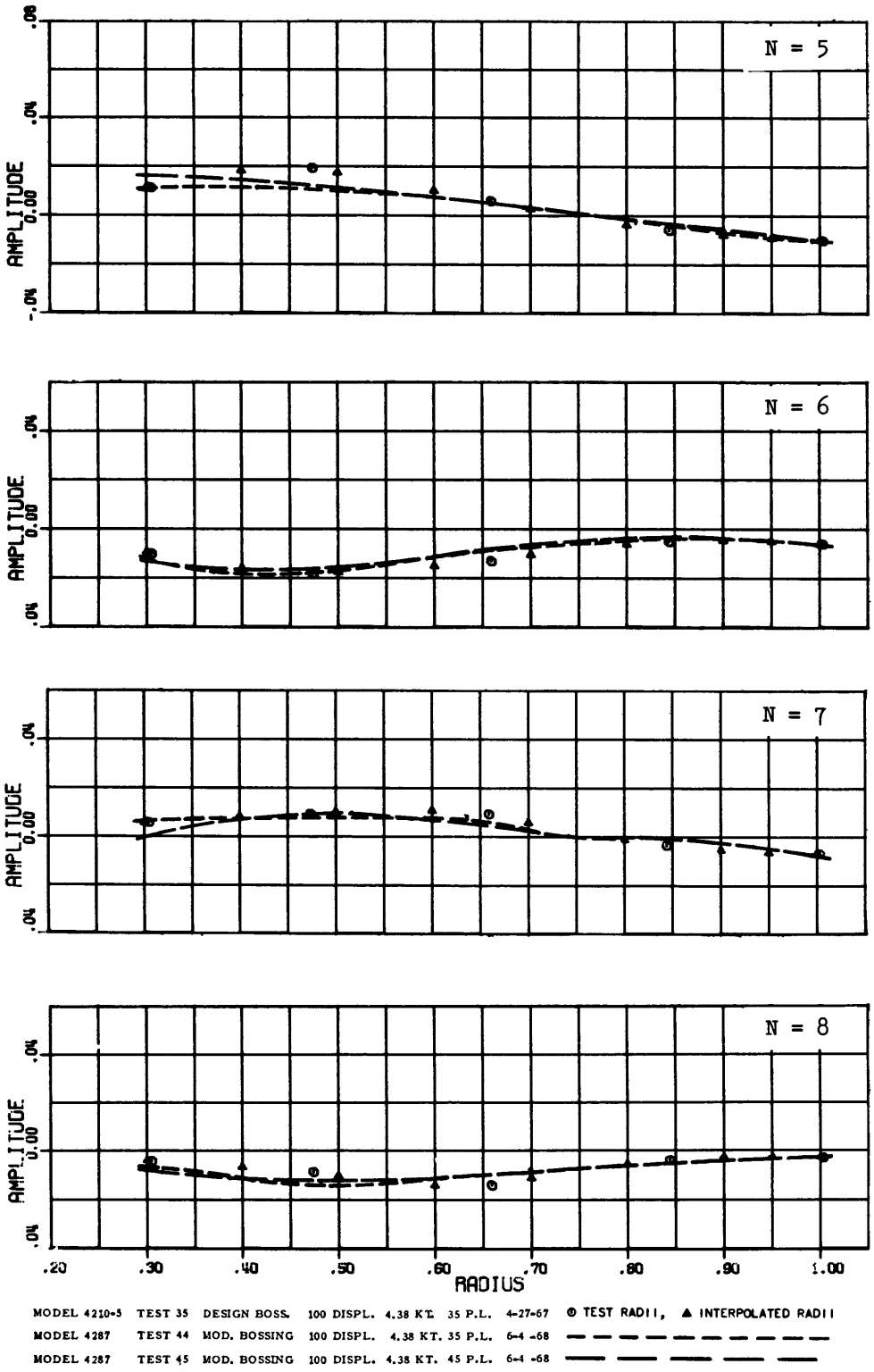

Figure C-9 – Radial Distribution of the Amplitudes of the Fifth through the Eighth Harmonic of the Circumferential Distribution of the Tangential Velocity Component Ratios for a Modified Bossing at Two Propeller Positions: Composite of Tests 35, 44, and 45

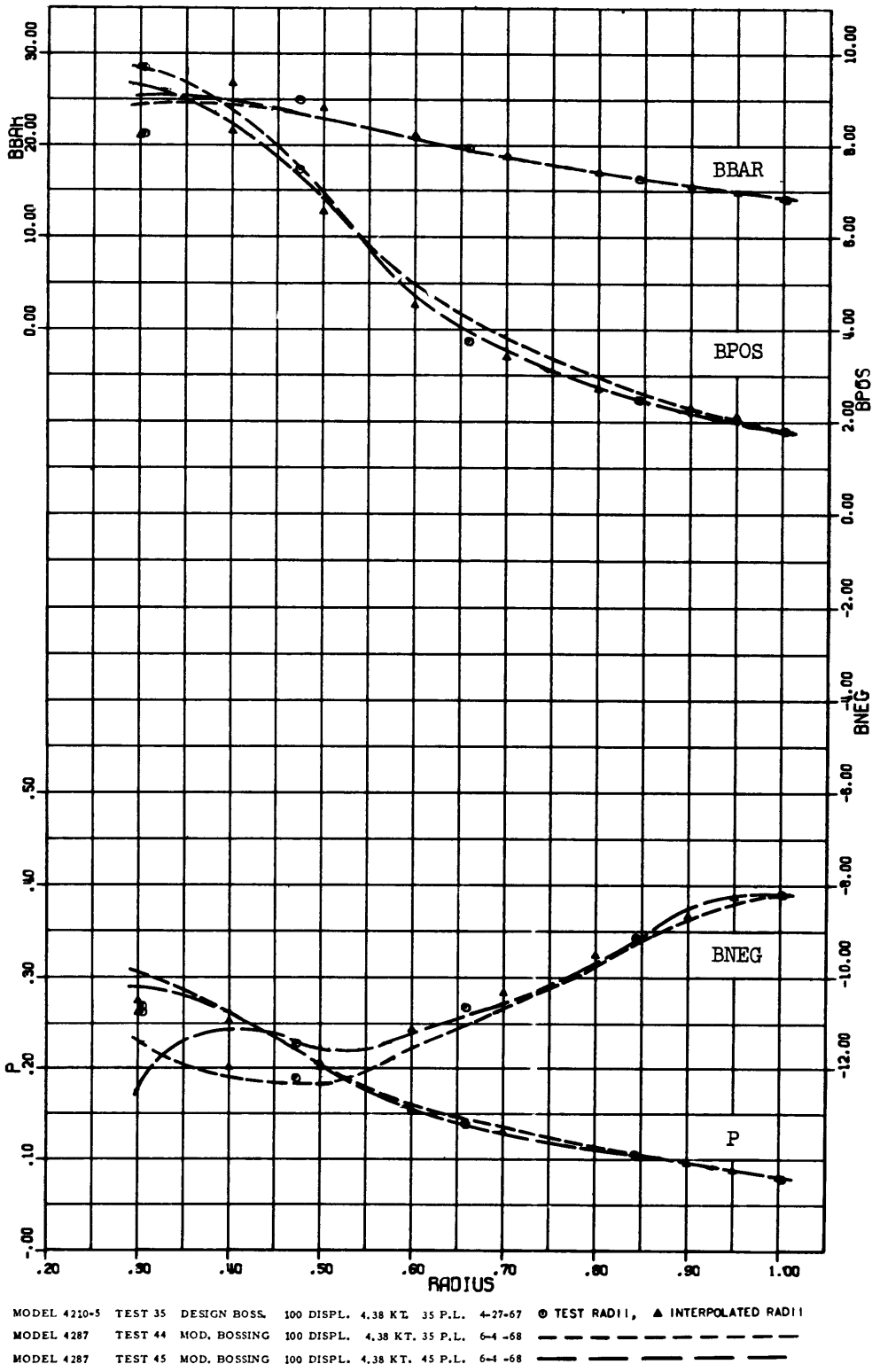

Figure C-10 – Radial Distribution of the Mean Advance Angle, the Maximum Variations of the Advance Angle, and the Pressure Factor for a Modified Bossing at Two Propeller Positions: Composite of Tests 35, 44, and 45

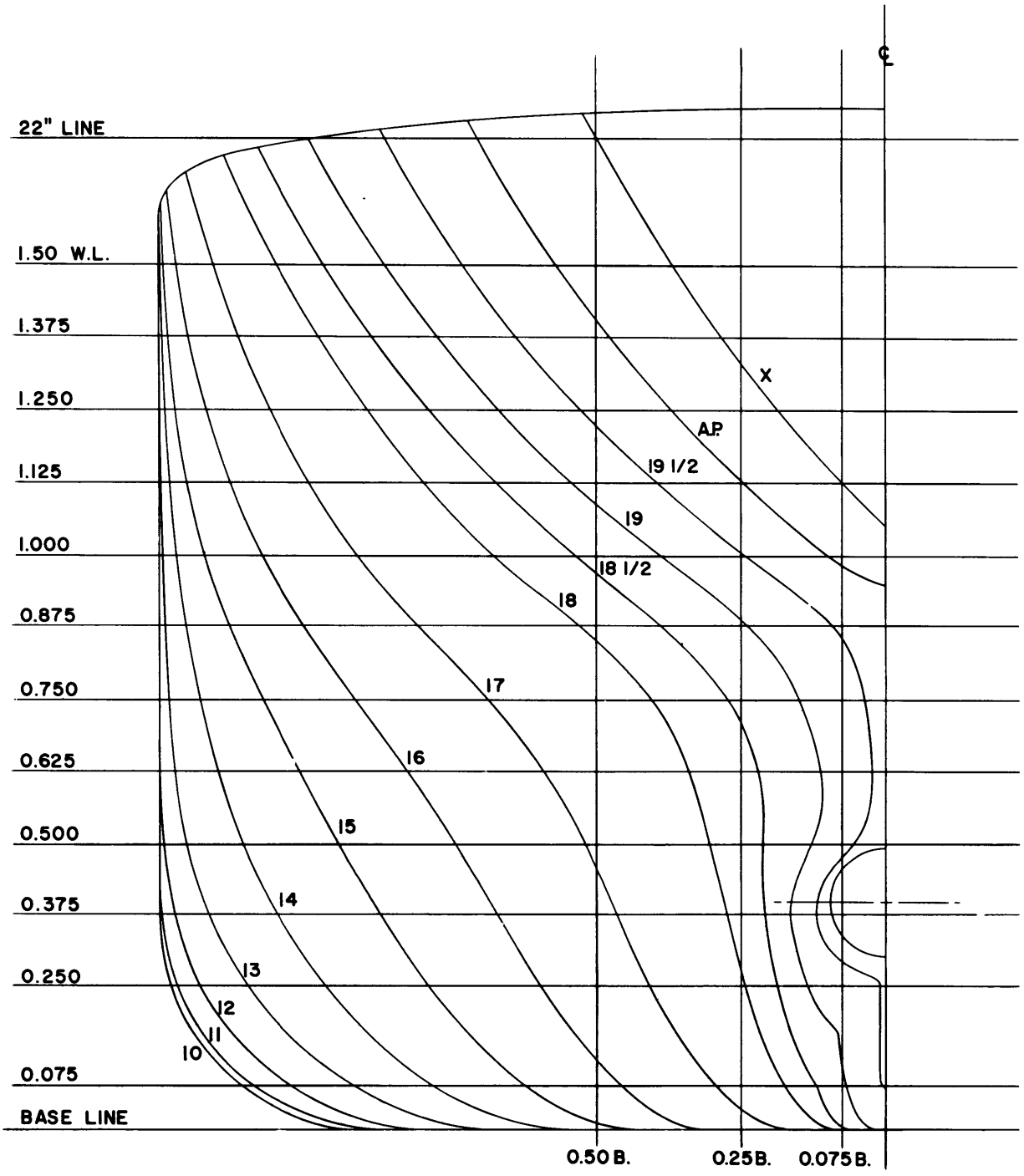

Figure C-11 – Afterbody Plan of Model 4287 with a Modified Bossing

APPENDIX D

CALCULATION PROCEDURES

An important element in any data acquisition system is the means by which the data will be handled, processed, and presented. In a testing procedure such as that involved in a wake survey, the water velocity is determined at approximately 450 points in the propeller plane. Since the processing of this large quantity of data is done by computer, it is important that the data be in a form which is acceptable to the computer. Care has been taken in the design of the instrumentation and the preparation of the computer programs to guarantee compatability between these systems.

Essentially, each record of test data consists of a pitot tube number, a model speed reading, an angular rake position, and four differential pressure readings. The data acquisition system encodes this information on paper punch tape in a predetermined format. These data can be processed directly or may be transcribed onto magnetic tape or IBM cards. Generally the data are converted into card form since they are more easily edited in this form.

The analysis of the test data is carried out in two parts. The first is the calculation of the velocity component ratios from raw test data. The computerized calculation routines, which use polynomials to represent the appropriate pitot-tube and pressure transducer calibration curves, follow the hand computation method described in Reference 8. Sample pitot-tube calibration curves are shown in Figures D-1 and D-2.

The calculation procedure takes advantage of the inherent redundancy of measurement in the five-hole pitot tube in that the longitudinal (V_x/V) velocity component ratio is calculated from two sets of data. Since pressure measurements are taken in two planes, i.e., the longitudinal-radial and the longitudinal-tangential planes, the longitudinal velocity component ratio is calculated in each of these planes. The reported ratio (V_x/V) is the average of these two values.

The dual-measurement feature of the five-hole pitot tube experimentally verifies the limitations of a spherical pitot tube in the extreme velocity gradients, which were discussed in the first section of the discussion. The velocity gradients are known to be greatest in those areas closest to the hull or an appendage of the hull. For single-screw merchant hulls with conventional sterns, the pitot-tubes pass closest to the hull in the vicinity of 0 and 180 deg. The experimental data collected in this series of tests clearly indicate that the velocity gradients are steep in these regions; the velocities determined in the dual planes were not within the ± 1 percentage points of the average longitudinal velocity component ratio (V_x/V). In the remainder of the disk, this ± 1 percent limit is quite realistie.

The output consists of the following:

1. A tabulated printout of the experimentally determined longitudinal, tangential, and radial velocity component ratios and the corresponding angular rake position at each test radius.

2. Intermediate calculations.

3. A deck of IBM cards containing the information in Item 1 above.

4. A magnetic tape with encoded instruction for the plotting of these data by the Calcomp Incremental Plotter.

The second part of the analysis uses as its input the deck of cards output from the first program. The input also consists of various constants and control numbers. Among these is the apparent advance coefficient (J_A), which is necessary to establish the geometrical relationships between the velocity component ratios. (The velocity diagram presented in Figure D-3 may help to clarify the geometrical relationships.)

The output from this program consists of the following:

1. A printout of velocity component ratios interpolated at increments of 2 1/2 deg at each test radius.

2. A printout of interpolated velocity component ratios at several other radius ratios.

3. A printout of the following at each interpolated angular position and radius ratio:
   a. The advance angle (β)

$$\arctan \left[\frac{(V_x/V)}{\frac{\pi(\bar{r}/R)}{J_A} + (V_t/V)} \right]$$

   b. The inflow velocity ratio squared

$$\left[\frac{V_x}{V}\right]^2 + \left[\frac{V_t}{V} + \frac{\pi(r/R)}{J_A}\right]^2$$

   c. The corrected longitudinal velocity component ratio (V_{xc}/V)

$$(V_x/V) - (V_t/V) \cdot \tan \beta$$

4. A printout of the harmonic content of each of the following functions using the 144 interpolated values at each radius ratio. The coefficients of the Fourier series are calculated as follows:

$$f(\theta) = a_0 + \sum_{n=1}^{h} a_n \cos(n\theta) + \sum_{n=1}^{h} b_n \sin(n\theta)$$

$$= a_0 + \sum_{n=1}^{h} c_n \sin(n\theta + \phi_n)$$

where h = 1/2 number of values of $f(\theta)$ used in the summation

= 72

$$a_0 = A(0) = \text{mean value of } f(\theta) = \frac{1}{144} \sum_{i=1}^{144} f(\theta_i)$$

for $f(\theta) = V_x/V$, $a_0 = \overline{V}_x/V$ = **VXBAR**

for $f(\theta) = V_t/V$, $a_0 = \overline{V}_t/V$ = **VTBAR**

for $f(\theta) = (V_b/V)^2$, $a_0 = (\overline{V}_b/V)^2$

for $f(\theta) = V_{x_c}/V$, $a_0 = \overline{V}_{x_c}/V$

$$a_n = A(N) = \frac{1}{h} \sum_{i=1}^{2h} f(\theta_i) \cos(n\theta)$$

$$b_n = B(N) = \frac{1}{h} \sum_{i=1}^{2h} f(\theta_i) \sin(n\theta)$$

$c_n = C(N)$ = AMPLITUDE = $(a_n^2 + b_n^2)$ 1/2

$\phi_n = PHI(N)$ = PHASE ANGLE = arctan (a_n/b_n)

5. A printout of the following at each radius ratio:
   a. The mean longitudinal velocity component ratio.
   b. The mean tangential velocity component ratio.
   c. The mean radial velocity component ratio.
   d. The volumetric velocity ratio.
   e. The volumetric mean wake velocity component ratio.
   f. The wake coefficient.
   g. The pressure factor.
   h. The mean advance angle.
   i. The variation of the maximum advance angle from the mean.
   j. The variation of the minimum advance angle from the mean.

6. A magnetic tape containing encoded instructions for the plotting of some of the output in Items 4 and 5 against radius ratio. At the present time, the following information is presented for single and twin-screw vessels:

a. *Single-Screw Vessels*

AMPLITUDE (a_n) for specified harmonics of V_x/V.

AMPLITUDE (b_n) for specified harmonics of V_t/V.

VXBAR ($\overline{V}_x/V$), $1 - WX\ (1 - w_x)$, P

BBAR ($\overline{\beta}$), BPOS ($+\Delta\beta$), BNEG ($-\Delta\beta$)

b. *Twin-Screw Vessels*

AMPLITUDE (c_n) and PHASE ANGLE (ϕ_n) for specified harmonics of V_x/V.

AMPLITUDE (c_n) and PHASE ANGLE (ϕ_n) for specified harmonics of V_t/V.

VXBAR ($\overline{V}_x/V$), VTBAR ($\overline{V}_t/V$), $1 - WX\ (1 - w_x)$

P, BBAR ($\overline{\beta}$), BPOS ($+\Delta\beta$), BNEG ($-\Delta\beta$)

CALIBRATION CONDITIONS:

1. C, R1, R2, T1, & T2 are pressure measurements at the corresponding pitot tube holes, converted to inches of water pressure.
2. T1 = T2, hence, $\beta_T = 0$ and $V_T = 0$.
3. β_{LR} is the angle in degrees between hole C and the direction of water flow. β_{LR} is positive when hole R2 is closer to the point of impact than hole R1.
4. V_{LR} is the velocity in ft/sec at which the pitot tube is towed.

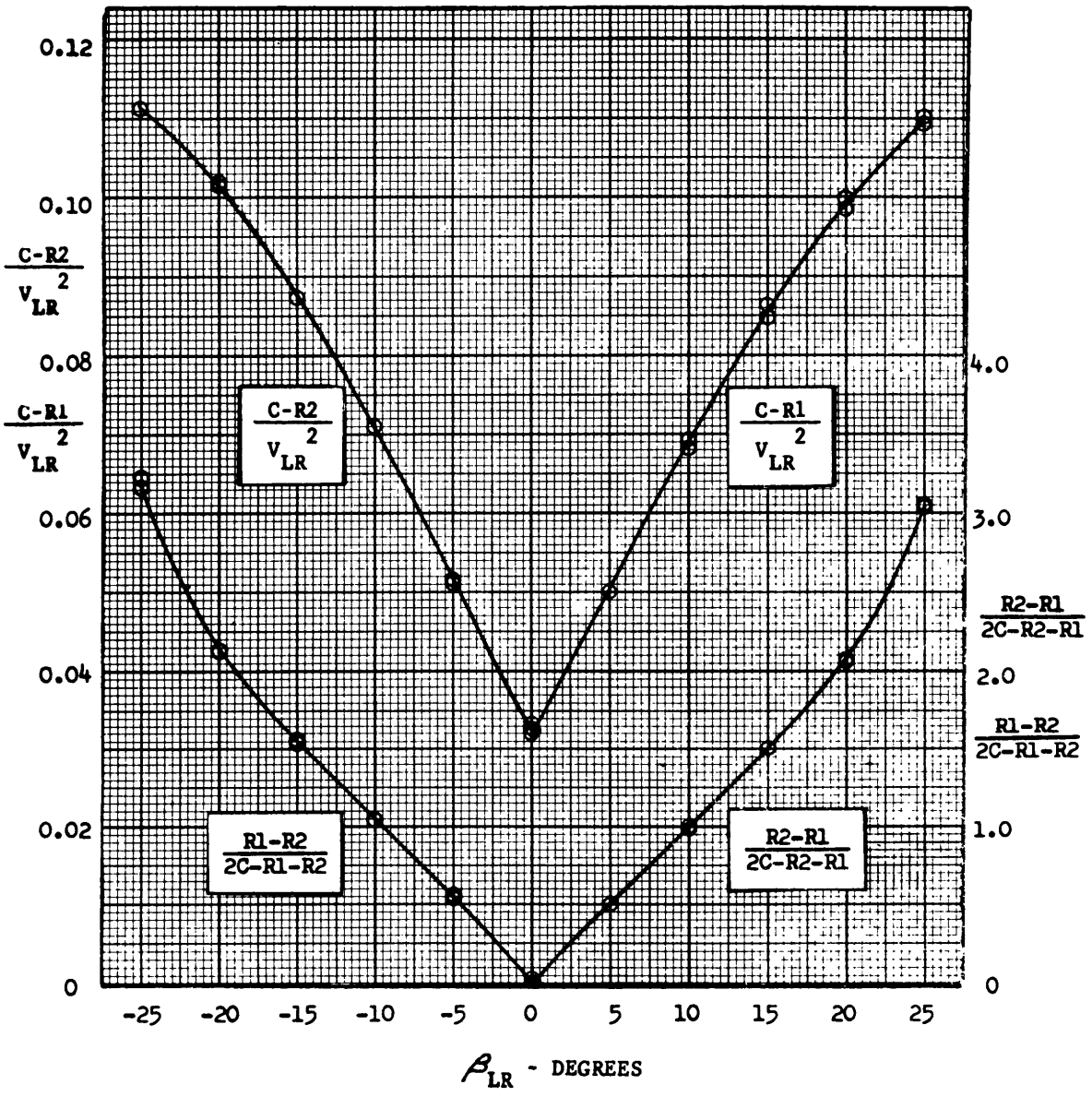

Figure D-1 – Calibration Curves of a Spherically Headed Pitot Tube in the Longitudinal-Radial Plane

CALIBRATION CONDITIONS:

1. C, T1, T2, R1, & R2 are pressure measurements at the corresponding pitot tube holes, converted to inches of water pressure.
2. R1 = R2, hence, $\beta_R = 0$ and $V_R = 0$.
3. β_{LT} is the angle in degrees between hole C and the direction of water flow. β_{LT} is positive when hole T2 is closer to the point of impact than hole T1.
4. V_{LT} is the velocity in ft/sec at which the pitot tube is towed.

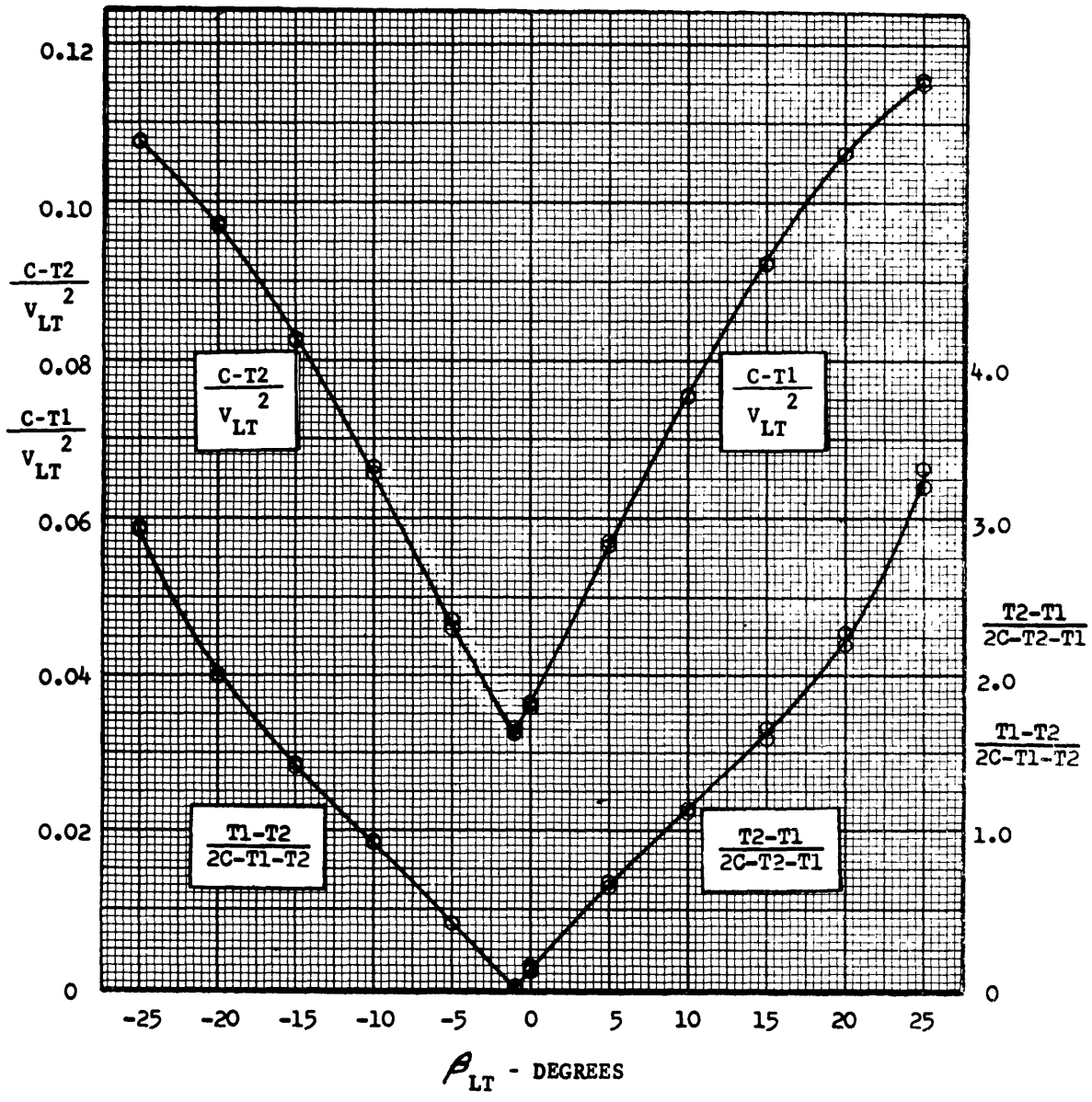

Figure D-2 – Calibration Curves of a Spherically Headed Pitot Tube in the Longitudinal-Tangential Plane

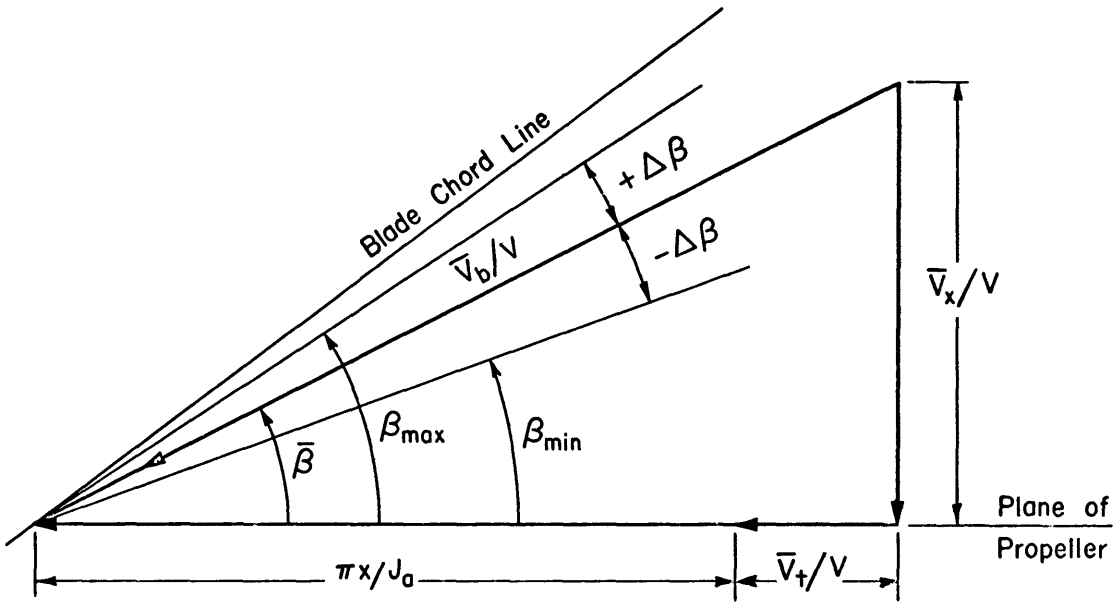

Figure D-3 – Velocity Diagram

REFERENCES

1. Cheng, H.M. and Hadler, J.B., "Wake Analysis of Ship Models, Single-Screw DE-Type," David Taylor Model Basin Report 1849 (Jun 1964).

2. Cheng, H.M. and Hadler, J.B., "Wake Analysis of Ship Models, Twin-Screw Military Types," David Taylor Model Basin Report 1928 (Dec 1954).

3. Cheng, H.M. and Hadler, J.B., "Wake Analysis of Ship Models, Single-Screw Merchant Types," David Taylor Model Basin Report 2076 (Nov 1965).

4. Cheng, H.M. and Hadler, J.B., "Wake Analysis of Ship Models, Twin-Screw Merchant Types," David Taylor Model Basin Report 2074 (Oct 1965).

5. Hadler, B. and Cheng, M., "Analysis of Experimental Wake Data in Way of Propeller Plane of Single and Twin-Screw Ship Models," Transactions of The Society of Naval Architects and Marine Engineers, Vol. 73 (1965).

6. Hadler, J.B. and Weaver, A.H., Jr., "Wake Analysis of a Series 60, 0.60 Block Coefficient Model, Model 4210-5," David Taylor Model Basin Report 2075 (Oct 1965).

7. Hadler, J.B., Discussion of "Correlation and Application of an Unsteady Flow Theory for Propeller Forces," by S. Tsakonas et al., Transactions of The Society of Naval Architects and Marine Engineers, Vol. 75, pp. 186–188 (1967).

8. Pien, P.C., "Five-Hole Spherical Pitot Tube," David Taylor Model Basin Report 1229 (May 1958).

9. Stuntz, G.R. et al., "Series 60 – The Effect of Variations in Afterbody Shape upon Resistance, Power, Wake Distribution, and Propeller-Excited Vibratory Forces," Transactions of The Society of Naval Architects and Marine Engineers, Vol. 68 (1960).

INITIAL DISTRIBUTION

Copies

10 ADMIN, MARAD
- 1 Ship Div
- 1 Coord of Res

4 NAVSHIPS
- 3 (SHIPS 2052)
- 1 (SHIPS 033)

9 NAVSEC
- 1 (SEC 6100)
- 2 (SEC 6110)
- 3 (SEC 6136)
- 1 (SEC 6144)
- 2 (SEC 6148)

1 NAVORDSYSCOM (ORD 05411)

3 NAVAIRSYSCOM
- 2 AIR 604
- 1 AIR 302

3 CHONR
- 2 Fluid Dyn (Code 438)
- 1 Sys and Res Gp (Code 492)

1 NUWC, Pasadena

1 DIR, Naval Weapons Center, China Lake

1 CDR, USNOL

1 DIR, USNRL

1 ONR, SAN FRAN

1 CO, ONR, BSN

1 CO, ONR, Pasadena

1 CO, ONR, Chicago

1 CO, ONR, London

1 NAVSHIPYD PTSMH

1 NAVSHIPYD BSN

1 NAVSHIPYD PUG

1 NAVSHIPYD PHILA

1 NAVSHIPYD CHASN

1 NAVSHIPYD LBEACH

1 CDR, NWL
Attn: Computation & Exterior Ballistic Lab

Copies

1 CO & DIR, NMDL

1 CO, USNROTC & NAVADMINUMIT

1 SUPT, USMA

1 SUPT, USNA

1 SUPT, USMMA

1 USNASL, Attn: Lib

1 CO, USNAVUWRES, Attn: Lib

1 CO, USNEL, Attn: Lib

1 CO & DIR, USNAVCIVENGRLAB

1 USNAVPGSCOL, Monterey

20 DDC

2 NASA
- 1 Dr. W.L. Habeman (Code MTY)
- 1 Dir of Res (Code RR)

1 CO, MSTS

1 BUSTAND, Attn: Lib

1 Lib of Congress

1 CMDT, USCG
Attn: Ship Const Comm

1 CDR, U.S. Army Transportation R&D, Fort Eustis, Va Attn: Marine Transp Div

1 Air Force Office of Sci Res, Attn: Mech Div

1 W-PAFB, Dayton, Attn: Wright Air Dev Div
Aircraft Lab

2 Langley Res Center, Langley Sta, Hampton, Va
- 1 Mr. I.E. Garrick
- 1 Mr. D.J. Marten

1 DIR, Natl Sci Found, Attn: Eng Sci Div

1 Chief, R&D, Office of Chief of Staff
Dept of the Army, The Pentagon

1 DIR, WHOI

1 NASA, College Park
Attn: Sci & Tech Infor Acq Br

Copies

1 CHOFENGRS, ENGINDIV, Dept Army
Attn: Tech Doc Center

1 DIR, ORL

1 Head, Dept NAME, MIT

4 CIT
1 Lib
1 Prof Acosta
1 Prof Plesset
1 Prof Wu

1 DIR, St. Anthony Hydraulics Lab, Univ of Minnesota

1 Univ of Notre Dame, Dept of Mech Eng, South Bend

1 DIR, Inst of Hydraulic Res, Univ of Iowa

1 Univ of Michigan, Dept NAME, Ann Arbor

2 Webb Inst of Nav Arch, Glen Cove
1 President
1 Lib

2 Univ of Calif, Berkeley
1 Lib
1 Head, Dept NAVARCH

2 State Univ of Colorado, Fort Collins
1 Dr. M.L. Albertson
1 Prof J.E. Germak

1 Cornell Univ, Graduate School of Aeronau Eng, Ithaca

1 Harvard Univ, Cambridge, Attn: Lib

2 Johns Hopkins Univ, Baltimore
1 Dept of Mechanics
1 Inst of Cooperative Res

4 State Univ of New York, Maritime College, Bronx
1 Lib
1 Prof J.J. Foody
1 Prof R. Zubaly
1 Prof J.G. McNeill

1 Princeton Univ, Princeton, New Jersey
Attn: Lib

1 Stanford Univ, Stanford, Calif
Attn: Dept of Civil Eng

Copies

1 Univ of Ill, Dept of Theoretical & Appl Mech Urbana

1 Johns Hopkins Univ, Fenton Kennedy Doc Center, Appl Phys Lab, Silver Spring

1 Cornell Aeronautical Lab, Buffalo

2 Davidson Lab, SIT, Hoboken
1 Director
1 Dr. Tsakonas

1 Rensselaer Polytechnic Inst, Dept of Math, Troy

1 Puget Sound Bridge & DDC, Seattle

1 Douglas Aircraft Co, Gen Appl Sci Lab Westbury, L.I.

1 ITEK Corp, Vidya Div, Palo Alto

1 TRG Inc, Melville, N.Y.

1 Therm Inc

1 Lockheed Missiles and Space, Sunnyvale
Attn: Dept 5701

1 Lockheed Missiles and Space, Palo Alto
Attn: Tech Info Center

1 Elec Boat Co, Gen Dyn Corp, Groton

1 Robert Taggart Inc, Fairfax

1 Oceanics

1 Gibbs & Cox

1 Litton Industries

1 NNS & DD

1 J.J. Henry

1 George G. Sharp, Inc.

1 Grumman Aircraft Corp., Bethpage

1 Hydronautics, Inc.

1 Martin Co, Baltimore

1 Boeing Aircraft, AMS Div, Seattle

1 United Aircraft, Hamilton Standard Div, Windsor Locks, Conn

1 AVCO, Lycoming Div, Washington

Copies

1 Baker Mfg, Evansville

2 General Dynamics–Convair, San Diego
1 Dr. B.R. Parkin
1 Chief of ASW/Marine Sciences

1 Curtiss-Wright Corp, Woodridge, N.J.

1 Pres, General Tech Services Inc, Cleveland

1 Dr. K.E. Schoenherr
7053 Western Ave, N.W.,
Washington, D.C.

1 Dr. S.F. Hoerner
148 Busteed Drive
Midland Park, N.J.

1 Radio Corp of America, Burlington, Mass
Attn: Hydrofoil Projects

1 U.S. Rubber Co, Res and Dev Dept, Wayne, N.J.

1 Midwest Res Inst, Kansas City, Mo
Attn: Lib

1 North American Aviation Inc, Oceans Systems Div,
Downey, Calif

1 Aerojet-General Corp, Azusa

1 SNAME

1 ASNE, Washington

1 ASME, Res Comm in Information, New York

1 Inst of Aerospace Sci, New York
Attn: Lib

14 KEY WORDS	LINK A		LINK B		LINK C	
	ROLE	WT	ROLE	WT	ROLE	WT
Ship Model Tests:						
Wake Surveys, Results and Analysis						
Variation of Several Parameters						
Effects of Stern Shapes						
Effects of Speed						
Effects of Propeller Position						
Effects of Displacement and/or Draft						
Effects of Trim						
Effects of Deadwood Area						
Wake Survey, Measurement-Instrumentation						

UNCLASSIFIED
Security Classification

DOCUMENT CONTROL DATA - R & D

(Security classification of title, body of abstract and indexing annotation must be entered when the overall report is classified)

1 ORIGINATING ACTIVITY (Corporate author)	2a. REPORT SECURITY CLASSIFICATION
Naval Ship Research and Development Center Washington, D. C. 20007	UNCLASSIFIED
	2b. GROUP

3 REPORT TITLE

THE EFFECTS OF VARIATIONS OF SEVERAL PARAMETERS ON THE WAKE IN WAY OF THE PROPELLER PLANE FOR SERIES 60–0.60 C_B MODELS

4. DESCRIPTIVE NOTES *(Type of report and inclusive dates)*

Research and Development

5 AUTHOR(S) *(First name, middle initial, last name)*

Jerald W. Grant and Alan C. M. Lin

6 REPORT DATE	7a. TOTAL NO OF PAGES	7b. NO OF REFS
June 1969	117	9

8a. CONTRACT OR GRANT NO	9a. ORIGINATOR'S REPORT NUMBER(S)
MARAD Purchase Order P1-MA66-939 b. PROJECT NO. Other Government Task 82881	3024
c. d.	9b. OTHER REPORT NO(S) *(Any other numbers that may be assigned this report)*

10 DISTRIBUTION STATEMENT

This document has been approved for public release and sale; its distribution is unlimited.

11 SUPPLEMENTARY NOTES	12 SPONSORING MILITARY ACTIVITY
	Maritime Administration

13 ABSTRACT

This report presents the results of a series of wake surveys conducted on Series 60–0.60 C_B models with three different afterbody configurations. These tests were conducted with variations of the following parameters: speed, propeller position, displacement, trim, and deadwood area.

This presentation includes the circumferential distributions of the longitudinal, tangential, and radial velocity component ratios; the radial distribution of the mean velocity component ratios; the radial distribution of the volumetric mean wake velocity ratio; the radial distribution of the amplitudes of the harmonics of the longitudinal and tangential velocity component ratios; and the radial distribution of the pressure factor and of the mean advance angle and the maximum positive and negative variations thereof.

The most pronounced effect was achieved by removing a portion of the deadwood in way of the stern aperture. This alteration yielded a higher mean longitudinal velocity while reducing the harmonic amplitudes. The displacement and speed also had an effect on the wake distribution. The testing of the moderate U- and V-shaped sterns, however, did not indicate changes of the magnitude that were anticipated.